Phase field modeling of ferroelectrics with point defects

Vom Fachbereich
Material- und Geowissenschaften
Technische Universität Darmstadt
zur Erlangung des akademischen Grades eines Doktor-Ingenieurs (Dr.-Ing.)
genehmigte Dissertation

von

Dipl. Ing. Yinan Zuo

geboren am 29. April 1983 in Shenyang, Liaoning, V. R. China

1. Gutachten Prof. PhD. Bai-Xiang Xu
2. Gutachten Dr. Yuri Genenko

Tag der Einreichung: 12. Jan. 2016
Tag der mündlichen Prüfung: 15. April 2016

D 17

Darmstädter Dissertationen
2016

Acknowledgement

First of all, I would like to gratefully and sincerely thank my advisor, Jun. Prof. Bai-Xiang Xu, for her admission to be her Ph. D. student and her guidance and especially her patience during the three years. Moreover, I would like to thank her for giving me the deep understanding for phase field modeling of materials. I have been very pleased to have worked with her for three years.

I would also like to thank Dr. Yuri Genenko and Apl. Prof. Andreas Klein. They gave me a lot of suggestions about the research on semiconducting feature of ferroelectrics. Only with their help, we were able to explain the results from calculations correctly from point of view of physics. I am grateful to Dr. Peter Stein, with whose help I have better knowledge for using Linux and relevant programs. I would like to thank Mr. Jan Hennecke for providing the help on computer problems. I would also thank Ms. Maria Bense for her work as secretary. I would like to thank Prof. Dr. Ralf Müller, Prof. Dr. Jürgen Rödel and Dr. Yuri Genenko for finding time from their schedules to attend the examination committee and to carefully read this thesis. I would specially thank Mr. David Swallow for their help on the English language for thesis writing. I would like to thank my previous colleagues and friends, Mr. Yangbin Ma, Ms. Ying Zhao, Min Yi, Ph.D., Habib Pouriayevali, Ph.D., Mr. Shuai Wang, Ms. Dagmar Eder-Goy, Jia Yuan and Chao He for setting up a nice working condition in the group and help from many aspects. Finally, and most importantly, I would also like to thank my wife Yuqing Guan for her support and kind encouragement. I thank my parents Yonghong Li and Ying Zuo, for all their education to me and allowing me to realize my own potential.

Contents

B_0	Initial configuration
B_t	Current configuration
t	Time (s)
X_i	Coordinate in initial configuration (m)
x_i	Coordinate in current configuration (m)
δ_{ij}	Kronekcer delta
ϵ_{ijk}	Levi-Civita symbol
F_{ij}	Deformation gradient
H_{ij}	Displacement gradient
ε_{ij}	Infinitesimal strain
S_{ij}	Second Piola stress
C_{ijkl}	Stiffness tensor (Nm^{-2})
n_i	surface normal vector
t_i	surface traction force vector (Nm^{-2})
dS	Line element in initial configuration (m)
ds	Line element in current configuration (m)
E_{ij}	Green strain tensor
r	Distance between two electric charges (m)
E_i	Electric field (Vm^{-1})
F_i	Electric force (N)
q	Unit electric charge (C)
ϵ_0	Vacuum permittivity (Fm^{-1})
W	Work (Nm)
ϕ	Electric potential (V)
s_i	Displacement between positive and negative charge (m)
E_i^{micro}	Microscopic electric field (Vm^{-1})
P_i^{micro}	Microscopic polarization (Cm^{-2})
D_i^{micro}	Microscopic electric displacement (Cm^{-2})
E_i^{ext}	External electric field (Vm^{-1})
E_i^{tot}	Total electric field (Vm^{-1})
D_i	Electric displacement (Cm^{-2})
A_{ij}	Permittivity (Fm^{-1})
b_{ijk}	Piezoelectric tensor $(Nm^{-1}V^{-1})$
ρ	Charge density (Cm^{-3})
ω	Surface charge density (Cm^{-2})
f_i	Volume force (Nm^{-3})
v_i	velocity (ms^{-1})

σ_{ij}	Cauchy stress (Nm^{-2})
σ_{ij}^{m}	Maxwell stress (Nm^{-2})
e	Internal energy (Nm^{-2})
r	Volume heat supply ($Nm^{-2}s^{-1}$)
q_i	Surface heat supply ($Nm^{-1}s^{-1}$)
f_i^{ext}	External volume force (Nm^{-3})
f_i^{ele}	Electric volume force (Nm^{-3})
m_{ij}	Force torque (Nm^{-2})
T	Temperature (K)
Q	Heat (Nm)
S	Entropy (Nm)
$\delta_{(\cdot)}(\cdot)$	Variational symbol
$N_{(\cdot)}$	Concentration of certain point defect (m^{-3})
N_C	Effective density of states in the conduction band (m^{-3})
N_V	Effective density of states in the valence band (m^{-3})
E_F	Fermi level (eV)
E_C	Conduction band edge (eV)
E_V	Valence band edge (eV)
$t_{(\cdot)}$	Ionization of certain point defect
$z_{(\cdot)}$	Valency of certain point defect
$F_{\frac{1}{2}}$	Fermi integral
$\mathcal{H}$	Free enery (Nm)
$\mathcal{D}$	Dissipation (Nm)
D	Diffusion coefficient (m^2s^{-1})
P_i	Spontaneous polarization (Cm^{-2})
M_{ij}	Domain mobility cofficient ($Cm^{-1}V^{-1}s^{-1}$)
κ_s	Domain wall energy calibration parameter
κ_i	Domain wall width calibration parameter
G	Domain wall energy (Jm^{-2})
ϵ	Domain wall width (m)
a_i	Domain separation energy polynomial coefficient
Σ_{ij}	Configurational stress tensor (Nm^{-2})
g_i	Configurational force vector (Nm^{-3})
N^I	Shape function
B^I	Differential operator
R_k^I	Residual vector

K_{kl}^{IJ}	Stiffness matrix
D_{kl}^{IJ}	Damping matrix
J_i	The J-integral
L_i	The L-integral
α	Tilt angle of domain wall $grad$
E_{ib}	Internal bias field Vm^{-1}
E_i^d	Internal bias field due to defect dipole Vm^{-1}
P_i^d	Defect dipole polarization Cm^{-2}
C_0	Constant
κ_0	Permitticity
P_i^t	Total polarization Cm^{-2}
E_i^e	External applied electric field Vm^{-1}
E_i^t	Total electric field Vm^{-1}
E_i^t	Total electric field Vm^{-1}
n_1	Number of particles whose energy is larger than G_1
n_2	Number of particles whose energy is larger than G_2
N	Total number of particles
ΔE^{i-j}	Energy barrier between position i and j eV
ν_0	Vibration frequency of a vacancy s^{-1}
c_i	Vibration frequency of a vacancy
K_{ij}	Coefficients s^{-1}
V_0	Unit cell volume m^3

Chapter 1

Introduction

1.1 Basics

1.1.1 Applications of ferroelectrics

The nonlinear feature of ferroelectric materials can be applied to make capacitors with tunable capacitance. Typically, a ferroelectric capacitor simply consists of a pair of electrodes sandwiching a layer of ferroelectric material. The permittivity of ferroelectrics is not only tunable but commonly also very high in absolute value, especially when close to the phase transition temperature. Because of this, ferroelectric capacitors are small in physical size compared to dielectric (non-tunable) capacitors of similar capacitance.

The spontaneous polarization of ferroelectric materials possesses a hysteresis effect which can be used in memory devices, and ferroelectric capacitors are used to make ferroelectric RAM for computers and RFID cards. In these applications thin films of ferroelectric materials are typically used, as this allows the field required to switch the polarization to be achieved with a moderate voltage. However, when using thin films a great deal of attention needs to be paid to the interfaces, electrodes and sample quality for devices to work reliably.

Ferroelectric materials are required by symmetry considerations to be also piezoelectric and pyroelectric. The combined properties of memory, piezoelectricity, and pyroelectricity make ferroelectric capacitors very useful, e.g. for sensor applications. Ferroelectric capacitors are used in medical ultrasound machines (the capacitors generate and then listen for the ultrasound ping used to image the internal organs of a body), high quality infrared cameras (the infrared image is projected onto a two dimensional array of ferroelectric capacitors capable of detecting temperature differences as small as millionths of a degree Celsius), fire sensors, sonar, vibration sensors, and even fuel injectors on diesel engines.

Another idea of recent interest is the ferroelectric tunnel junction (FTJ) in which a contact made up by nanometer-thick ferroelectric film placed between metal electrodes. Thickness of the ferroelectric layer is small enough to allow tunneling of electrons. The piezoelectric and interface effects as well as the depolarization field may lead to a giant electroresistance (GER) switching effect. Yet another hot topic is multiferroics, where researchers are looking for ways to couple magnetic and ferroelectric ordering within a material or heterostructure; there are several recent reviews on this topic.

1.1.2 Development history

As early as 1894, Pockels in Göttingen reported some unusual dielectric and piezoelectric properties of sodium potassium tartrate tetrahydrate ($NaKC_4H_4O_6 \cdot 4H_2O$), which is better known as Rochelle salt. But it was not until 1920 that Valasek found that there was a hysteresis effect in the field-polarization curve in this material, and a large dielectric and piezoelectric response near the ferroelectric region as well [1]. In 1935, the first series of ferroelectric isomorphous crystals were produced by Busch and Scherer in Zurich [2].

Later in the 1940s, people found that barium titanate ceramic had an extremely large dielectric constant of more than 1000 at room temperature. Shortly after that ferroelectricity in the same material was reported by Wul and Goldman [3, 4].

Due to many of its anomaly properties, $BaTiO_3$ became the most intensively investigated ferroelectric material. Some new ferroelectric materials like $KNbO_3$, $KTaO_3$ [5], $LiNbO_3$ and $LiTaO_3$ [6], and $PbTiO_3$ [7] were discovered in the following years. In the $1950'$s, a lot of studies on ferroelectric materials have been made. Widespread use of barium titanate ($BaTiO_3$) based ceramics in capacitor applications and piezoelectric sensors and actuators was made. Since then, many other ferroelectric ceramics including lead titanate ($PbTiO_3$), lead zirconate titanate (PZT), lead lanthanum zirconate titanate (PLZT), and relaxor ferroelectrics like lead magnesium niobate (PMN) have been developed and utilized for a variety of applications. As ceramic processing and thin film technology developed, many new applications have appeared. The most common use of ferroelectric ceramics has been in the areas such as dielectric ceramics and capacitor applications. Other applications include piezoelectric materials for medical ultrasound imaging and actuators, ferroelectric thin films for non-volatile memories, and electro-optic materials for data storage and displays.

An important group of ferroelectrics is known as the perovskites, which gets its name from the mineral perovskite $CaTiO_3$. The perfect perovskite structure can be described by chemical formula ABO_3, where A is a bivalent metal ion and B is a tetravalent one in the case of $BaTiO_3$ (Fig. 1.1). These ferroelectrics are cubic and nonpiezoelectric in the unpolarized state.

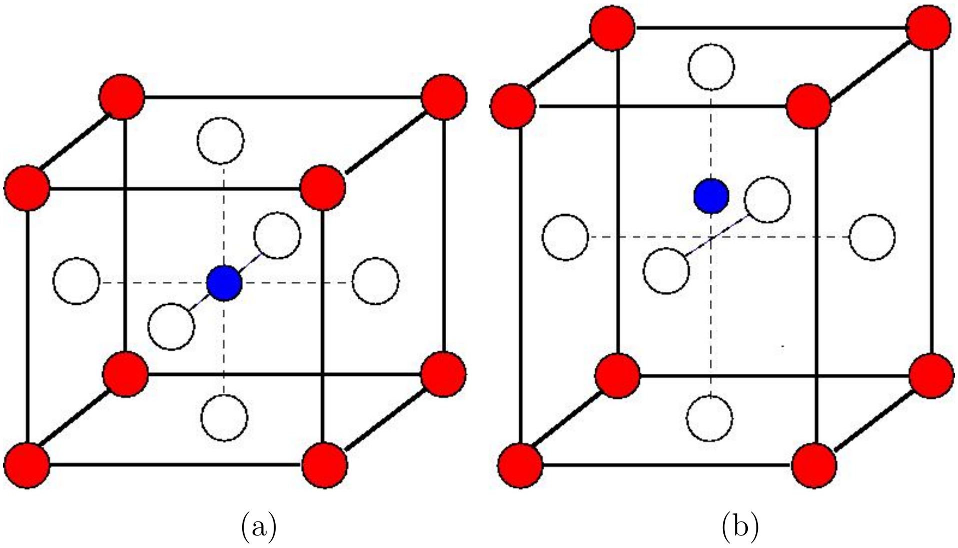
(a) (b)

Figure 1.1: (Color online) Perovskite-type structure ABO_3: cubic phase and tetragonal phase

1.1.3 Working principle

The ferroelectricity usually exists in a certain temperature range. Above certain temperature the ferroelectricity vanishes and the material becomes paraelectric. The temperature at which the paraelectric-ferroelectric phase transition takes place is called Curie temperature. Spontaneous polarization is the result of dipoles in the crystal and it reveals the self ordering of the system. In the phase transition theory, one introduces an order parameter to describe the ordering of the system. For ferroelectrics, the order parameter can be chosen as spontaneous polarization or total polarization.

One fundamental parameter to understand ferroelectrics is polarization, more exactly, how the spontaneous polarization takes place, how it is related to the crystal and electronic structure, and how the polarization states evolve under certain boundary and electric/mechanical loading conditions. The ferroelectric polarization is a polar vector. The configuration of the atoms in the lattice arrange themselves so that the positive and negative charges are displaced and an electric dipole comes into being. Only crystals that belong to certain point groups can possess spontaneous polarization.

Now a model of a hypothetical ferroelectric crystal is introduced in order to explain the essence of the ferroelectric phenomenon and the formation of domains. Here an extreme oversimplification is made for a two-dimensional crystal having the composition of AB comprising of only element

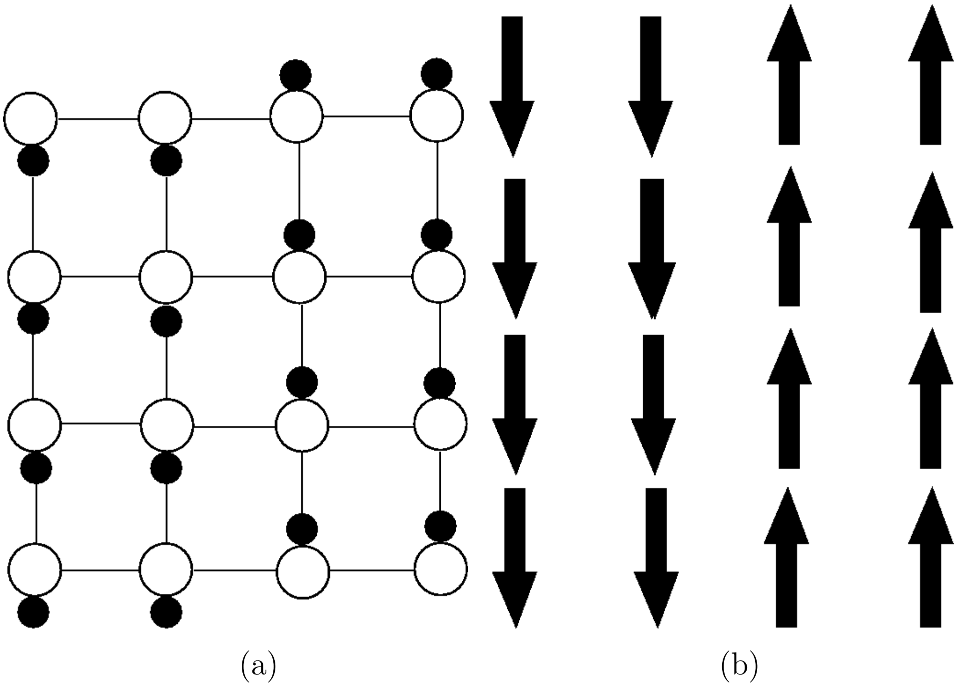

Figure 1.2: (Color online) Schematic structure of a fictitious ferroelectric crystal

A and B and has a structure as depicted in Fig. 1.2 (a). The A ions carry a negative charge and they are located on the lattice point of the lattice. The B ions carry the positive charge and they are located on the horizontal lines joining the A ions. In an equilibrium position, the B ions lie closer to one of the two adjacent A ions than to the other. There are two possible equilibrium positions for B, corresponding to the same minimum value of energy. If the necessary energy to overcome the energy barrier δE is supplied, the B ions can jump from one equilibrium position to the other, finding a new equilibrium position. A corresponding domain structure for the simplified case is illustrated in Fig. (1.2 (b)). The polarization is defined as the electric dipole moment, as will be shown later.

Alignment of the electric dipoles may extend only over a certain region of the crystal, while in another region the orientation of spontaneous polarization may be reversed. Such regions of uniform polarization are defined as domains and the regions between the domains are defined as domain walls. The energy of a domain wall is the difference between the systems before and after the domain wall was created. This value is defined as energy per unit wall area. The theoretical calculation of domain wall energy is very complicated and can also be solved only in special simple cases. Additionally, the problem of thickness of the domain wall needs to be considered. In the most anisotropic ferroelectrics, the direction of spontaneous polarization deviates little from the ferroelectric axis. The polarization vector will not change its orientation within the domain wall, but will decrease its magnitude to zero, and then increases in another direction on the other side.

A crystal belongs to the class ferroelectrics if it has spontaneous polarization which can be switched by an applied electric field. Many of the most common ferroelectric materials possess a perovskite lattice structure. A ferroelectric material is characterized by the fact that it can be switched from one spontaneous polarization state to another. In tetragonal case, either 90 degree or 180 degree switching takes place. Generally a uniform polarization in one direction can not be achieved because of the depolarization field. Rather the solid is divided into small polarized uniform zones. The polarization of the ferroelectrics evolves as the external electric field changes. Now the case is considered that there is a perfect insulated ferroelectric crystal with a uniform spontaneous polarization. The charge induced on the surfaces will give rise to a depolarizing electric field whose energy is proportional to the volume of the crystal and the square of the polarization. This results in a crystal that is subdivided into domains having antiparallel directions of spontaneous polarization. This is a more stable state of energy because it reduces the depolarizing electric field. The process proceeds and a certain amount of energy is stored in the domain walls. When the increase of overall wall energy balances the decrease in the depolarizing field energy, then an equilibrium configuration is reached at the considered temperature. An applied electric field gives rise to new domains or changes the size of existing domains. It can be seen from Fig. 1.3 that, as the electric field reaches the P_2 point, the crystal becomes a single domain one.

If an electric field is applied to the ferroelectric crystal, the domains in which the polarization is already oriented in the direction of the field will remain so aligned. Those in which the polarization is oriented different from the field show a tendency to reverse their orientation. This phenomenon of polarization reversal takes place by way of a nucleation process and domain wall motions. Again a simplified case is considered here. Suppose that the crystal is initially composite of positive and negative domains (e.g. domains oriented to the left and domains oriented to the right), which means that the overall polarization of the crystal is zero. First, a small electric field is applied in the positive direction, which causes the relationship between P and E to be linear. This is because the electric field is not large enough to reverse any of the domains, but their size may change. The ferroelectric behaves like a normal dielectric. If the electric field reaches a critical value, a number of the negative domains will switch over in the positive direction and the positive polarization will increase rapidly as shown by portion P_1P_2 in Fig. (1.3) until a state in which all the domains are aligned in the positive direction is reached. The crystal now consists of a single domain and this is a state of saturation (portion P_2P_3).

If the field strength is decreased, the polarization will not return to zero, but rather follow the path P_3P_4 of Fig. 1.3. When the field is reduced to zero, some of the domains will remain aligned in the positive direction and the ferroelectric exhibits a remnant polarization P_r (OP_4). The extrapolation of the linear portion P_2P_3 of the curve back to the polarization axis represents the spontaneous polarization P_s (OP_5). Thus, it is necessary to employ an electric field in the opposite direction to eliminate the overall polarization of the crystal. The electric field required

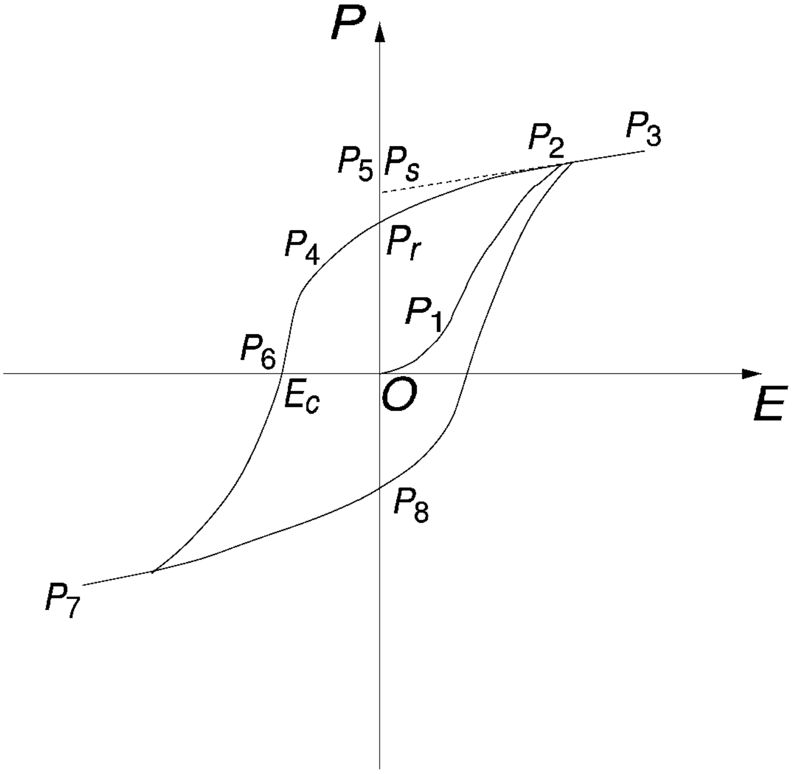

Figure 1.3: (Color online) Ferroelectric hysteresis loop.

to reduce P to zero(OP_6) is called the coercive field E_c. The alignment of the dipoles in this direction(P_6P_7) will be achieved if the electric field in this direction is further strengthened. By reversing the field again($P_7P_8P_3$), a cycle can be finished. A hysteresis loop($P_3P_4P_7P_8P_3$) can be depicted to represent the relationship between P and E.

However, it is assumed above that the crystals are perfect, which is not true in reality. The domain configuration observed in a given crystal is a result of compromise between the energetic requirements of a perfect crystal and perturbing effects of conductivity, strain and imperfections in a real crystal. The mentioned effect may proceed slowly with time, thus the observed domain configuration is a metastable state. Among those defects, oxygen vacancies are common ones in ferroelectric perovskites. They have relatively high mobility and interesting electrical properties. They are main factors for fatigue and aging in ferroelectrics, which is the main topic of the current study.

1.2 Fatigue and aging of ferroelectrics due to point defects

There has been a lot of interest in ferroelectric thin films and non-volatile memory applications. The decrease of switchable polarization, or polarization fatigue, which arises during working conditions, has severely hindered the better application of ferroelectric memories. A large amount of experimental data related to fatigue has been collected. It is believed that the fatigue is closely related to the existence of point defects in ferroelectrics.

$Pb(Zr, Ti)O_3$ and PZT capacitors with Pt electrodes are likely to be fatigued. Many works have reported on the degradation of the switchable polarization to occur between 10^4 and 10^7 cycles. The fatigue properties can be largely improved by applying conductive oxide electrodes [8, 9, 10]. Oxide electrodes can postpone the fatigue initiation up to 10^9-10^{12} cycles.

Some papers have plotted the switching polarization P_{sw} as a function of the logarithm of the number of polarization cycles N. Other functions like $P_{sw} = kN^{-1/4}$, $P_{sw} = k(aN + 1)^{-m}$ or $P_{sw} = A + k\exp(-aN)$ have also been suggested [11, 12]. It has also been reported that with the onset of the fatigued state that not only the remanent polarization is reduced, but the hysteresis loop shape is modified and the loop body is tilted as well. Many articles have addressed the effect of doping on fatigue endurance in ferroelectric thin film capacitors.

The typical change of the hysteresis loop shape induced by the initiation of the fatigued state comprises of a decrease of the remanent polarization. This is always accompanied with a tilt of the loop. If leakage degradation does not take place together with fatigue, the coercive field is almost not influenced by cyclic loading. In the case in which fatigue is accompanied by this sort of degradation, the shape of the hysteresis loops can be largely modified becoming rounded with increased magnitudes of E_c. In many articles [13, 14, 15, 16], examples of fatigue induced evolution of the hysteresis loops, which show those trends can be found.

Many articles have addressed the influence of doping on fatigue endurance in ferroelectric thin-film capacitors. Rather contradictory conclusions can be made from the publications for single element donor doping, e.g., for Nb doping, the results include an improvement [17],[18] or deterioration [19] with increasing dopant concentration. Doping with acceptor species such as Ce [15] and Fe [20] has been found to affect the fatigue resistance positively. It has been found that combined donor Nb, Ta-acceptor Sc, Mg, Zn doping may help improve fatigue endurance as well.

The DC conduction in both the room temperature thermoionic emission and low-temperature tunneling emission regimes and dielectric breakdown is substantially influenced by the polarization fatigue in Pt/PZT/Pt capacitors. According to recent publications the influence of fatigue on thermionic and tunneling emission are two-way: the thermionic emission is suppressed [21], whereas the tunneling emission is enhanced [22]. Investigation on constant-current breakdown in the Pt/PZT/Pt system has shown that the polarization fatigue leads to an appreciable reduction of the charge-to-breakdown [23]. It should by noted Scott et al. have shown that, for the case of conduction at room temperature a different trend, i.e., a rise of conduction at room temperature in fatigued Pt/PZT/Pt systems can be observed [24]. The study on modeling of fatigue and aging of ferroelectrics will be reviewed in Chapter 3.

1.3 Modeling of ferroelectrics

There are different models of ferroelectrics: sharp interface models, micromechanics models and phennomenological models.

Among the sharp interface models, Davi obtained a 3D continuum model for deformable ferroelectrics in the polarized phase characterized by the spontaneous polarization under the hypothesis that the domain walls are sharp interfaces [25]. Kessler and Balke treated the domain walls in a good approximation as sharp interfaces and specialized the general formulations for the driving force per unit area of the domain walls to domain walls in piezoelectric crystals [26]. Mueller et al. found that point defects have the ability to reduce the driving force on the domain wall where point defects are modelled as anisotropic centers of dilatation and the domain walls are modelled as sharp interfaces [27].

Bassiouny et al. first considered the multi-axial loading case. They introduced the Helmholtz free energy and used the yield surface in plasticity and work hardening as a source of reference. The theory described the initial polarization and the hysteresis loop under cyclic loading, but did not present the butterfly-loop [28, 29]. Based on the motion of domain walls, Huber et al. developed a micromechanical constitutive law, which is similar to crystal sliding [30]. Chen et al. develpoed a model which introduced volume fraction of domains as an internal variable, considering the interaction between crystals by a mean field method and obtained the behaviour of polycrystalline ferroelectrics [31]. Lu et al. conducted a study based on micromechanics and established a criterion taking into account the difference between the 90° switching and the 180° switching by a thermodynamic approach [32]. Shaikh et al. proposed a domain switching criterion for a generalized electromechanical loading based on an estimation of the existing domain switching criteria for ferroelectrics [33]. Kamlah and Tsakmakis constructed a phenomenological model of ferroelectricity for general loading histories [34]. Kamlah et al. also presented a complete phennomenological theory. They introduced several nonlinear functions to describe the switching behaviour and defined the domain switching driving forces for different loading cases [35]. McMeeking et al. presented a phenomenological theory. They defined the domain switching criterion similar to the yield surface in plasticity theory [36, 37]. Based on domain-switching mechanisms, Zhang et al. proposed a new domain-switching criterion [38].

As shown in the above, it is believed that the existence of point defects is one of the main factors that cause fatigue and aging in ferroelectrics. However, the mechanisms of the fatigue and aging introduced by the point defects are not totally known and are under debate. More studies are needed on this topic, especially on the domain structure level, to help the understanding of the material and to improve the design and widen the application range.

There have been sufficient studies on fatigue and aging in perovskite ferroelectrics. Dawber and Scott have given an analytic expression for fatigue the dependence of $P(N)$, the switched charge per unit area versus number of switching cycles in ferroelectric thin films [39]. Beale and Duiker postulated a model involving both the diffusion and trapping of charged defects. It was believed that the dendrites from opposite sides of the sample can grow together and this can cause the electrical shorting of the sample [40]. Duiker et al. presented a theoretical model of fatigue in thin-film ferroelectrics memories based on impact ionization, resulting in dendritic growth of oxygen-vacancy filaments. The model captures the experiment results well [41]. Brennan proposed a model based on the Landau theory, stating that fatigue in ferroelectrics is mainly due to the appearance of mesoscopic structures of interaction between charged lattice defects and opposing domains [42]. This explains the spatial orientation of the fatigue observed in bulk materials. Jiang et al. have reported on the arising of electric fatigue from the pinning of domains by space charges or injected carriers or from microcracking [43].

Based on a gradual domain switching model, Yu and Yu formulated a constitutive model for investigating the hysteresis behavior of ferroelectrics by radiation damage and fatigue. The influence of point defects and domain wall pinning by space charges are considered in the ferroelectric fatigue model [44]. Warren et al. found that that electronic charge trapping at domain walls can lock domain walls and lead to the suppression of the switchable polarization in perovskite thin films and the suppressed polarization can be recovered significantly to its initial value by injecting charge carriers into the material in several loading cases [45]. Du and Chen observed that injected electrons, together with oxygen vacancies, produced during cyclic loading, are proposed as the defects which are responsible for electric fatigue [46]. Yoo and Desu proposed a fatigue model for ferroelectric thin films on the basis of one-directional movement of defects due to asymmetric polarization under alternating pulses, defect trapping at electrode-ferroelectric interface, and the polarization loss at these surfaces due to structural change [47]. Portelles et al. explained the aging of this system by the existence of two different polar populations, fast aging polarized macroregions characterized by aging time t_1 and polar microregions associated with slow relaxing microstructures characterized by t_2 [48]. On the defect dipoles in ferroelectric perovskite, Poykko and Chadi have shown that oxygen-vacancy-platinum impurity pairs are tightly bound dipolar defects, which may cause a suppression of switchable polarization [49].

In a word, phase field models appear as an attractive model, particularly for the evolution of microstructure in inhomogeneous materials, e.g. domain structure evolution in ferroelectrics. However, there is very little phase field modeling for the study of fatigue and aging of ferroelectrics. It should be very promising, because the phase field model is able to depict the domain structure level behavior. It is posible to combine the phase field approach with the defect modeling in order to reveal the mechanisms of fatigue and aging, i.e., the exact roles of point defects in modifying the overall properties. This is the goal of this thesis.

1.4 Outline

In this thesis, a comprehensive study on how point defects can influence the overall properties in perovskite ferroelectrics will be conducted. The phase field and finite element simulations have been carried out to reveal different mechanisms of point defects. The model treats the spontaneous polarization as an order parameter and its evolution obeys the Landau-Ginzburg equation. For the influence of point defects depending on what hypotheses are made, two models are put forward: the defect dipole model and the space charge model. The first model assumes that the oxygen vacancy on a face of the perovskite unit cell can be associated with the impurity cation and they form an electric dipole. An internal electric field will arise due to the defect dipole and this is supposed to have an influence on the self organization of the spontaneous polarization. The latter assumes that ferroelectrics are semiconductors with space charges due to donors and electronic charge carriers. One aims to investigate using the models how point defects can modify the overall behaviour of ferroelectrics.

The rest of the thesis is organized as follows. Therefore, in Chapter 2 the basics of continuum mechanics are introduced. One starts from the case of large deformation, and it is restricted to the infinitesimal strain case which is valid for perovskite ferroelectric solids. And after introducing the basic concepts of electromagnetism, one moves to the continuum theory for electromechanical solids which serve as prerequisite for the phase field model of ferroelectrics. Relevant balance laws and thermodynamics are referred to. After that, electric Gibbs energy is chosen as the initial point of the modeling and corresponding variational formulation is made which enable us to solve the physical problem in an approximating approach by discretizing the geometry of the problem, i. e. the finite element method.

In Chapter 3, based on the balance equations of microforce by Gurtin, the Landau-Ginzburg equation is derived in a thermodynamically consistent way. The phase field model for tetragonal ferroelectrics is then established, by which a kinematic description of domain switching in ferroelectric solids is obtained. The physical meaning and the values of the parameters are shown. The following chapter discusses the implementation of the phase field model. The domain structure evolution concerns the change of material microstructure, therefore it should be referred to as change in 'initial configuration', therefore the concept 'configurational force' is the suitable tool to depict this change. The configurational force and moment for the case of infinitesimal elasticity, piezoelectricity and the phase field model for ferroelectrics will be derived, respectively.

Chapter 4 is dedicated to semiconducting feature in ferroelectrics. Significant effect of semiconductor properties on domain configurations in ferroelectrics is demonstrated, especially for doped ones. Phase field simulations are performed for ferroelectrics with space charges due to donors and electronic charge carriers. It is shown that the free charges introduced act as a source for charge compensation at domain walls with uncompensated polarization bound charges. Results show that the equilibrium position of a domain wall with respect to its rotation in a head-to-head or a tail-to-tail domain configuration depends on the charge defect concentration and the Fermi level position.

In Chapter 5, the conductivity of head-to-head and tail-to-tail domain walls are studied.

In Chapter 6, one deals with the polarization switching behavior of aged ferroelectrics with the presence of point defects by a phase field model. In the model, the defect dipole formed by oxygen vacancy and the neighboring impurity cation is incorporated. Two typical domain configurations, i.e., rank-1 and rank-2 domain configurations, are taken as the initial domain configuration in the simulation. The so-called memory effect and the increase of the coercive field caused by the defect dipoles are predicted, and a double hysteresis loop is reproduced. This provides an insight into the role of point defects in modifying the overall properties of ferroelectrics. In Chapter 7, it is also shown that, at higher temperature, switching of defect dipoles becomes more significant due to switching of spontaneous polarization by applying a cyclic electric field, and aged ferroelectric samples can be deaged.

A summary and outlook on possible future work on those topics will be discussed in Chapter 8.

In the appendix, details on numerical implementation, codes and etc are given.

Chapter 2

Electromechanics in continua

This thesis aims to discuss the phase field study of ferroelectrics with point defects. Phase field models are developed in the context of continuum theory. Ferroelectrics are continua which have coupling effects of mechanics and electrostatics. Some basics of continuum mechanics and electrostatics from the continuum point of view are introduced.

2.1 Basics of continuum mechanics

Continuum mechanics is the subject which deals with the motion and deformation of continuous materials under certain boundary conditions. This branch of science treats materials as continua and disregards the microstructures. People also have attempted to include many physical phenomena (e.g. dislocation glide, phase transition, chemical reaction, electromagnetic effect, damage, etc) into the continuum model, even many of those essentially take place on a microscopic level and this subject has been extended into a broader one: continuum physics. There are many textbooks on classical continuum mechanics. The book by Malvern provides a unified presentation of the concepts and general principles common to all branches of solid and fluid mechanics [50]. The book by Holzaplfel provides a comprehensive approach and includes vital information on variational principles constituting the cornerstone of the finite element method [51]. Liu focuses on representations of tensor functions, material symmetry and thermodynamics in his book [52]. The book by Bonet and Wood considers nonlinear geometrical behaviour and nonlinear hyperelastic materials, and the numerics needed to model such phenomena [53]. Other books include Ogden [54], Haupt [55] and Tsakmakis [56]. Interested readers can refer to those

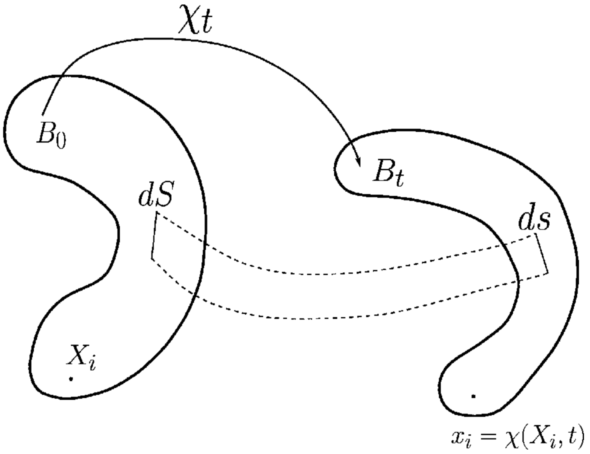

Figure 2.1: (Color online) Mapping between The reference body B_0 and the deformed body B_t.

books.

2.1.1 Deformation

In continuum mechanics, the bodies are usually considered to be existing in a Euclidean space E^3. A material body can occupy different space regions at different times. As one wishes, one can denote one of them as reference configuration B_0 and a point $X_i \in B_0 (i = 1, 2, 3)$ as a material point. Then a motion of the material body is defined as a smooth mapping from the reference configuration to a current configuration which resides at time point t (Fig. 2.1),

$$x_i = \phi_i(X_j, t), \tag{2.1}$$

where X_i and x_i stand for coordinates in reference configuration and current configuration, respectively. The tensor field

$$F_{ij} = \frac{\partial x_i}{\partial X_j} \tag{2.2}$$

is defined as the deformation gradient. As a measure of deformation, strain is defined to be able to give the change in length between two neighboring material points with infinitesimal distance. If the vector between the two points in the reference configuration and current configuration are dX_i and dx_i. Then the squared distance in the two configurations is

$$dS^2 = dX_i dX_i, \quad ds^2 = dx_i dx_i. \tag{2.3}$$

By using the relationship $dx_j = F_{ij} dX_j$, one can write the squared distance in current configuration in terms of coordinates in reference configuration,

$$ds^2 = dx_i dx_i = F_{ij} dX_j F_{ik} dX_k = dX_i F_{ki} F_{kj} dX_j. \tag{2.4}$$

Then one writes the difference of the squared distance between the reference configuration and current configuration as

$$ds^2 - dS^2 = dX_i(F_{ki}F_{kj} - \delta_{ij})dX_j = dX_i 2E_{ij}dX_j, \tag{2.5}$$

where $E_{ij} = \frac{1}{2}(F_{ki}F_{kj} - \delta_{ij})$, which is the Green-Lagrange strain tensor. If the displacement gradient tensor is defined as

$$H_{ij} = \frac{\partial(x_i - X_i)}{\partial X_j} = F_{ij} - \delta_{ij} = \frac{\partial u_i}{\partial X_j}. \tag{2.6}$$

Then the Green-Lagrange strain tensor becomes

$$E_{ij} = \frac{1}{2}((H_{ki} + \delta_{ki})(H_{kj} + \delta_{kj}) - \delta_{ij}) = \frac{1}{2}(H_{ij} + H_{ji} + H_{ki}H_{kj}). \tag{2.7}$$

In the case $\|H_{ij}\| \ll 1$ it may be said that the deformation is an infinitesimal and the Green-Lagrange strain tensor can be approximated by an infinitesimal strain tensor,

$$E_{ij} \approx \varepsilon_{ij} = \frac{1}{2}(H_{ij} + H_{ji}). \tag{2.8}$$

It can be seen that the infinitesimal tensor is a symmetric one.

2.1.2 Balance principles

In continuum mechanics, both the free energy and the second Piola-Kirchhoff stress tensor are functions of the deformation gradient,

$$\psi = \psi(F_{ij}), \quad S_{ij} = S_{ij}(F_{kl}). \tag{2.9}$$

It is known that the second Piola-Kirchhoff stress tensor is derived as,

$$S_{ij} = 2\frac{\partial\bar{\psi}(C_{ij})}{\partial C_{ij}}. \tag{2.10}$$

As one knows, the unstrained configuration yields no stress,

$$S_{ij}(F_{kl})|_{F_{kl}=\delta_{kl}} = 0. \tag{2.11}$$

The derivation is now calculated and the value in the vicinity of unstrained state is obtained,

$$\frac{\partial S_{ij}}{\partial(\frac{1}{2}C_{kl})}|_{F_{kl}=\delta_{kl}} = \mathbb{C}_{ijkl}. \tag{2.12}$$

The tensor $\mathbb{C}_{ijkl}$ is defined as the stiffness tensor. By using the Taylor expansion of S_{ij} around the unstrained state, one has

$$S_{ij}(C_{kl}) = \frac{1}{2}\mathbb{C}_{ijkl}(C_{kl} - \delta_{kl}) + h.o.t. = \mathbb{C}_{ijkl}E_{kl} + h.o.t.. \tag{2.13}$$

In small strain case, one has $E_{ij} \approx \varepsilon_{ij}, S_{ij} \approx \sigma_{ij}$, therefore,

$$\sigma_{ij} = \mathbb{C}_{ijkl}\varepsilon_{kl}, \tag{2.14}$$

which is the constitutive relationship for infinitesimal elasticity. The following study is restricted to only infinitesimal elasticity, since common perovskite ceramics can not undergo large deformation. The balance law for linear momentum reads

$$\int_{\partial B_t} \sigma_{ij} n_j dA + \int_{B_t} f_i dV = 0. \tag{2.15}$$

And for angular momentum,

$$\int_{\partial B_t} \epsilon_{jki} x_j \sigma_{kl} n_l dA + \int_{B_t} \epsilon_{jki} x_j f_k dV = 0. \tag{2.16}$$

From Eq.(2.15), using divergence theorem, one has

$$\int_{B_t} \sigma_{ij,j} dV + \int_{B_t} f_i dV = 0, \tag{2.17}$$

$$\sigma_{ij,j} + f_i = 0. \tag{2.18}$$

From Eq.(2.16), also using divergence theorem, one has

$$\begin{aligned}
\int_{B_t} \frac{\partial}{\partial x_l}(\epsilon_{jki} x_j \sigma_{kl}) dV + \int_{B_t} \epsilon_{jki} x_j f_k dV = 0, \\
\int_{B_t} \epsilon_{jki}(x_{j,l}\sigma_{kl} + x_j \sigma_{kl,l}) dV + \int_{B_t} \epsilon_{jki} x_j f_k dV = 0, \\
\int_{B_t} \epsilon_{jki} x_{j,l} \sigma_{kl} dV + \int_{B_t} \epsilon_{jki} x_j (f_k + \sigma_{kl,l}) dV = 0.
\end{aligned} \tag{2.19}$$

After using Eq.(2.18) and $x_{i,j} = \delta_{ij}$, there is

$$\epsilon_{jki}\delta_{jl}\sigma_{kl} = 0. \tag{2.20}$$

After using the substituting property of δ_{jl} and multiplying the whole with ϵ_{mni}, this yields

$$\epsilon_{mni}\epsilon_{lki}\sigma_{kl} = 0. \tag{2.21}$$

Using the relationship $\epsilon_{mni}\epsilon_{lki} = \delta_{ml}\delta_{nk} - \delta_{mk}\delta_{nl}$, this becomes

$$\begin{aligned}
(\delta_{ml}\delta_{nk} - \delta_{mk}\delta_{nl})\sigma_{kl} = 0, \\
\delta_{ml}\delta_{nk}\sigma_{kl} = \delta_{mk}\delta_{nl}\sigma_{kl}, \\
\sigma_{nm} = \sigma_{mn}.
\end{aligned} \tag{2.22}$$

Therefore in the case without distributed volume torque the Cauchy stress tensor σ_{ij} is symmetric. Since the infinitesimal strain tensor is also symmetric $\varepsilon_{ij} = \varepsilon_{ji}$ and the strain energy is a positive definite square function of strain, the stiffness tensor does not only have main symmetry, but also have secondary symmetry. That is: $C_{ijkl} = C_{klij} = C_{jikl} = C_{ijlk}$.

2.2 Basics of electrostatics

2.2.1 Electric charge and electric field

There are two kinds of electric charges, positive and negative. Experiments show that charges of the same kind reject each other, whereas those of the opposite kind attract each other. One calls this Coulomb's law, which reads

$$F_i^{1\to2} = \frac{1}{4\pi\epsilon_0}\frac{q_1q_2}{\|r_i^{1\to2}\|^3}r_i^{1\to2}, \tag{2.23}$$

where $r_i^{1\to2}$ is the position vector pointing from charge q_1 to charge q_2, ϵ_0 is the vacuum permittivity and $F_i^{1\to2}$ is the force that q_1 acts on q_2. The electric charge is one of the basic properties of matter. The smallest unit of charge is that of one electron: $q_e = 1.602\times10^{-19}C$. The electric field is defined as the the force acting on a positive unit electric charge in that electric field,

$$E_i = F_i/q_e. \tag{2.24}$$

It is known that the electric force is a conservative force: the work done by an electric field to a charge to move it along a close path $\boldsymbol{p}$ is zero,

$$\mathcal{W} = \oint_{\boldsymbol{p}} E_i dS_i = 0. \tag{2.25}$$

That is, the electrostatic field is a conservative field. One can divide the path $\boldsymbol{p}$ into two parts $\boldsymbol{p} = \boldsymbol{p_1}\bigcup\boldsymbol{p_2} = (\boldsymbol{x}_0 \to \boldsymbol{x})_1 \bigcup (\boldsymbol{x} \to \boldsymbol{x}_0)_2$,

$$\mathcal{W} = \int_{(\boldsymbol{x}_0\to\boldsymbol{x})_1} E_i dS_i + \int_{(\boldsymbol{x}\to\boldsymbol{x}_0)_2} E_i dS_i = 0. \tag{2.26}$$

Therefore,

$$\int_{(\boldsymbol{x}_0\to\boldsymbol{x})_1} E_i dS_i = -\int_{(\boldsymbol{x}\to\boldsymbol{x}_0)_2} E_i dS_i = \int_{(\boldsymbol{x}_0\to\boldsymbol{x})_2} E_i dS_i. \tag{2.27}$$

It is seen that the work done to one Coulomb charge from $\boldsymbol{x}_1$ to $\boldsymbol{x}_2$ in an electric field does not depend on the path. One defines this integration as electric potential,

$$\phi = -\int_{(\boldsymbol{x}_0\to\boldsymbol{x})} E_i dS_i. \tag{2.28}$$

In most of the cases, the reference point is chosen to be infinity. It can be seen that the electric field can be obtained by taking the negative gradient of the electric potential,

$$E_i = -\frac{\partial\phi}{\partial x_i}. \tag{2.29}$$

2.2.2 Electric moment

Now two point charges which are displaced from each other by a distance s_i are considered. This pair of point charges is defined as an electric dipole and the notion of electric moment should be introduced to describe it. Think of a negative point charge located at x_i and a positive point charge located at $x_i + s_i$, then one can define the electric moment of the pair as

$$p_i = e(x_i + s_i) - ex_i = es_i. \tag{2.30}$$

2.2.3 Microscopic electric field and electric force

The section provides a simple introduction on microscopic theory of electric field. One can refer to relevant monographs for more details [57, 58]. The whole system is divided into some composite particles which again are made from positive and negative particles (Fig. 2.2). The microscopic electric field E_i^{micro} at x_i by a number point charges can be obtained by the Maxwell-Lorentz equation,

$$E_{k,k}^{micro} = \sum_r q^r \delta(x_i^r - x_i). \tag{2.31}$$

The electric force F^s on a point particle with charge e^s at position x^s is

$$F_k^s = e^s E_k^{tot}(x_i^s). \tag{2.32}$$

The total electric field is a superposition of external electric field and field generated by all the other point charges in the solid,

$$E_i^{tot}(x_k^s) = E_i^{ext}(x_k^s) + \sum_{t \neq s} E_i^t(x_k^s) = E_i^{ext}(x_k^s) + \sum_{t \neq s} \frac{1}{4\pi\epsilon_0} \frac{e^t}{\|x_i^t - x_i^s\|^2}(x_i^t - x_i^s). \tag{2.33}$$

Then the electric force is

$$F_i^s = e^s E_i^{ext}(x_k^s) + \sum_{t \neq s} \frac{1}{4\pi\epsilon_0} \frac{e^t e^s}{\|x_i^t - x_i^s\|^2}(x_i^t - x_i^s). \tag{2.34}$$

Now one considers a dielectric solid which comprises of unit cells. Those unit cells are made up of many particle charges. If the mass center of the sth unit cell is x_i^s, and the position vector of the tth charge of the sth unit cell is $x_i^{st} = x_i^s + r_i^{st}$. Since it is known that r^{st} is of the order of unit cell size so that one has $r^{st} \ll r^s$, in this system the Maxwell-Lorentz equation is written as

$$E_{k,k}^{micro} = \sum_{s,t} q^{st} \delta(x_i^s + r_i^{st} - x_i). \tag{2.35}$$

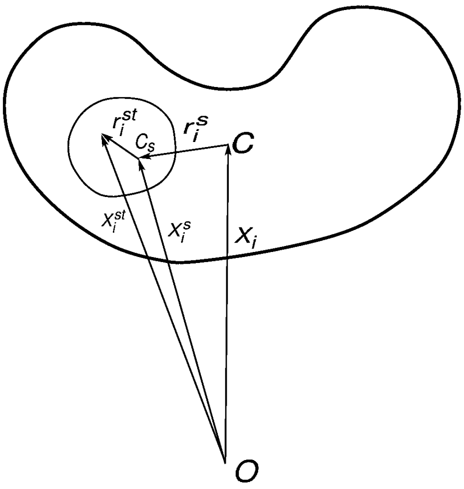

Figure 2.2: (Color online) Set of particles with charges

The right hand side may be expanded into a Taylor expansion,

$$E^{micro}_{k,k} = \sum_{s,t} q^{st}[\delta(x_i^s - x_i) - \frac{\partial}{\partial x_i}\delta(x_i^s - x_i) r_i^{st} + \frac{\partial^2}{\partial x_i^2}\delta(x_i^s - x_i)(r_i^{st})^2 - h.o.t.]. \tag{2.36}$$

If one neglects higher order terms (multiple moment) and writes $q = \sum_{s,t} q^{st}\delta(x_i^s - x_i)$ and $P_i^{micro} = \sum_{s,t} q^{st} r_i^{st}\delta(x_i^s - x_i)$, one has

$$E^{micro}_{i,i} = q - P^{micro}_{i,i}. \tag{2.37}$$

2.2.4 Power of electric force

Now one considers only power of external field and the interaction between particles in attributed into the internal free energy. The power of external field on a unit cell is the sum of power over all particles,

$$\mathcal{W}_e = \sum_{s,t} q^{st} E_i^{ext}(x_i^{st}, t)\dot{x}_i^{st}. \tag{2.38}$$

The electric field may be written into a Taylor expansion, so that there is

$$\mathcal{W}_e = \sum_{s,t} q^{st}[E_i^{ext}(x_i^s, t) + r_j^{st} E_{i,j}^{ext}(x_i^s, t)](\dot{x}_i^s + \dot{r}_i^{st}). \tag{2.39}$$

After expanding them,

$$\begin{aligned}\mathcal{W}_e = \sum_{s,t} q^{st} E_i^{ext}(x_i^s,t)\dot{x}_i^s + \sum_{s,t} q^{st} E_i^{ext}(x_i^s,t)\dot{r}_i^{st} + \sum_{s,t} q^{st} r_j^{st} E_{i,j}^{ext}(x_i^s,t)(\dot{x}_i^s + \dot{r}_i^{st}) \\ = \sum_s (\sum_t q^{st}) E_i^{ext}(x_i^s,t)\dot{x}_i^s + \sum_s (\sum_t q^{st}\dot{r}_i^{st}) E_i^{ext}(x_i^s,t) + \sum_s (\sum_t q^{st} r_j^{st}) E_{i,j}^{ext}(x_i^s,t)\dot{x}_i^s \\ = q^s \dot{x}_i^s E_i^{ext}(x_i^s,t) + \dot{x}_i^s E_{i,j}^{ext}(x_i^s,t) p_i^s + \dot{p}_i^s E_i^{ext}(x_i^s,t).\end{aligned} \tag{2.40}$$

For a stationary frame one has

$$W^{ext} = qE_i v_i + P_j E_{i,j} v_i + E_i \dot{P}_i. \tag{2.41}$$

For a quasi-static case, only the third term on the right side remains.

2.2.5 Electric displacement

One rearranges Eq.(2.37) and defines $D_i^{micro} = E_i^{micro} + P_i^{micro}$,

$$\begin{aligned} E_{i,i}^{micro} + P_{i,i}^{micro} &= q, \\ D_{i,i}^{micro} &= q. \end{aligned} \tag{2.42}$$

D_i^{micro} is called microscopic electric displacement. After averaging the equation over volume, one has

$$D_{i,i} = \rho_e, \tag{2.43}$$

which is called the Gauss law. In dielectrics the electric field causes the bound charges in the material to slightly separate, inducing a local electric dipole moment. The electric displacement field D_i is defined as

$$D_i = \epsilon_0 E_i + P_i^{rev} + P_i^{irr}. \tag{2.44}$$

In which the P_i^{rev} comprises of dielectric and piezoelectric contribution and P_i^{irr} is the spontaneous polarization,

$$\begin{aligned} P_i^{rev} &= \epsilon_0 \chi_{ij} E_j + e_{ijk}\varepsilon_{jk}, \\ P_i^{irr} &= P_i^s. \end{aligned} \tag{2.45}$$

The susceptibility is related to permittivity in the way

$$\chi_{ij} = \epsilon_{ij}^r - \delta_{ij}. \tag{2.46}$$

Therefore, the electric displacement can also be written as

$$\begin{aligned} D_i &= \epsilon_0 E_i + \epsilon_0(\epsilon_{ij}^r - \delta_{ij})E_j + e_{ijk}\varepsilon_{jk} + P_i^s \\ &= \epsilon_0 \epsilon_{ij}^r E_j + e_{ijk}\varepsilon_{jk} + P_i^s = A_{ij}E_j + e_{ijk}\varepsilon_{jk} + P_i^s. \end{aligned} \tag{2.47}$$

2.2.6 Energy in static electric field

In this section one talks about the energy of solids in a static electric field, then one can go further to the topic of thermodynamics and balance laws. Recall that the electric potential at x_i generated by a point charge q' at position x'_i is

$$\phi = \frac{1}{4\pi\epsilon_0}\frac{q'}{\|x_i - x'_i\|}. \tag{2.48}$$

The work needed to be done to move an electric charge q_b from infinity to position x_i^b in the electric field generated by q_a at x_i^a is

$$W = \frac{1}{4\pi\epsilon_0}\frac{q_a q_b}{\|x_i^a - x_i^b\|}. \tag{2.49}$$

Then for many particles, there is

$$W = \frac{1}{2}\frac{1}{4\pi\epsilon_0}\sum_{k=1}^{N}\sum_{l=1}^{N}\frac{q_k q_l}{\|x_i^k - x_i^l\|} \quad (k \neq l). \tag{2.50}$$

There is a factor of 1/2 because, for each pair of charges, the work has been counted twice. Since the elecrtric potential at x_i^l is the superposition of elecrtric potential of all the other particles,

$$\phi(x_i^l) = \frac{1}{4\pi\epsilon_0}\sum_{k=1}^{N}\frac{q_k}{\|x_i^k - x_i^l\|} \quad (k \neq l). \tag{2.51}$$

The total energy can therefore be written as

$$W = \sum_{l=1}^{N} q_l \phi(x_i^l). \tag{2.52}$$

If the particles are considered as a continuum, the total energy can be written into an integral,

$$\mathcal{W} = \int \rho\phi(x_i)dV(x_i), \tag{2.53}$$

in which,

$$\phi(x_i) = \frac{1}{4\pi\epsilon_0}\int\frac{\rho(x'_i)}{\|x_i - x'_i\|}dV(x'_i). \tag{2.54}$$

Since it is known that,

$$\rho = D_{i,i}. \tag{2.55}$$

The variation of the energy then can be written into

$$\delta\mathcal{W} = \int_\Omega \delta D_{i,i}\phi dV = \int_\Omega (\delta D_i\phi)_{,i} - \delta D_i\phi_{,i}dV = \int_{\partial\Omega}\delta D_i\phi n_i dA + \int_\Omega \delta D_i E_i dV. \tag{2.56}$$

Therefore the energy in dielectrics is obtained.

2.3 Thermodynamics

As one studies a problem of thermodynamics, one usually call the objects studied a system, and the objects around it: the environment. The parameters used to describe the state of the system are called state parameters, like density ρ, temperature T, entropy s, electric displacement D_i, etc. According to thermodynamics, a characteristic function can determine the properties of equilibrium uniquely. The attitude of homogeneous elastic dielectrics can be characterized by temperature T, entropy S, strain ε_{ij}, stress σ_{ij}, electric field E_i and electric displacement D_i. Mostly the differential of the function is used. According to the first law of thermodynamics, the change of the total internal energy is

$$dU = dQ + dW, \tag{2.57}$$

where dQ is the heat the system absorbs, dW is the work done to the system. For elastic dielectrics, the work comprise of mechanical and eletrostatic work,

$$dW = \sigma_{ij} d\varepsilon_{ij} + E_i dD_i. \tag{2.58}$$

For reversible processes one has

$$dQ = TdS. \tag{2.59}$$

Therefore the change of internal energy is

$$dU = TdS + \sigma_{ij} d\varepsilon_{ij} + E_i dD_i. \tag{2.60}$$

After introducing the electrical enthalpy, one has

$$H = U - E_i D_i, \tag{2.61}$$

$$dH = dU - d(E_i D_i) = TdS + \sigma_{ij} d\varepsilon_{ij} + E_i dD_i - E_i dD_i - D_i dE_i = TdS + \sigma_{ij} d\varepsilon_{ij} - D_i dE_i. \tag{2.62}$$

For more details about thermodynamic characteristic functions, please refer to Appendix A.

2.4 Electromechanics

This section deals with the electromechanics of continua and focuses on dielectrics. Energy balance is formulated for an infinitesimal deformable dielectrics which is necessary for describing the constitutive behavior of the system. In the second section the basics of physics of semiconducting solids is introduced.

2.4.1 Balance laws in dielectric media

One aims to derive balance laws in electromechanical media. The conservation of mass is

$$\frac{d}{dt}\int_{B_t}\rho dV = 0. \tag{2.63}$$

The conservation of linear momentum is

$$\int_{B_t} f_i dV + \int_{\partial B_t} t_i dA = \frac{d}{dt}\int_{B_t}\rho v_i dV. \tag{2.64}$$

And the conservation of angular momentum,

$$\int_{B_t}\epsilon_{ijk}x_i f_j dV + \int_{\partial B_t}\epsilon_{ijk}x_i t_j dA = \frac{d}{dt}\int_{B_t}\rho\epsilon_{ijk}x_i v_j dV. \tag{2.65}$$

It follows that the sum of Cauchy stress and Maxwell stress is symmetric,

$$\sigma_{ij} + \sigma^m_{ij} = \sigma_{ji} + \sigma^m_{ji}. \tag{2.66}$$

the rate of external work to the system is

$$\frac{dW}{dt} = \int_{B_t} f_i v_i dV + \int_{\partial B_t} t_i v_i dA + \int_{B_t}\phi\frac{d}{dt}(qdV) + \int_{\partial B_t}\phi\frac{d}{dt}(\omega dS). \tag{2.67}$$

After making use of material time derivatives of field variables in volume and surface elements, the balance of linear momentum and divergence theorem, the equation is transformed into

$$\frac{dW}{dt} = \int_{B_t}[E_i\frac{dD_i}{dt} + (\sigma_{ij} + \sigma^M_{ij} - E_i D_j + E_k D_k\delta_{ij})\frac{\partial v_i}{\partial x_j} + \rho\frac{dv_i}{dt}v_i]dV. \tag{2.68}$$

According to the first law of thermodynamics, one has

$$\frac{dU}{dt} = \frac{dW}{dt} + \frac{dQ}{dt}. \tag{2.69}$$

The rate of change of internal energy and heat transfer are written as

$$\frac{dU}{dt} = \frac{d}{dt}\int_{B_t} udV + \frac{d}{dt}\int_{B_t}\frac{1}{2}\kappa_0 E_i E_i dV + \frac{d}{dt}\int_{B_t}\frac{1}{2}\rho v_i v_i dV, \tag{2.70}$$

$$\frac{dQ}{dt} = \int_{B_t}\dot{r}dV - \int_{\partial B_t} q_i n_i dS. \tag{2.71}$$

Based on Eq. (2.68-2.70), one gets a local form of first law of thermodynamics,

$$\frac{dU}{dt} = (\sigma_{ij} + \sigma^M_{ij} - E_i P_j + E_k P_k\delta_{ij})\frac{\partial v_i}{\partial x_j} + E_i\frac{dP_i}{dt} + \dot{r} - \frac{\partial q_i}{\partial x_i}. \tag{2.72}$$

The second law of thermodynamics says

$$\frac{d}{dt}\int_{B_t} sdV \geqslant \int_{B_t} \frac{\dot{r}}{T}dV - \int_{\partial B_t} \frac{q_i n_i}{T}dS. \tag{2.73}$$

If one defines the Helmholtz energy per unit volume,

$$\psi = U - Ts. \tag{2.74}$$

Then one has

$$\frac{d\psi}{dt} = \frac{dU}{dt} - \frac{dT}{dt}s - T\frac{ds}{dt}. \tag{2.75}$$

After combining the equations in the above, it follows,

$$\frac{du}{dt} = (\sigma_{ij} + \sigma_{ij}^M - E_i P_j + E_k P_k \delta_{ij})\frac{\partial v_i}{\partial x_j} + E_i \frac{dP_i}{dt} - s\frac{dT}{dt} - \frac{d\psi}{dt} - \frac{q_i}{T}\frac{\partial T}{\partial x_i} \leqslant 0. \tag{2.76}$$

Since the Helmholtz free energy is expressed as $\psi = \psi(\varepsilon_{ij}, P_i, T)$, one has

$$\frac{d\psi}{dt} = \frac{\partial \psi}{\partial \varepsilon_{ij}}\frac{d\varepsilon_{ij}}{dt} + \frac{\partial \psi}{\partial P_i}\frac{dP_i}{dt} + \frac{\partial \psi}{\partial T}\frac{dT}{dt}. \tag{2.77}$$

Then the equation can be modified into

$$(\sigma_{ij} + \sigma_{ij}^M - E_i P_j + E_k P_k \delta_{ij} - \frac{\partial \psi}{\partial \varepsilon_{ij}})\frac{dv_i}{dx_j} + (E_i - \frac{\partial \psi}{\partial P_i})\frac{dP_i}{dt} - (s + \frac{\partial \psi}{\partial T})\frac{\partial T}{\partial t} - \frac{q_i}{T}\frac{\partial T}{\partial x_i} \leqslant 0. \tag{2.78}$$

After Legendre transformation, one gets the electric enthalpy,

$$H = \psi - D_i E_i. \tag{2.79}$$

Then Eq.(2.76) becomes

$$(\sigma_{ij} + \sigma_{ij}^m - E_i P_j + E_k P_k \delta_{ij}) - \frac{\partial H}{\partial \varepsilon_{ij}})\frac{d\varepsilon_{ij}}{dt} + (D_i - \frac{\partial H}{\partial E_i})\frac{dE_i}{dt} - (s + \frac{\partial H}{\partial T})\frac{\partial T}{\partial t} - \frac{q_i}{T}\frac{\partial T}{\partial x_i} \leqslant 0. \tag{2.80}$$

An estimation has been made that the Maxwell stress is much smaller than the Cauchy stress and the electrostatic force can be neglected under regular conditions [35], i.e.,

$$f_i^m = 0, m_{ij} = 0, \|\sigma_{ij}^m\| = 0. \tag{2.81}$$

If one limits to isothermal processes, Eq.(2.80) further becomes

$$(\sigma_{ij} - \frac{\partial H}{\partial \varepsilon_{ij}})\frac{d\varepsilon_{ij}}{dt} + (D_i - \frac{\partial H}{\partial E_i})\frac{dE_i}{dt} \leqslant 0. \tag{2.82}$$

Then the equations can be simplified,

$$\begin{aligned} \sigma_{ij,j} + f_i = 0, \\ \sigma_{ij} = \sigma_{ji}, \\ D_{i,i} - \rho = 0, \\ \varepsilon_{ij} = \frac{1}{2}(H_{ij} + H_{ji}). \\ E_i = -\phi_{,i}. \end{aligned} \tag{2.83}$$

Then one can get the corresponding quantities after taking the derivative of the energy funtional with respect to the conjugate field variables,

$$\sigma_{ij} = \frac{\partial H}{\partial \varepsilon_{ij}}, D_i = -\frac{\partial H}{\partial E_i}. \tag{2.84}$$

2.4.2 Features of semiconducting solids

This section aims to give a very fundamental introduction on semiconducting solids. For more thorough explanation, one can refer to Sze's book [59]. Metals and insulators are different mainly because valence band is totally filled and the conducting band is totally empty. On the other hand, in metal at least one band is partially filled. One important characteristic measure of an insulator is the energy band gap E_g, which is the energy difference between the highest filled band and the bottom of the lowest empty band. In a case where the temperature is not zero, some of electrons can jump across the band gap into the conducting band, leaving behind unoccupied levels in the valence band. Those materials whose band gaps are not so wide that, below the melting temperature enough electrons can be thermally exited into the conducting band and conductivity can be observed are categorized as semiconductors. At 0K, the valence band is totally filled and the conduction band is totally empty. At this time the solid can not transfer electric current. The energy of electrons in the valence band increases as the temperature rises and those electrons can be stimulated into the conduction band at a higher temperature. Therefore empty levels appear in the valence band which are called electron holes. Those electrons and holes are not caused by material doping or lattice defects and take place only in pure ion lattices. Therefore, the concentration of holes is exactly the same as that of electrons. The quasi-free electrons in the conduction band and the holes in the valence band can move under an electric field and make the crystal conductive. The direction of motion of the electrons and holes is opposite to each other.

The equilibrium of the spontaneous appearance of electrons and holes depends on the electron distribution on the permitted energy levels and it obeys the Fermi distribution. The number of eletrons which have energy E_i is

$$N_i = \frac{g_i}{1 + exp(\frac{E_i - E_f}{k_B T})}. \tag{2.85}$$

In the case $\frac{E_i - E_f}{k_B T} \gg 1$ the last equation can be approximated as

$$N_i = g_i exp(\frac{E_f - E_i}{k_B T}). \tag{2.86}$$

The number of electrons can be obtained by integrating the product of the number of states of certain energy level and corresponding occupancy,

$$n = \int_{E_C}^{\infty} N(E)F(E)dE. \tag{2.87}$$

where the density of states $N(E)$ is approximated by

$$N(E) = M_C \frac{\sqrt{2}}{\pi^2} \frac{m_{eff}^{3/2}(E - E_C)^{1/2}}{\hbar^3}. \tag{2.88}$$

The occupancy is represented by the Fermi-Dirac distribution function,

$$F(E) = \frac{1}{1 + exp((E - E_F)/k_B T)}. \tag{2.89}$$

Then the integral in Eq. 2.87 turns into

$$n = \int_{E_C}^{\infty} N(E)F(E)dE = \int_{0}^{\infty} N(E)F(E)dE = \int_{0}^{\infty} c_{coeff} \frac{(\frac{E_i - E_C}{k_B T})^{1/2}}{1 + exp(\frac{E_i - E_C - (E_F - E_C)}{k_B T})} dE. \tag{2.90}$$

After changing the variable, $\eta = (E_i - E_C)/(K_B T)$ and $\eta_f = (E_F - E_C)/(K_B T)$,one has

$$n = \int_{0}^{\infty} c_{coeff} \frac{\eta^{1/2}}{1 + exp(\eta - \eta_f)} d\eta. \tag{2.91}$$

Then the Fermi integral can be defined as

$$F_{\frac{1}{2}}(\eta) = \int_{0}^{\infty} \frac{\eta^{1/2}}{1 + exp(\eta - \eta_f)} d\eta. \tag{2.92}$$

In dielectrics both dopant atoms and intrinsic point defects can be donors and acceptors which make the material a n-type or p-type semiconductor. Depending on the electric potential, a certain portion of donors or acceptors is ionized and the electrons or holes are available. In this work, all possible point defect species are considered. The expression of the local space charge will be shown in the next chapter according to the general semiconducting theory.

2.5 Variational formulation in electromechanics

In this part one formulates the electromechanical problem in a variational framework in the material body. The variation of free energy is

$$\delta\mathcal{H} = \int_\Omega \delta H(\varepsilon_{ij}, E_i, P_i, P_{i,j})dV = \int_\Omega \frac{\partial H}{\partial \varepsilon_{ij}}\delta\varepsilon_{ij} + \frac{\partial H}{\partial E_i}\delta E_i + (\frac{\partial H}{\partial P_i} - (\frac{\partial H}{\partial P_{i,j}})_{,j})\delta P_i dV. \tag{2.93}$$

The virtual work of external forces is

$$\delta\mathcal{W} = \delta\mathcal{W}_u + \delta\mathcal{W}_\phi + \delta\mathcal{W}_P = \int_\Omega f_i\delta u_i dV + \int_{\partial\Omega_t} t_i\delta u_i dA - \int_\Omega q\delta\phi dV - \int_{\Omega_{\partial\omega}} \omega\delta\phi dA. \tag{2.94}$$

The dissipation is

$$\delta\mathcal{D} = \int_\Omega \frac{1}{M}\dot{P}_i\delta P_i dV. \tag{2.95}$$

According to principle of virtual work, for a system in equilibrium, the work of external forces equals the virtual change of internal free energy for any virtual change $\delta u_i, \delta\phi, \delta P_i$. In other words, the internal free energy is balanced by the external work done to the material, i.e.,

$$\delta\mathcal{H} - \delta\mathcal{W} + \delta\mathcal{D} = 0. \tag{2.96}$$

This is the basis of FEM implementation of the physical problem studied.

Chapter 3

Phase field modeling for ideal ferroelectrics and configurational force theory

This chapter presents a finite element method based phase field model for ideal ferroelectrics without defects. This model will be modified in different aspects in Chapter 4,5,6 and 7 to taken into account the influences of defects, such as space charges and defect dipoles. The second part of the chapter presents the theory of configurational force theory which is applied in Chapter 4 for the stability study of charged domain wall.

3.1 The phase field modeling of ideal ferroelectrics

3.1.1 Introduction to phase field modeling

Microstructures are compositional and structural inhomogeneities that take place during manufacturing and processing of materials. Microstructure evolution is common in many fields, including phase transformations, chemical reactions, and fracture. Material microstructures comprise of phases of different compositions and crystal structures which are distributed spatially. There are also other materials microstructures like grains, which are oriented differently, domains of different structural variants (domains of different electric or magnetic polarizations), and other structural defects. These structural features possess an intermediate mesoscopic size scale in the range from nanometers to microns. The size, shape, pattern and spatial arrangement of the local structural features in a microstructured material play an important role in the overall properties of a material. Microstructures evolve so that the total free energy (including the interfacial energy, elastic energy, magnetic energy, electrostatic energy and coupling energy) is minimized under applied external fields (applied stress, electrical, temperature, and magnetic fields).

A phase field model is a mathematical model for solving interfacial problems. It has been applied to many fields of study (e.g. solidification), but it has also been applied to other situations such like phase transformation in ferroelectrics, ferromagnetics and fracture. The method substitutes boundary conditions at the interface by a partial differential equation for the evolution of an auxiliary field (the phase field) that takes the role of an order parameter.

In the conventional way to model microstructure evolution, the zones separating the structural domains are considered as sharp interfaces, across which the material properties experience a jump. For complicated three-dimensional microstructures, tracking the interface becomes impractical. The phase field modeling has become one of the most powerful methods for modeling the microstructure evolution in materials. A phase field model describes a microstructure as a whole by a set of field variables. The field variables are continuous across different phase regions, and the interfaces in phase field models are diffuse. The original idea to use a diffuse interface was given by van der Waals [60]. Cahn and Hilliard also have attempted to treat the free energies of an interface for the free energy of a system which has a spatial variation of one of its scalar variables and the interface between two coexisting phases is diffuse [61, 62]. For more details on the theory and application of phase field methods in materials science one can refer to Chen's paper [63].

3.1.2 History of phase field modeling of ferroelectrics

Based on the Landau theory, the free energy of a ferroelectric material may be written as a Taylor expansion in terms of the order parameter (for which one has several options, as will be shown later) in the absence of an electric field and applied stress. The free energy can be given by a sixth order polynomial.

There is a transition region between two domains known as a domain wall. Since the domain wall region involves both electrical and elastic deformation, the relavant energy penalty which is associated with the spontaneous polarization gradients is added. This extended phenomenological theory is usually called the Ginzburg-Landau theory because Ginzburg and Landau first applied the gradient terms for describing the superconducting transition [64].

The behaviour of ferroelectrics on the scale of domain structure is described by phase field models which are then based on the Landau-Ginzburg equations. Mueller first applied thermodynamics in ferroelectrics by expressing the free energy in a polynomial of polarization and strain of different power [65, 66, 67]. The thermodynamical theory by Devonshire et al. is one of the most important theories. Ginzburg and Devonshire developed the method further. This thermodynamical theory is the application and development of the phase transition theory of Landau [68, 69]. Therefore it is called the Landau-Ginzburg theory and remains one effective method in studying ferroelectrics.

In treating the phase transition in ferroelectrics, the Landau theory does not only consider the spontaneous polarization, but also the its coupling with other parameters. In the phase field model the spontaneous polarization is taken as an order parameter. Devonshire developed the primary thermodynamic theories of phase transitions in ferroelectric crystals by expanding the total free energy in a power series with respect to two independent variables: one from the polarization and electric field, and the other from the strain and stress.

Phase field methods are used widely for the study of domain structures in ferroelectrics recent years. Cao et al. first introduced a gradient energy in the order parameter to account for interphase boundaries energy of the tetragonal phase in perovskites [70]. Some works also extended the free energy to include dipole-dipole interaction in the phase field model. Li et al. raised a phenomenological model. They introduced remanent polarization and remanent strain as an internal variable which only consider the single-axial case [71]. Wang et al. simulated polarization switching in ferroelectrics using a phase field model based on the Ginzburg-Landau equation. The phase field model takes both multiple-dipole-dipole-elastic and multiple-dipole-dipole-electric interactions into account [72]. Zhang and Bhattacharya formulated a phase field model which can predict the macroscopic behavior and the microstructural evolution of ferroelectrics under electro-mechanical boundary conditions [73]. Soh et al. have also done phase field simulations and the results have shown that the coupled electro-mechanical loading change both the symmetry of hysteresis loops and the coercive field of ferroelectric materials [74]. Su and Landis devised a continuum thermodynamic framework to model the evolution of domain structures in ferroelectrics [75]. Schrade et al. established a continuum physics model which is descretized with finite element method. In contrast to other phase field models, the model takes the spontaneous polarization as primary order parameter [76, 77]. Size dependent domain configurations and dead layers in ferroelectrics have also been studied by phase field models [78, 79]. Phase transition induced by mechanical stress in ferroelectrics has also been studied by phase field models [80, 81].

3.1.3 A finite-element phase field model for ideal ferroelectrics

Higher order terms of the order parameter are included in the Helmholtz free energy. In the phase field model, an order parameter P_i is introduced. The power of the microforces can be written as

$$\int_{\Omega} (\zeta_{ij} n_j) \dot{P}_i dA, \int_{\Omega} \pi_i \dot{P}_i dV, \int_{\Omega} \gamma_i \dot{P}_i dV, \tag{3.1}$$

where the second term is power expended due to the evolution of the microstructure and the first term and the third term are the power due to certain external source. It is expected that there is an equilibrium equation between the microstress and the internal and the external microforces,

$$\int_{\partial\Omega} (\zeta_{ij} n_j) dA + \int_{\Omega} (\gamma_i + \pi_i) dV = 0. \tag{3.2}$$

Locally it reads,

$$\zeta_{ij,j} + \pi_i + \gamma_i = 0. \tag{3.3}$$

According to the second law of thermodynamics,

$$\int_{\partial\Omega} \sigma_{ij} n_j \dot{u}_i + D_i n_i \dot{\phi} + (\zeta_{ij} n_j) \dot{P}_i dA + \int_{\Omega} f_i \dot{u}_i - \rho \dot{\phi} + \gamma_i \dot{P}_i dV - \frac{d}{dt} \int_{\Omega} H dV \geqslant 0. \tag{3.4}$$

Making use of equilibrium equations, this yields

$$(\sigma_{ij} - \frac{\partial H}{\partial \varepsilon_{ij}}) \dot{\varepsilon}_{ij} - (D_i + \frac{\partial H}{\partial E_i}) \dot{E}_i + (\zeta_{ij} - \frac{\partial H}{\partial P_{i,j}}) \dot{P}_{i,j} - (\pi_i + \frac{\partial H}{\partial P_i}) \dot{P}_i - \frac{\partial H}{\partial \dot{P}_i} \ddot{P}_i \geqslant 0. \tag{3.5}$$

Thus one more constitutive relationship can be obtained in addition to Eq. (2.84),

$$\sigma_{ij} = \frac{\partial H}{\partial \varepsilon_{ij}}, D_i = -\frac{\partial H}{\partial E_i}, \zeta_{ij} = \frac{\partial H}{\partial P_{i,j}}. \tag{3.6}$$

It is assumed that the free energy does not depend on the rate of the polarization, it follows,

$$-(\pi_i + \frac{\partial H}{\partial P_i}) \dot{P}_i \geqslant 0. \tag{3.7}$$

Therefore the terms in the bracket can be defined as dissipative microforce,

$$\pi_i^{diss} = \pi_i + \frac{\partial H}{\partial P_i}. \tag{3.8}$$

For inequality to be satisfied, one can assume

$$\pi_j^{diss} = -\beta_{ij} \dot{P}_i. \tag{3.9}$$

then the total dissipation reads,

$$\mathcal{D}^{diss} = -\int_{\Omega} \pi_i^{diss} \dot{P}_i dV = \int_{\Omega} \dot{P}_i \beta_{ij} \dot{P}_j dV \geqslant 0. \tag{3.10}$$

Then the microforce has the form,

$$\pi_i = \pi_i^{diss} - \frac{\partial H}{\partial P_i} = -\beta_{ij} \dot{P}_j - \frac{\partial H}{\partial P_i}. \tag{3.11}$$

By using Eq. (3.3), one has

$$\beta_{ij}\dot{P}_j = \zeta_{ij,j} + \gamma_i - \frac{\partial H}{\partial P_i}. \tag{3.12}$$

With the ignorance of external microforce and the multiplication of the inverse of the β_{ij} on the both sides, one has

$$\dot{P}_k = \beta_{ik}^{-1}(-\frac{\partial H}{\partial P_i} + (\frac{\partial H}{\partial P_{i,j}})_{,j}). \tag{3.13}$$

After redefining the $M_{ki} = \beta_{ik}^{-1}$, the equation turns into

$$\dot{P}_k = M_{ki}(-\frac{\partial H}{\partial P_i} + (\frac{\partial H}{\partial P_{i,j}})_{,j}). \tag{3.14}$$

The terms in the bracket on the right side is the functional derivative of the free energy with respect to P_i, then the equation again turns into

$$\dot{P}_k = -M_{ki}\frac{\delta H}{\delta P_i}. \tag{3.15}$$

This is the common form of the Landau-Ginzburg equation.

3.1.4 Phase field potentials

Now the free energy is written into a form where each term and parameter has a specific physical meaning [82],

$$H = H^{ent}(\varepsilon_{ij}, E_i, P_i) + H^{sep}(P_i) + H^{grad}(P_{i,j}), \tag{3.16}$$

in which,

$$H^{ent}(\varepsilon_{ij}, E_i, P_i) = \frac{1}{2}(\varepsilon_{ij} - \varepsilon_{ij}^{\circ})[\mathbb{C}_{ijkl}(\varepsilon_{kl} - \varepsilon_{kl}^{\circ})] - (\varepsilon_{ij} - \varepsilon_{ij}^{\circ})(e_{kij}E_k) - \frac{1}{2}E_i(A_{ij}E_j) - P_iE_i, \tag{3.17}$$

$$H^{sep}(P_i) = \kappa_s\frac{\gamma}{\varepsilon}\psi(P_i), \tag{3.18}$$

$$H^{grad}(P_{i,j}) = \frac{1}{2}\kappa_i\frac{\gamma\varepsilon}{P_0^2}\|P_{i,j}\|^2. \tag{3.19}$$

They are electric enthalpy, domain separation energy and gradient energy respectively. The domain separation energy is expressed as a sixth degree polynomial, indicating four and six possible polarized states in the 2D and 3D case,

$$\begin{aligned}\psi(P_i) = a_0 + \frac{a_1}{P_0^2}(P_1^2 + P_2^2 + P_3^2) + \frac{a_2}{P_0^4}(P_1^4 + P_2^4 + P_3^4) + \frac{a_3}{P_0^4}(P_1^2P_2^2 + P_1^2P_3^2 + P_2^2P_3^2) \\ + \frac{a_4}{P_0^6}(P_1^6 + P_2^6 + P_3^6).\end{aligned} \tag{3.20}$$

By evaluating the equation Eq. (3.6), one gets the constitutive equations,

$$\sigma_{ij} = \mathbb{C}_{ijkl}(\varepsilon_{kl} - \varepsilon^0_{kl}) - e_{kij}E_k, \tag{3.21}$$

$$D_i = e_{ijk}(\varepsilon_{jk} - \varepsilon^0_{jk}) + A_{ij}E_j + P_i, \tag{3.22}$$

$$\dot{P}_j = -M_{ji}\frac{\delta H}{\delta P_i}. \tag{3.23}$$

3.1.5 Interpretation of the Parameters

A single 180° interface is used in a 1D setting. By neglecting the bulk energy, one is able to identify the phase field parameters γ and ε as the energy and the interface width. κ_i and κ_s are selected as calibration constants. The latter one is approximately twice as large as the former one.

Generally elastic, piezoelectric, dielectric constants and eigenstrain $\mathbb{C}_{ijkl}(P_m)$, $b_{ijk}(P_m)$, $\epsilon_{ij}(P_i)$ and $\varepsilon^0_{ij}(P_m)$ depend on the order parameter P_i. For simplicity, it is assumed that $\mathbb{C}_{ijkl}$ is an isotropic stiffness tensor and $\epsilon_{ij} = \epsilon$ is a constant. For piezoelectric tensor one assumes [35]

$$b_{kij}(P_m) = (\frac{\|P_m\|}{P_0})^3\{b_{\|}p_ip_jp_k + b_{\perp}(\delta_{ij} - p_ip_j)p_k + \frac{1}{2}b_{=}[(\delta_{ij} - p_kp_i)p_j + (\delta_{kj} - p_kp_j)p_i]\}. \tag{3.24}$$

The spontaneous strain is a purely deviatoric [35],

$$\varepsilon^0_{ij} = \frac{3}{2}\varepsilon^0(\frac{\|P_m\|}{P_0})^2(p_ip_j - \frac{1}{3}\delta_{ij}). \tag{3.25}$$

In the equations above, $p_i = P_i/||P_i||$.

3.2 Finite element implementation

In this thesis, one solves the field equations by the finite element method. The finite element method (FEM) is a way of numerically solving boundary value problems for partial differential equations by subdividing the whole problem domain into small regions. Thus the solution of the original problem is obtained by approximation. The first use of FEM originated from the necessity of solving complex structural problems in civil engineering. The first development of FEM was promoted by Argyris and Clough. For more information on standard finite element techniques one can refer to e.g. Zienkiewicz & Taylor [95], Hughes [96], and Wriggers [97].

The starting point of the finite element formulation is the weak form of the corresponding field equations. Since the variation of displacement, electric potential and spontaneous polarization is arbitrary chosen, Eq. (2.94) can be splitted into

$$\int_{B_0} \frac{\partial H}{\partial \varepsilon_{ij}} \delta\varepsilon_{ij} dV = \int_{B_0} f_i \delta u_i dV + \int_{\partial B_0^t} t_i \delta u_i dA, \tag{3.26}$$

$$\int_{B_0} \frac{\partial H}{\partial E_i} \delta E_i dV = -\int_{B_0} \rho \delta\phi dV - \int_{\partial B_0^\omega} \omega \delta\phi dA, \tag{3.27}$$

$$\int_{B_0} [\frac{\partial H}{\partial P_i} - (\frac{\partial H}{\partial P_{i,j}})_{,j}] \delta P_i dV = -\int_{B_0} \frac{1}{M} \dot{P}_i \delta P_i dV. \tag{3.28}$$

After applying the constitutive equations $\frac{\partial H}{\partial \varepsilon_{ij}} = \sigma_{ij}$ and $\frac{\partial H}{\partial E_i} = -D_i$ and making use of the symmetry of tensor σ_{ij}, the Eqs. (3.26) and (3.27) turn into

$$\int_{B_0} \sigma_{ij} \delta u_{i,j} dV = \int_{B_0} f_i \delta u_i dV + \int_{\partial B_0^t} t_i \delta u_i dA, \tag{3.29}$$

$$\int_{B_0} D_i \delta\phi_{,i} dV = -\int_{B_0} \rho \delta\phi dV - \int_{\partial B_0^\omega} \omega \delta\phi dA. \tag{3.30}$$

After rewriting $\delta u_{i,j} = v_{i,j}^u$, $\delta\phi = v^\phi$ and $\delta P_i = v_i^P$, one has

$$\int_{\partial B} t_i v_i^u dS + \int_B -\sigma_{ij} v_{i,j}^u + f_i v_i^u dV = 0, \tag{3.31}$$

$$\int_{\partial B} -\omega v_i^\phi dS + \int_B -D_i v_{,i}^\phi - \rho v^\phi dV = 0, \tag{3.32}$$

$$\begin{gathered} \int_B (\frac{1}{M} \dot{P}_i + \frac{\partial H}{\partial P_i} - (\frac{\partial H}{\partial P_{i,j}})_{,j}) v_i^P dV = 0, \\ \int_B (\frac{1}{M} \dot{P}_i + \frac{\partial H}{\partial P_i}) v_i^P - (\frac{\partial H}{\partial P_{i,j}} v_i^P)_{,j} + \frac{\partial H}{\partial P_{i,j}} v_{i,j}^P dV = 0. \end{gathered} \tag{3.33}$$

One defines $k = \kappa_i \gamma \epsilon$ and makes use of the flux free condition of polarization $P_{i,j} n_j = 0$. One has

$$\begin{gathered} \int_B (\frac{1}{M} \dot{P}_i + \frac{\partial H}{\partial P_i}) v_i^P - (2k P_{i,j} v_i^P)_{,j} + 2k P_{i,j} v_{i,j}^P dV = 0, \\ \int_B (\frac{1}{M} \dot{P}_i + \frac{\partial H}{\partial P_i}) v_i^P + 2k P_{i,j} v_{i,j}^P dV + \int_{\partial B} -2k P_{i,j} n_j v_i^P dA = 0, \\ \int_B (\frac{1}{M} \dot{P}_i + \frac{\partial H}{\partial P_i}) v_i^P + 2k P_{i,j} v_{i,j}^P dV = 0. \end{gathered} \tag{3.34}$$

Within each element, the value of each field variable is approximated by the sum of the product of the nodal value and its corresponding shape function N^I,

$$\begin{gathered} u_i = \Sigma N^I u_i^I, \quad \phi = \Sigma N^I \phi^I, \quad P_i = \Sigma N^I P_i^I, \\ {}^u v_i = \Sigma N^I\, {}^u v_i^I, \quad {}^\phi v = \Sigma N^I\, {}^\phi v^I, \quad {}^P v_i = \Sigma N^I\, {}^P v_i^I. \end{gathered} \tag{3.35}$$

Here the Voigt notation is adopted, $\varepsilon_{ij} = (\varepsilon_{11}, \varepsilon_{22}, \gamma_{12})^T$, where $\gamma_{12} = u_{1,2} + u_{2,1}$. Then the gradient quantities can be formulated as

$$\varepsilon_{ij} = \Sigma\ {}^{u}B^{I}_{ijk} u^{I}_{k}, \quad E_i = -\Sigma\ {}^{\phi}B^{I}_{i} \phi^{I}, \quad P_{i,j} = \Sigma\ {}^{P}B^{I}_{ijk} P^{I}_{k}, \tag{3.36}$$

in which the differential operator matrices are obtained by derivation of the shape functions,

$$ {}^{u}B^{I}_{ijk} = \begin{pmatrix} N^{I}_{,1} & 0 \\ 0 & N^{I}_{,2} \\ N^{I}_{,2} & N^{I}_{,1} \end{pmatrix}, {}^{\phi}B^{I}_{i} = \begin{pmatrix} N^{I}_{,1} \\ N^{I}_{,2} \end{pmatrix}, {}^{P}B^{I}_{ijk} = \begin{pmatrix} N^{I}_{,1} & 0 \\ 0 & N^{I}_{,2} \\ N^{I}_{,2} & 0 \\ 0 & N^{I}_{,1} \end{pmatrix}. \tag{3.37}$$

The element residuals for node I have the form,

$$ {}^{u}R^{I}_{k} = \int (-\ {}^{u}B^{I}_{ijk} \sigma_{ij} +\ {}^{u}N^{I} f_k) dV + \int\ {}^{u}N^{I} t_k dA, \tag{3.38}$$

$$ {}^{\phi}R^{I} = \int (-\ {}^{\phi}B^{I}_{k} D_k -\ {}^{\phi}N^{I} \rho) dV - \int\ {}^{\phi}N^{I} \omega dA, \tag{3.39}$$

$$ {}^{P}R^{I}_{k} = \int\ {}^{P}N^{I} (\frac{1}{M} \dot{P}_k + \frac{\partial H}{\partial P_k}) + 2k\ {}^{P}B^{I}_{ijk}\ {}^{P}P^{I}_{i,j} dV. \tag{3.40}$$

If one defines the global vector of degrees of freedom, then,

$$R_m = R_m(d_m, \dot{d}_m). \tag{3.41}$$

The velocities for the degree of freedom are approximated by Euler backward integration,

$$\dot{d}_m = \frac{d^{n+1}_m - d^{n}_m}{\Delta t_n}. \tag{3.42}$$

With respect to the time discretization, the indices n and $n+1$ denote quantities at the current and next time step in each Newton iteration, respectively. It is noted that the time discretization is only needed in the residual due to the occurrence of P. The residual is then a function of the time-discretized degrees of freedom. At time step t_{n+1} the residual should vanish and then a linear equation system is obtained,

$$R_m(d^{n+1}) = 0. \tag{3.43}$$

The stiffness and damping matrix was calculated by deriving with respect to the degrees of freedom,

$$\boldsymbol{K}^{IJ} = (\boldsymbol{R}^{I}_{,u_i}, \boldsymbol{R}^{I}_{,\phi}, \boldsymbol{R}^{I}_{,P_i}) = \begin{pmatrix} {}^{\sigma\sigma}K^{IJ}_{2\times2} & {}^{\sigma D}K^{IJ}_{2\times1} & {}^{\sigma P}K^{IJ}_{2\times2} \\ {}^{D\sigma}K^{IJ}_{1\times2} & {}^{DD}K^{IJ}_{1\times1} & {}^{DP}K^{IJ}_{1\times2} \\ {}^{P\sigma}K^{IJ}_{2\times2} & {}^{PD}K^{IJ}_{2\times1} & {}^{PP}K^{IJ}_{2\times2} \end{pmatrix}, \tag{3.44}$$

$$\boldsymbol{D}^{IJ} = (\boldsymbol{R}^{I}_{,\dot{u}_i}, \boldsymbol{R}^{I}_{,\dot{\phi}}, \boldsymbol{R}^{I}_{,\dot{P}_i}) = \begin{pmatrix} 0_{2\times2} & 0_{2\times1} & 0_{2\times2} \\ 0_{1\times2} & 0_{1\times1} & 0_{1\times2} \\ 0_{2\times2} & 0_{2\times1} & {}^{PP}D^{IJ}_{2\times2} \end{pmatrix}. \tag{3.45}$$

The global system matrix is obtained by assembling the element matrices. Since the matrix is derived from one free energy functional, it is a symmetric matrix.

3.3 Configurational force and moment

The basic equations of thermodynamics introduced earlier describe the behavior of material bodies with certain constitutive law under external influence. The description is unique and is not limited to the assumption that the materials are homogeneous. However, considering there are domain structures in ferroelectrics which is heterogeneous in some sense and the evolution of domain structure has determined direction and strives for certain target. It would be beneficial to define the force of evolution or driving force on the domain structure. One wishes that this ′driving force′ does not only give the trend of evolution of the total energy of the system, but also where exactly the evolution due to imhomogeinity is going to take place.

On the aspect of formulation of domain wall motion, the idea of a generalized force acting on a defect traces back to Peach and Koehler [83] for the study on dislocation in crystal and Eshelby [84, 85] for the study on inclusion problem in elasticity. Configurational forces present a basic concept of continuum physics and require their own balance [86]. They serve as a powerful tool in identifying the driving force on an interface between phases [87]. Motion of a discontinuity or a singularity in continua is characterized by the concept of configurational force and level set method [88]. Budiansky and Rice have defined the path-independent integrals for rotation and expansion of inhomogeneities for infinitesimal elasticity [89]. Eischen and Herrmann have made an attempt to connect the energy release rate and the path-independent integrals [90]. By postulating balance laws, energy release rate and configurational moment were derived for a crack tip evolution by Agiasofitou and Kalpakides [91]. Xu et al. [92] generalized the configurational force theory for ferroelectrics with domain structures and investigated the energy release rate at the crack tip in the material.

In the research on the behavior of defects, one question is important: how the state quantities change, as defects move relatively with respect to the material. For example, the dislocation can glide and climb in the crystal lattice, inclusions and pores can change their form, and cracks can grow. Each body stands in interaction with its environment. Not only the energy of material with defects, but also the energy of the surroundings which interacts with the defect is considered. The energy of the material body depends on the position of the defect. The negative derivative of energy with respect to the position parameter can be understood as a general physical force. In order to determine this ′material force′, one has to calculate the change of energy with respect to the displacement of a defect. Due to the motion, the deformation of the body and the energy can change. The configuration of the defect is then described by a parameter which one calls the material coordinate. Therefore, the energy of the body depends on the position of the defects. The negative derivative of total energy with respect to this parameter can be interpreted as a ′general force′ physically. In order to determine this ′material force′, one has to calculate the energy change during the position change of the defects.

The motion of defects do not have to really take place like one has conceived: the motion can be virtual. The calculation deliver the answer about the position change of a defect, but not the information about the direction and at what velocity the change takes place. There are different approaches to derive Σ_{ij}. Here the approach of Kienzler is adopted [93].

3.3.1 Linear elastic body

First one considers an elastic dielectric body B_0 with its surface S. The total energy is

$$\diamond = \int_{B_0} (W+P)dV - \int_{\partial B_0^t} \sigma_{ij}^* n_j u_i dA - \int_{\partial B_0^u} \sigma_{ij} n_j u_i^* dA, \tag{3.46}$$

where $W(X_i, u_{i,j}) = \frac{1}{2}\varepsilon_{ij}\mathbb{C}_{ijkl}\varepsilon_{kl}$ is the total energy of the elastic dielectrics. The components of Cauchy stress can be derived as

$$\sigma_{ij} = \frac{\partial W}{\partial u_{i,j}}. \tag{3.47}$$

It is assumed that the volume force f_i can be derived from one potential,

$$f_i = -\frac{\partial P}{\partial u_i}. \tag{3.48}$$

If the body is subject to a virtual displacement, then the first variation of the total energy vanishes according to the principle of the virtual displacement. After the variational operation, one gets the equilibrium equations,

$$\begin{aligned} \sigma_{ij,j} + f_i &= 0, && \text{in } B_0, \\ \sigma_{ij} n_j &= t_i^*, && \text{on } S_t, \\ u_i &= u_i^*, && \text{on } S_u. \end{aligned} \tag{3.49}$$

Now one thinks about the variation which keeps the volume integral Eq. (3.46) constant. Here one means by δ_u the variation which has impact on variables u_i. The calculation of variation yields

$$\begin{aligned} \delta_u \mathcal{A} = \delta_u \int_{B_0} (W+P)dV = \int_{B_0} (\delta_u W + \delta_u P)dV = \int_{B_0} (\sigma_{ij}\delta_u u_{i,j} - f_i \delta_u u_i)dV \\ = \int_{B_0} ((\sigma_{ij}\delta_u u_i)_{,j} - \sigma_{ij,j}\delta_u u_i - f_i\delta_u u_i)dV = \int_{B_0} (\sigma_{ij}\delta_u u_i)_{,j} dV = \int_{B_0^u} \sigma_{ij}\delta_u u_i n_j dA, \end{aligned} \tag{3.50}$$

With the variation of displacement state, the physical balance laws and the path independent integrals can be derived. The forces on defects which move relatively to the material should be calculated based on the material balance laws. Besides the variation of dependent variables, the variation of independent variable X_i is also allowed. The variated variables are denoted with a prime,

$$\delta X_i = X_i' - X_i, \tag{3.51}$$

$$\delta u_i = u_i'(X_i') - u_i(X_i) = u_i'(X_i') + \frac{\partial u_i'(X_i)}{\partial X_j}\delta X_j - u_i(X_i) + h.o.t. = \delta_u u_i + u_{i,j}\delta X_j + h.o.t., \tag{3.52}$$

The variation of total energy comprises of the local variation due to displacement and a convective part,

$$\delta(W+P) = \delta_u(W+P) + (W+P)_{,j}\delta X_j + h.o.t.. \tag{3.53}$$

Now the change of integral is calculated using these equations,

$$\begin{aligned}
\delta\mathcal{A} &= \int_{B_0'}(W'+P')dV' - \int_{B_0}(W+P)dV \\
&= \int_{B_0}\left\{\left[(W+P) + \delta_u(W+P) + (W+P)_{,j}\delta X_j\right](1+\delta X_{l,l}) - (W+P)\right\}dV \\
&= \int_{B_0}(W+P)\delta X_{l,l} + \delta_u(W+P) + (W+P)_{,j}\delta X_j dV.
\end{aligned} \tag{3.54}$$

It should be noted that the higher order of variations are neglected. Making use of Eq.(3.50), one gets

$$\begin{aligned}
\delta\mathcal{A} &= \int_{B_0}(W+P)\delta X_{l,l} + (\sigma_{ij}\delta_u u_i)_{,j} + (W+P)_{,j}\delta X_j dV \\
&= \int_{B_0}(W+P)\delta X_{l,l} + \sigma_{ij,j}\delta_u u_i + \sigma_{ij}\delta_u u_{i,j} + (W+P)_{,j}\delta X_j dV.
\end{aligned} \tag{3.55}$$

It further follows, by using Eq.(3.52),

$$\begin{aligned}
\delta\mathcal{A} &= \int_{B_0}(W+P)\delta X_{l,l} + \sigma_{ij,j}(\delta u_i - u_{i,l}\delta X_l) + \sigma_{ij}(\delta u_{i,j} \\
&- \frac{\partial u_{i,j}}{\partial X_l}\delta X_l - \frac{\partial u_{i,k}}{\partial X_{l,k}}\delta X_{l,j}) + (W+P)_{,j}\delta X_j dV \\
&= \int_{B_0}(W+P)\delta X_{l,l} + \sigma_{ij,j}(\delta u_i - u_{i,l}\delta X_l) + \sigma_{ij}(\delta u_{i,j} \\
&- u_{i,jl}\delta X_l - u_{i,l}\delta X_{l,j}) + (W+P)_{,j}\delta X_j dV \\
&= \int_{B_0}(W+P)_{,j}\delta_{jl}\delta X_l - (\sigma_{ij,j}u_{i,l} + \sigma_{ij}u_{i,lj})\delta X_l \\
&+ ((W+P)\delta_{jl} - \sigma_{ij}u_{i,l})\delta X_{l,j} + \sigma_{ij,j}\delta u_i + \sigma_{ij}\delta u_{i,j}dV \\
&= \int_{B_0}(((W+P)\delta_{jl} - \sigma_{ij}u_{i,l})\delta X_l)_{,j} + (\sigma_{ij}\delta u_i)_{,j}dV.
\end{aligned} \tag{3.56}$$

With the divergence theorem this becomes

$$\begin{aligned}
\delta\mathcal{A} &= \int_{B_0}(((W+P)\delta_{jl} - \sigma_{ij}u_{i,l})\delta X_l + \sigma_{ij}\delta u_i)_{,j}dV \\
&= \int_{B_0}(((W+P)\delta_{ij} - \sigma_{ki}u_{k,j})\delta X_i + \sigma_{ij}\delta u_i)n_j dA.
\end{aligned} \tag{3.57}$$

It can be seen that the physical balance law is contained in this integral. For a material translation of the defect, there is: $\delta X_i = C_i, \delta u_i = 0$. Then,

$$\delta \mathcal{A} = C_i \int_{B_0} ((W + P)\delta_{ij} - \sigma_{ki} u_{k,j}) n_j dA = C_i \int_{B_0} \Sigma_{ij} n_j dA, \tag{3.58}$$

in which $\Sigma_{ij} = (W + P)\delta_{ij} - \sigma_{ki} u_{k,j}$ is defined as configurational stress tensor, and the corresponding configurational force vector is $g_i = -(W + P)_{,i} - u_{j,i} f_j$. This has the same form as presented in Eshelby's work [85].

3.3.2 Linear piezoelectrics

The piezoelectric effect is the linear electromechanical interaction between the mechanical and the electrical state in crystalline materials with no inversion symmetry. For linear piezoelectric model,

$$W = \frac{1}{2}\varepsilon_{ij}\mathbb{C}_{ijkl}\varepsilon_{kl} - \varepsilon_{ij} b_{kij} E_k - \frac{1}{2} E_i E_j A_{ij}. \tag{3.59}$$

The components of electric displacement can be derived as

$$D_i = -\frac{\partial W}{\partial E_i}. \tag{3.60}$$

The charge density ρ can be derived from one potential,

$$\rho = \frac{\delta W}{\delta \phi}. \tag{3.61}$$

After the variational operation, besides the mechanical equilibrium, one gets the equilibrium equations,

$$\begin{aligned} D_{i,i} &= \rho, && \text{in } B_0, \\ D_i n_i &= \omega^*, && \text{on } S_\omega, \\ \phi &= \phi^*, && \text{on } S_\phi. \end{aligned} \tag{3.62}$$

Besides the variation of displacement, the variation of electric potential reads

$$\delta\phi = \phi'(X_i') - \phi(X_i) = \phi'(X_i') + \frac{\partial \phi'(X_i)}{\partial X_j}\delta X_j - \phi(X_i) + h.o.t. = \delta_\phi \phi + \phi_{,j}\delta X_j + h.o.t.. \tag{3.63}$$

The variation of total energy comprises of the local variation due to the displacement, the electric potential and a convective part,

$$\delta(W + P) = \delta_u(W + P) + \delta_\phi(W + P) + (W + P)_{,j}\delta X_j + h.o.t.. \tag{3.64}$$

Then the variation of total energy with respect to displacement is

$$\begin{aligned}\delta_u \mathcal{W} &= \int_{B_0} \mathbb{C}_{ijkl} u_{k,l} \delta_u u_{i,j} + u_{i,j} b_{kij} \delta_u \phi_{,k} + \phi_{,k} b_{kij} \delta_u u_{i,j} - \phi_{,i} \epsilon_{ij} \delta_u \phi_{,j} dV \\ &= \int_{B_0} \sigma_{ij} \delta_u u_{i,j} + D_i \delta_u \phi_{,i} dV.\end{aligned} \tag{3.65}$$

Then,

$$\delta_u(\mathcal{W} + \mathcal{P}) = \int_{B_0} (\sigma_{ij} \delta_u u_i)_{,j} + (D_i \delta_u \phi)_{,i} dV. \tag{3.66}$$

Similarly one has

$$\delta_\phi(\mathcal{W} + \mathcal{P}) = \int_{B_0} (\sigma_{ij} \delta_\phi u_i)_{,j} + (D_i \delta_\phi \phi)_{,i} dV. \tag{3.67}$$

Now one calculates the change of integral,

$$\begin{aligned}
\delta \mathcal{A} &= \int_{B_0'} (W' + P') dV' - \int_{B_0} (W + P) dV \\
&= \int_{B_0} ((W + P) dV + \delta_u (W + P) + \delta_\phi (W + P) + (W + P)_{,j} \delta X_j)(1 + \delta X_{l,l}) - (W + P)) dV \\
&= \int_{B_0} (W + P) \delta X_{l,l} + \delta_u (W + P) + \delta_\phi (W + P) + (W + P)_{,j} \delta X_j dV \\
&= \int_{B_0} (W + P) \delta X_{j,j} + (W + P)_{,j} \delta X_j + \sigma_{ij,j} \delta_u u_i + \sigma_{ij} \delta_u u_{i,j} + D_{j,j} \delta_u \phi + D_j \delta_u \phi_{,j} + \sigma_{ij,j} \delta_\phi u_i \\
&+ \sigma_{ij} \delta_\phi u_{i,j} + D_{j,j} \delta_\phi \phi + D_j \delta_\phi \phi_{,j} dV \\
&= \int_{B_0} (W + P) \delta X_{j,j} + (W + P)_{,j} \delta X_j + \sigma_{ij,j} (\delta_u u_i + \delta_\phi u_i) + \sigma_{ij} (\delta_u u_{i,j} + \delta_\phi u_{i,j}) \\
&+ D_{j,j} (\delta_u \phi + \delta_\phi \phi) + D_j (\delta_u \phi_{,j} + \delta_\phi \phi_{,j}) dV \\
&= \int_{B_0} (W + P) \delta X_{j,j} + (W + P)_{,j} \delta X_j + \sigma_{ij,j} (\delta u_i - u_{i,k} \delta X_k) + \sigma_{i,j} (\delta u_{i,j} - u_{i,kj} \delta X_k \\
&- u_{i,k} \delta X_{k,j}) + D_{j,j} (\delta \phi - \phi_{,k} \delta X_k) + D_j (\delta \phi_{,j} - \phi_{,jk} \delta X_k - \phi_{,k} \delta X_{k,j}) dV \\
&= \int_{B_0} (W + P) \delta X_{j,j} + (W + P)_{,j} \delta X_j - \sigma_{kj,j} u_{k,i} \delta X_i - \sigma_{kj} u_{k,ij} \delta X_i - \sigma_{kj} u_{k,i} \delta X_{i,j} \\
&+ \sigma_{ij,j} \delta u_i + \sigma_{ij} \delta u_{i,j} + E_{i,j} D_j \delta X_i + E_i D_{j,j} \delta X_i + E_i D_j \delta_{i,j} + D_{j,j} \delta \phi + D_j \delta \phi_{,j} dV \\
&= \int_{B_0} (((W + P) \delta_{jl} - \sigma_{ij} u_{i,l} + E_l D_j) \delta X_l + \sigma_{ij} \delta u_i + D_j \delta \phi)_{,j} dV.
\end{aligned} \tag{3.68}$$

And the corresponding configurational force vector is $g_i = -(W + P)_{,i} - u_{j,i} f_j + \rho \phi_{,i}$. This has the same form as presented in Maugin's work [94].

3.3.3 Ferroelectrics

$$\begin{aligned}\delta\mathcal{A} &= \int_{B_0'}(H'+P')dV' - \int_{B_0}(H+P)dV\\ &= \int_{B_0}((H+P)dV + \delta_u(H+P) + \delta_\phi(H+P) + \delta_P(H+P) + \delta_{\triangledown P}(H+P)\\ &+ (H+P)_{,j}\delta X_j)(1+\delta X_{l,l}) - (H+P))dV.\end{aligned} \tag{3.69}$$

Since one can write the phase field model in the way,

$$\frac{\partial H}{\partial P_i} - (\frac{\partial H}{\partial P_{i,j}})_{,j} + \frac{1}{M}\dot{P}_i = 0. \tag{3.70}$$

Thus one can treat the term $\frac{1}{M}\dot{P}_i$ as certain kind of volume force. If one writes $\kappa_i\gamma\varepsilon$ as k, one has

$$\begin{aligned}\delta\mathcal{A} &= \int(((H+P)\delta_{jl} - \sigma_{ij}u_{i,l} + E_iD_j)\delta X_l + \sigma_{ij}\delta u_i + D_j\delta\phi)_{,j}dV + \int_{B_0}\delta_P(H+P)dV\\ &+ \int_{B_0}\delta_{\triangledown P}(H+P)dV\\ &= \int_{B_0}(((H+P)\delta_{jl} - \sigma_{ij}u_{i,l} + E_iD_j)\delta X_l + \sigma_{ij}\delta u_i + D_j\delta\phi)_{,j}dV + \int_{B_0}(\frac{\partial H}{\partial P_{i,j}})_{,j}\delta_P P_i dV\\ &+ \int_{B_0}\frac{\partial H}{\partial P_{i,j}}\delta_{\triangledown P}P_{i,j}dV\\ &= \int_{B_0}(((H+P)\delta_{jl} - \sigma_{ij}u_{i,l} + E_iD_j)\delta X_l + \sigma_{ij}\delta u_i + D_j\delta\phi)_{,j}dV + \int_{B_0}2kP_{i,jj}\delta_P P_i dV\\ &+ \int_{B_0}2kP_{i,j}\delta_{\triangledown P}P_{i,j}dV\\ &= \int_{B_0}(((H+P)\delta_{jl} - \sigma_{ij}u_{i,l} + E_iD_j)\delta X_l + \sigma_{ij}\delta u_i + D_j\delta\phi)_{,j}dV\\ &+ \int_{B_0}2kP_{i,jj}(\delta P_i - P_{i,l}\delta X_l) + 2kP_{i,j}(\delta P_{i,j} - P_{i,jl}\delta X_l - \frac{\partial P_{i,j}}{\partial X_{j,l}}\delta X_{j,l})dV\\ &= \int_{B_0}(((H+P)\delta_{jl} - \sigma_{ij}u_{i,l} + E_iD_j)\delta X_l + \sigma_{ij}\delta u_i + D_j\delta\phi)_{,j}dV\\ &+ \int_{B_0}-2kP_{k,ij}P_{k,j}\delta X_i - 2kP_{k,i}P_{k,jj}\delta X_i - 2kP_{k,i}K_{k,j}\delta X_{i,j} + 2kP_{i,jj}\delta P_i + 2kP_{i,j}\delta P_{i,j}dV\\ &= \int_{B_0}(((H+P)\delta_{ij} - \sigma_{kj}u_{k,i} + E_iD_j)\delta X_i + \sigma_{ij}\delta u_i + D_j\delta\phi)_{,j}dV + \int_{B_0}((-2kP_{k,j}P_{k,i})\delta X_i)_{,j}\\ &+ (\frac{\partial H}{\partial P_{i,j}}\delta P_i)_{,j}dV\\ &= \int_{B_0}(((H+P)\delta_{ij} - \sigma_{kj}u_{k,i} + E_iD_j - P_{k,i}\frac{\partial H}{\partial P_{k,j}})\delta X_i + \sigma_{ij}\delta u_i + D_j\delta\phi + \frac{\partial H}{\partial P_{i,j}}\delta P_i)_{,j}dV.\end{aligned} \tag{3.71}$$

Therefore,

$$\Sigma_{ij} = (H+P)\delta_{ij} - \sigma_{kj}u_{k,i} + E_iD_j - P_{k,i}\frac{\partial H}{\partial P_{k,j}}. \tag{3.72}$$

And the corresponding configurational force vector is $g_i = (-H+P)_{,i} - u_{j,i}f_j + \rho\phi_{,i} + \frac{1}{M}P_{j,i}\dot{P}_j$. This has the same form as presented in the work [92].

3.3.4 Numerical evaluation of configurational force and moment

Mueller and Maugin shows that how the discrete configurational forces are calculated in a computational setting [99]. If one multiplies the equilibrium equation with a test function, one has

$$\int_{B_0}(\Sigma_{ij,j} + g_i)\eta_i dV = 0. \tag{3.73}$$

Integration by parts yields

$$\int_{\partial B_0}\Sigma_{ij}n_j\eta_i dA - \int_{B_0}\Sigma_{ij}\eta_{i,j}dV + \int_{B_0}g_i\eta_i dV = 0. \tag{3.74}$$

Assume that the vector η_i vanishes on the boundary and if one writes the Σ_{ij} and $\eta_{i,j}$ into vector $\underline{\Sigma}_i$ and $\underline{\nabla\eta}_i$, one has

$$-\int_{B_e}\underline{\Sigma}_i(grad\eta)_i dV + \int_{B_e}g_i\eta_i dV = 0, \tag{3.75}$$

where $\underline{\Sigma}_i$ is the Voigt notation of the configurational stress tensor. If one approximates the value of test function and its derivative by multiplying the nodal value with its shape function and differential operator, one has

$$\Sigma\eta_j^I\left(-\int_{B_e}B_{ij}^I\underline{\Sigma}_i dV + \int_{B_e}N^I g_j dV\right) = 0. \tag{3.76}$$

Then the discrete configurational force is introduced as

$$G_j^{e,I} = \int_{B_e}N^I g_j dV = \int_{B_e}B_{ij}^I\underline{\Sigma}_i dV. \tag{3.77}$$

For certain node K, the configurational force is the summation of those from all adjacent nodes,

$$G_i^K = \cup_{e=1}^{n_e}G_i^e, \tag{3.78}$$

where n_e are all the elements sharing the node K.

Chapter 4

Influence of space charges on domain structure

Ferroelectric perovskites are insulators in general and the band gap is larger than zero. However, because in perovskites usually impurities exists, they are semiconductors and it is important to treat them as semiconductors and do investigations. Phase field modeling has also been applied to ferroelectrics with semiconducting features in some studies. For instance, the depletion layers near the electrodes were predicted and the interaction between the donors and the different domain structures were investigated [100, 101]. In a recent study, it was found that, with increased concentration of charged domain walls, the piezoelectric properties are enhanced [103]. It has also been experimentally demonstrated that the charged head-to-head domain wall shows stable metallic-type conductivity [104]. In the model one treats the spontaneous polarization as an order parameter, whose evolution subordinates to the Landau-Ginzburg equation in a thermodynamically consistent way. In Chapter 3, a phase field model has been presented for the study of the domain evolution in a barium titanate single crystal with space charges. Within the frame of the phase field model we have developed, by introducing a new quantity, the space charge density ρ, one aims to study the ferroelectrics according to semiconducting features.

This chapter is organized in the following way. In Section 1, expression for the space charge density in perovskites due to point defects is given. The numerical calculation of Fermi-integral is included in Section 2. In Section 3, two illustrative examples, depletion layers and head-to-head domain walls, are first studied in Section 4.3 to show the accumulation of free electronic charges near the electrodes and at non-compensated domain walls. In Section 4, one focuses stability of head-to-head domain structure. For a quantitative study of stabilization of the domain walls with uncompensated polarization charges by free space charges, the concept of configurational force is applied. To start with, the driving force and moment along a domain wall between two head-to-head hard domains is numerically calculated for sharp interfaces in Section 5in Section 4.4.1. The effect of an external electric field, the domain wall orientation and the charge compensation on the tendency of motion of the domain wall is demonstrated. The results of the pressure on the domain wall agree well with those by Mokrý et al. [105]. However, the results reveal additionally a tendency of domain wall rotation besides the domain wall motion in the normal direction. The driving moment resulted from inhomogeneity of the electric field can affect the equilibrium position of the domain wall in a head-to-head or tail-to-tail domain configuration. This is then investigated by the phase field simulations in Section 6. It is also shown that the equilibrium angle of the domain wall depends on the donor concentration.

4.1 Space charge formulation and phase field model

In dielectrics both dopant atoms and intrinsic point defects can be donors and acceptors which make the material a n-type or p-type semiconductor. In particular, oxygen vacancies are common point defects, whose appearance is inevitable in the device production and working cycles. Depending on the electric potential, a certain portion of donors or acceptors is ionized and the electrons or holes are available. According to the general semiconducting theory, the local space charge consists of four parts [59],

$$\begin{aligned}\rho(\phi) = &-qN_C F_{1/2}(\frac{E_F - E_C + q\phi}{k_B T})\\ &+qN_V F_{1/2}(\frac{E_V - E_F - q\phi}{k_B T})\\ &+qz_d N_d t_d(\phi) - qz_a N_a t_a(\phi),\end{aligned} \tag{4.1}$$

in which

$$t_d(\phi) = 1 - \frac{1}{1 + \frac{1}{g_d}\exp(\frac{E_d - E_F - q\phi}{k_B T})}, \tag{4.2}$$

$$t_a(\phi) = 1 - \frac{1}{1 + g_a\exp(\frac{E_a - E_F - q\phi}{k_B T})}. \tag{4.3}$$

In the equations q is the electron charge, N_C and N_V are effective densities of states in the conduction band and the valence band, and E_F is the Fermi level. According to the work by Xiao et al. [100], the Fermi level in the material is taken as the Fermi level of the electrode, for instance the platinum electrode. E_C and E_V are the conduction and the valence band edges, respectively. N_d and N_a are the concentrations of donors and acceptors, whose ionized portion are denoted by t_d and t_a. z_d and z_a are the donor valency and the acceptor valency, respectively. k is the Boltzmann constant, T is the absolute temperature, and $F_{1/2}$ is the Fermi integral. The Fermi integral is numerically calculated according to the scheme by van Halen et al. [98]. Thus space charge density is coupled with donor concentration, electric potential and temperature at the same time. In this study no acceptor is considered and it is assumed that the donors have a homogeneous distribution and possess no mobility. The values of parameters used in the simulation are listed in Table 5.2 according to the reference [100]. Note that z_d is set to be 2 here, instead of 1. It was demonstrated in first principle calculations that in barium titanate doubly charged oxygen vacancies are dominant in the n-type region [50].

Table I: Parameters used in the simulation

C_{11}	$14 \cdot 10^{10}\mathrm{Nm}^{-2}$	A_{12}	0.0	P_0	$0.4\mathrm{Cm}^{-2}$
C_{12}	$1.4 \cdot 10^{10}\mathrm{Nm}^{-2}$	A_{21}	0.0	S_0	0.003
C_{13}	0.0	A_{22}	$6.0 \cdot 10^{-9}\mathrm{CV}^{-1}\mathrm{m}^{-1}$	E_F	$-5.300\mathrm{eV}$
C_{21}	$1.4 \cdot 10^{10}\mathrm{Nm}^{-2}$	M	$1.0 \cdot 10^{3}\mathrm{AV}^{-1}\mathrm{m}^{-1}$	E_C	$-3.600\mathrm{eV}$
C_{22}	$34 \cdot 10^{10}\mathrm{Nm}^{-2}$	γ	$0.067\mathrm{Jm}^{-2}$	E_V	$-6.600\mathrm{eV}$
C_{23}	0.0	ϵ	$1.6 \cdot 10^{-7}\mathrm{m}$	E_d	$-4.000\mathrm{eV}$
C_{31}	0.0	κ_s	0.70	E_a	$-6.200\mathrm{eV}$
C_{32}	0.0	κ_i	0.17	z_d	2
C_{33}	$16 \cdot 10^{10}\mathrm{Nm}^{-2}$	a_1	1.0	z_a	2
b_{11}	0.0	a_2	$5.824 \cdot 10^{-2}\mathrm{m}^4\mathrm{C}^{-2}$	g_d	2
b_{12}	0.0	a_3	$-117.9\mathrm{m}^8\mathrm{C}^{-4}$	g_a	1/2
b_{13}	$13.0\mathrm{Cm}^{-2}$	a_4	$214.4\mathrm{m}^8\mathrm{C}^{-4}$	N_C	$10^{24}\ \mathrm{m}^{-3}$
b_{21}	$-5.2\mathrm{Cm}^{-2}$	a_5	$490.6\mathrm{m}^{12}\mathrm{C}^{-6}$	N_V	$10^{24}\ \mathrm{m}^{-3}$
b_{22}	$-1.5\mathrm{Cm}^{-2}$	q	$1.6022 \cdot 10^{-19}\mathrm{C}$	N_d [118]	
b_{23}	0.0	k_B	$1.3807 \cdot 10^{-23}\mathrm{J}$	N_a	0
A_{11}	$6.0 \cdot 10^{-9}\mathrm{CV}^{-1}\mathrm{m}^{-1}$	T	300K		

The space charge is plotted as a function of electric potential in Fig.(4.1). For defect-free barium titanate, the material remains space charge neutral in the range of $-1.30\mathrm{V} < \phi < 1.70\mathrm{V}$, which corresponds to $(E_V - E_F)/q < \phi < (E_C - E_F)/q$. For $\phi > 1.70\mathrm{V}$ a large amount of electrons move to the conducting band, whereas for $\phi < -1.30\mathrm{V}$ holes move into the valence band. After introducing oxygen vacancies as donors, a sufficiently low electric potential favors the ionization and thus positive charge carriers dominate. From Fig.(4.1), it is seen that the potential difference between the commence of electron jumping into the conduction band and the point when 1/3 of donors are ionized, is about 0.4V. This value corresponds to $(E_C - E_D)/q$. The space charge due to the ionization of donors is proportional to the donor concentration.

As an example to demonstrate the formation of space charges, a periodic domain structure in a barium titanate thin film sandwiched between two electrodes is studied. Results show that the charge carriers diffuse away in a certain thickness near the electrodes, giving rise to a depletion layer (Fig. 4.2). A built-in potential arises in the interior of the material slab, and the charge density increases in the depletion layer from interior to the edge (Fig. 4.3). The result indicates

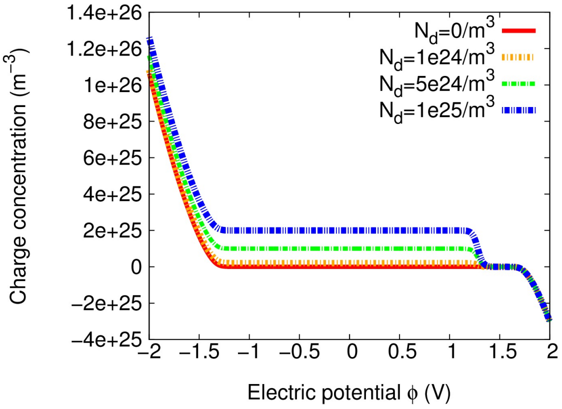

Figure 4.1: (Color online) Variation of the space charge with respect to the electric potential in ferroelectrics with semiconducting features according to Eq. (2.14) with $N_a = 0$.

that the sample is positively charged. This should be due to the asymmetry of the defect system considered here. Likewise, an acceptor-dominant sample was shown to be negatively charged in the work by Genenko et al. [106]. Donors are almost fully ionized in the depletion layers, whereas the ionized proportion of donors is only about 10% in the interior. Those results are consistent with the features demonstrated in Fig. 4.4.

4.2 Numerical implementation of space charge

For the case of ferroelectrics with space charge induced by semiconducting feature, an additional ρ arises in the residual ${}^{\phi}R^{I}$ in Eq. (3.39), which is express by Eq. (4.1). The space charge ρ includes two main species: The space charge from electrons or holes and from ionized acceptors or donors. The latter equals to the product of the unit charge, valency, defect concentration and the proportion of ionization which is some exponential function of ϕ. It can be evaluated directly. The first part contains an integral of the form $\int_0^\infty \frac{\epsilon^j d\epsilon}{1+exp(\epsilon-x)}$ whose value is not so obtained in a straightfoward way. A numerical scheme suggested by van Halen and Pulfrey is applied [98]. The numerical evaluation of t_d and t_a, which are some type of exponential functions of ϕ is a trivial job. However, the determination of the space charge from electrons in conduction band and holes in valence band involves the value of the Fermi integral expressed in (4.1), which is numerically very costly. There have been many attempts to evaluate, tabulate and approximate the integral.

The Fermi-Dirac integral for $j = -\frac{1}{2}, \frac{1}{2}$ is approximated with a finite series with $r = 1, 2, ..., 7$ as

$$\begin{aligned}
&if \quad x \leqslant 0, \quad F_{1/2} = \Sigma_{r=1,\ldots,7}(-1)^{(r+1)} a_r^{\frac{1}{2},1} exp(rx) \\
&if \quad 0 < x \leqslant 2, \quad F_{1/2} = \Sigma_{r=1,\ldots,7} a_r^{\frac{1}{2},2} x^{r-1} \\
&if \quad 2 < x \leqslant 4, \quad F_{1/2} = \Sigma_{r=1,\ldots,7} a_r^{\frac{1}{2},3} x^{r-1} \\
&if \quad 4 < x, \quad F_{1/2} = x^{\frac{3}{2}} \Sigma_{r=1,\ldots,7} a_r^{\frac{1}{2},4} \frac{1}{x^{2(r-1)}}
\end{aligned} \tag{4.4}$$

$$\begin{aligned}
&if \quad x \leqslant 0, \quad F_{1/2} = \Sigma_{r=1,\ldots,7}(-1)^{(r+1)} a_r^{-\frac{1}{2},1} exp(rx) \\
&if \quad 0 < x \leqslant 2, \quad F_{1/2} = \Sigma_{r=1,\ldots,7} a_r^{-\frac{1}{2},2} x^{r-1} \\
&if \quad 2 < x \leqslant 4, \quad F_{1/2} = \Sigma_{r=1,\ldots,7} a_r^{-\frac{1}{2},3} x^{r-1} \\
&if \quad 4 < x, \quad F_{1/2} = x^{\frac{3}{2}} \Sigma_{r=1,\ldots,7} a_r^{-\frac{1}{2},4} \frac{1}{x^{2(r-1)}}
\end{aligned} \tag{4.5}$$

Details of the implementation in Fortran can be found in Appendix C.

4.3 Depletion layer

In order to study the influence of oxygen vacancy on the domain evolution, a 2D computational scheme based on the model described in the previous section is developed and the simulation is conducted for $BaTiO_3$ with different domain structure types under a cycling electric field. The applied material parameters are listed in the reference. For the realization of discretization, 4-node elements are applied and for each node five degrees of freedom are assigned, spontaneous polarization components P_1, P_2, the electric potential ϕ and the two displacements u_1, u_2. The time derivative is realized with an Euler backward method. The discretization leads to a non-linear equation system of the unknown nodal values. After each advance of time step, sufficient Newton-iterations are conducted, until the calculation converges.

A good estimation has been done for space charge layers in semiconducting ferroelectrics [107]. Transmission optical microscopy shows that the domain walls in barium titanate are pinned after long time aging and thus the domain structure is stabilized by presumably space charge [108]. As it is known, two types of domain walls, i.e. 180° and 90° domain walls, are found as common equilibrium domain configurations of ferroelectrics free of space charges. Both of them are free of non-compensated polarization charges. However, in the case of ferroelectrics with free space charges, the otherwise unstable non-compensated domain walls can be stabilized. Several possibilities of domain structure stabilization have been discussed for Mn-doped barium titanate [109].

First-principle calculations have also confirmed that by inserting charged atomic layers, head-to-head and tail-to-tail domain structures are stabilized [110]. Gureev et al. show that charged

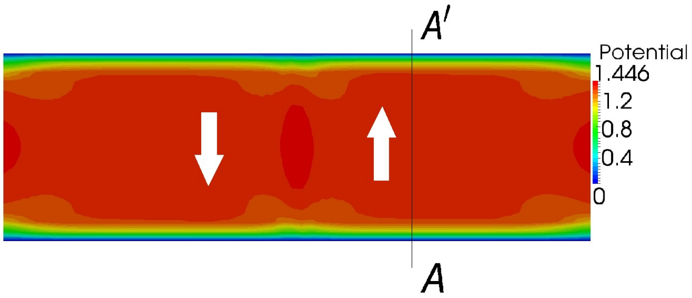

Figure 4.2: (Color online) Distribution of the electric potential in a barium titanate film with donor concentration of $N_d = 5 \cdot 10^{24}\,\mathrm{m}^{-3}$. The upper and lower surfaces are assumed to be potential-free, corresponding to a short circuit condition.

domain walls are energetically more favorable and can make head-to-head and tail-to-tail domain structures more stable [111]. Mokrý et al. [105] has obtained an analytic solution of the pressure acting on a head-to-head domain wall and studied the influence of charge compensation and the external electric field. In a subsequent work, Gureev et al. [112] also analytically studied the interaction of electric field with charged domain walls, which points out that the free charge carried by the wall depends on the size of the adjacent domains. A study of conductivity distribution across a charged domain wall has been performed for both head-to-head and tail-to-tail domain configurations, and accumulation of electrons around head-to-head domain walls was predicted [113].

The width of the depletion layer can vary with the concentration of donors (Fig. 4.4). The larger the concentration is, the thinner the depletion layer becomes. This is related to the fact that for larger concentration of donors, the distance to be covered in order to build up certain value of electric potential is also smaller. The built-in potential can modify the polarization distribution to a certain extent. The polarization component increases on the side favored by the electric field due to the built-in potential, whereas the component decreases on the other side (Fig. 4.5). These results are in agreement with those by Xiao et al. [100].

4.4 Stability of head-to-head domain structure

The head-to-head domain configuration is generally not a stable one in non-semiconducting case, since the non-compensated charges due to the polarization lead to high energy density and result in a driving force on the domain wall. However, when the free space charge is available, the domain configuration can be stabilized.

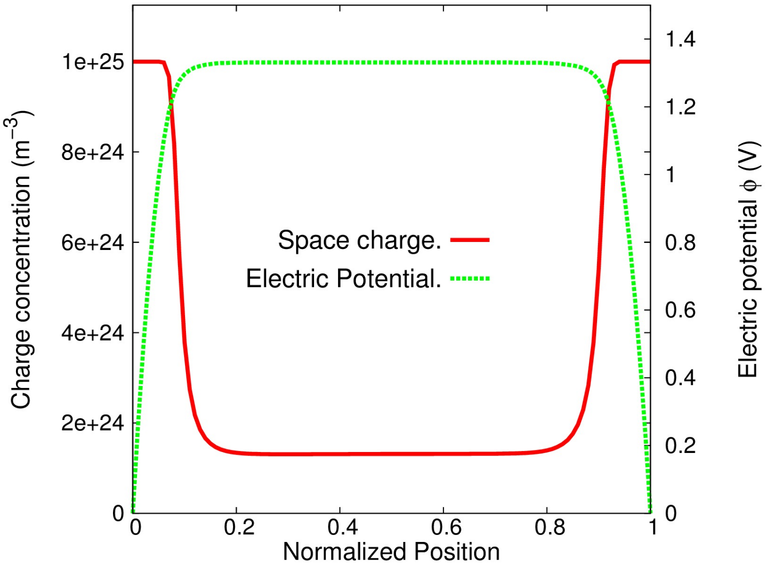

Figure 4.3: (Color online) Distribution of the electric potential and of the space charge along the cross section AA′ depicted in Fig. 1.3.

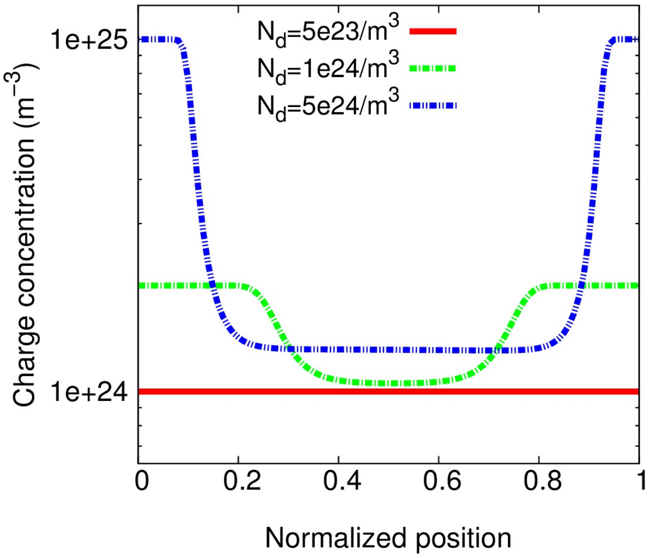

Figure 4.4: (Color online) The formed depletion layers for different concentrations of donors.

In this subsection the phase field model is applied to study the evolution of a 180° head-to-head domain wall for the cases with and without semiconducting features, respectively. Fig. 4.6(a) illustrates the initial configuration for the simulations. The left and right edges are short circuited, i.e. the electric boundary condition for the two edges are set to be potential-free, whereas, the

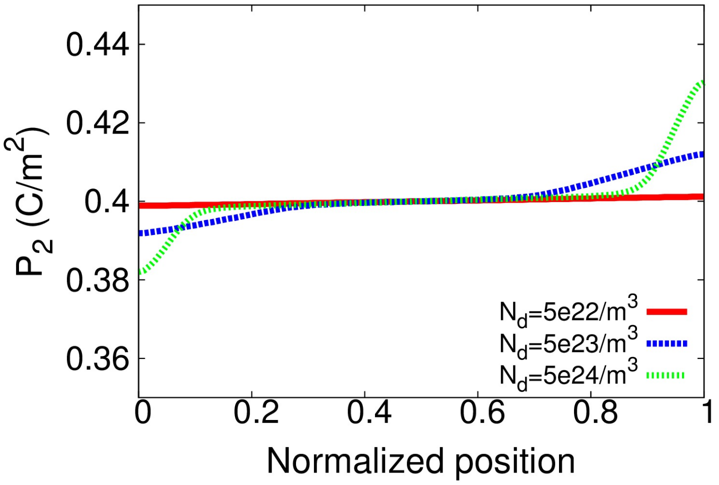

Figure 4.5: (Color online) Variation of P_2 due to the built-in potential.

system is periodically extended in the vertical direction. All the boundaries are supposed to be traction-free. Fig. 4.6(b) shows the obtained equilibrium domain configuration for the case that the space charge due to the semiconducting features is excluded. This lamellar domain structure is virtually charge-free. Unlike the phase field modeling by Wang and Kamlah [119], where the domain configuration in a ferroelectric nanotube was manipulated by prescribed surface charge density, the lamellar domain structure is introduced here by a periodical boundary setup. On the other hand, if the space charge of semiconducting nature is considered, the obtained equilibrium domain configuration remains almost the same as the initial one (Fig. 4.6(c)). The domain wall becomes simply thicker, as suggested by experimental observations [120]. Results indicate that the uncompensated polarization charges along the initial domain wall are now compensated by the free space charges from the semiconducting material (Fig. 4.7). In Fig. 4.7 the energy band of the electrons is also demonstrated. In this way the electrostatic energy due to the uncompensated polarization charges is counteracted by the contribution of the semiconductor space charges. This may also be justified by the distribution of the resultant electric potential and of the resultant polarization presented in Fig. 4.8.

4.4.1 Domain structure stability in the context of sharp interface model

This section is devoted to a quantitative study on the stability of the uncompensated domain walls and the influence of the space charges. To start with, one considers a domain wall between two hard domains with head-to-head polarization configuration, illustrated in Fig. 4.9. The

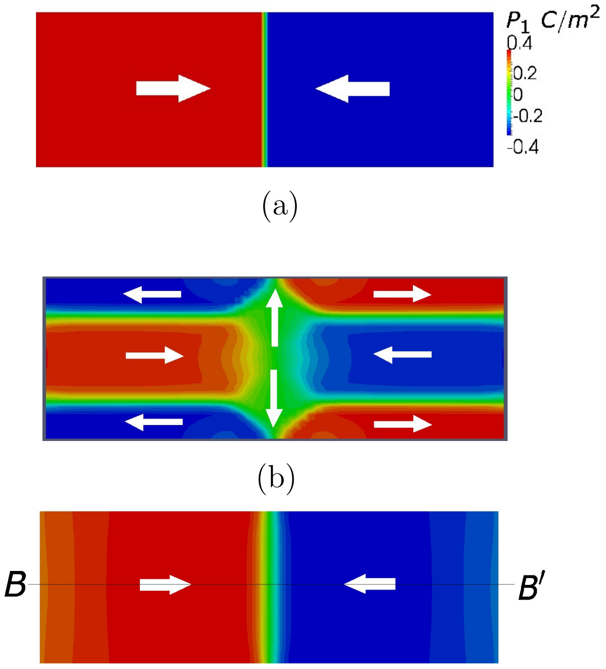

(a)

(b)

(c)

Figure 4.6: (a) The initial head-to-head domain configuration. (b) The equilibrium domain configuration without semiconducting features. (c) The equilibrium domain configuration with a donor concentration of $N_d = 5 \cdot 10^{23}\ \mathrm{m}^{-3}$.

driving force acting on the domain wall will be computed through numerically calculated nodal configurational forces.

According to Maugin [94], and as has been shown in Eq. (3.68), the Eshelby tensor for piezoelectricity has the form

$$\Sigma_{ij} = \Psi \delta_{ij} - u_{k,i}\sigma_{kj} + D_i E_j, \tag{4.6}$$

where Ψ denotes the free energy of the system which has the form expressed in Eq. (3.59). The corresponding configurational force vector is

$$g_i = -u_{j,i} f_j + \rho \phi_i, \tag{4.7}$$

where f_i is the volume force. In this study f_i is neglected. The condition

$$\Sigma_{ij,j} + g_i = 0, \tag{4.8}$$

must hold. That is, Σ_{ij} and g_i correlate to each other in a similar way as the Cauchy stress tensor and the volume force do. For a dielectric solid with an interface between two phases,

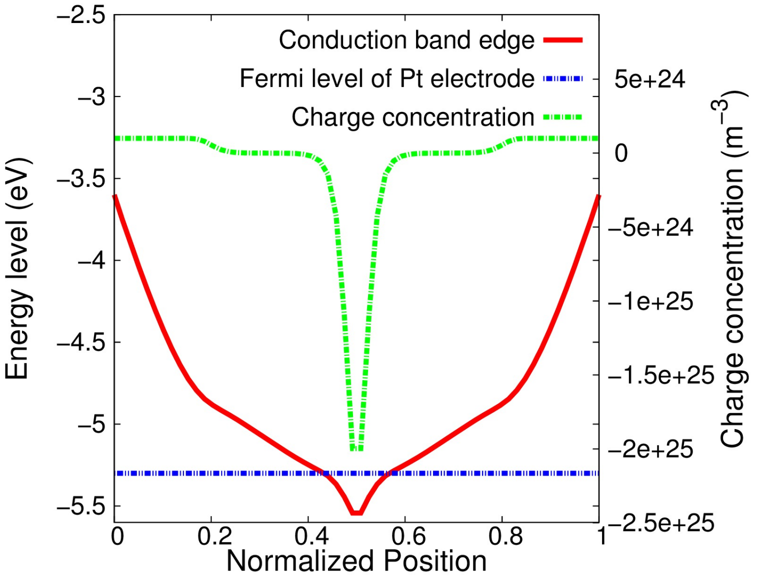

Figure 4.7: (Color online) Distribution of the conduction band edge and of the space charge along the cross section BB′ highlighted in Fig. 4.6. The donor concentration in this example is $N_d = 5 \cdot 10^{23}\ \mathrm{m}^{-3}$.

Σ_{ij} experiences a jump across the interface. The configurational force vector g_i is then concentrated at the interface, which can be interpreted as the driving force on the interface. For a selected control volume V_c the overall driving force and driving moment on the interface which is circumvented in the control volume V_c, is given [89, 86]

$$J_i = -\int_{V_c} g_i dV, \tag{4.9}$$

$$L_i = -\int_{V_c} \epsilon_{jki} x_j g_k dV, \tag{4.10}$$

where x_i is the location vector of the material point and ϵ_{ijk} denotes the Levi-Civita symbol. The volume integral may be rewritten into a path integral around the control volume according to the Gauss′ law. For the considered head-to-head domain configuration in Fig. 6.4, the integral path can be chosen as any path which circumvents the whole domain wall. Since there is no inhomogeneity inside both of the domains, no configurational force will appear in the interior of the domains. The configuration force appears merely along the domain wall. Therefore one can simply take the line along the domain wall as the integral path. In the FEM simulation, Σ_{ij} is calculated from the obtained field quantities, according to Eq. (3.73). The configurational force g_i at one element node is then calculated by summing up all the contributions from all adjacent elements around the node. After Eq. (3.74-3.78), the nodal driving force G_i^I at the node I is

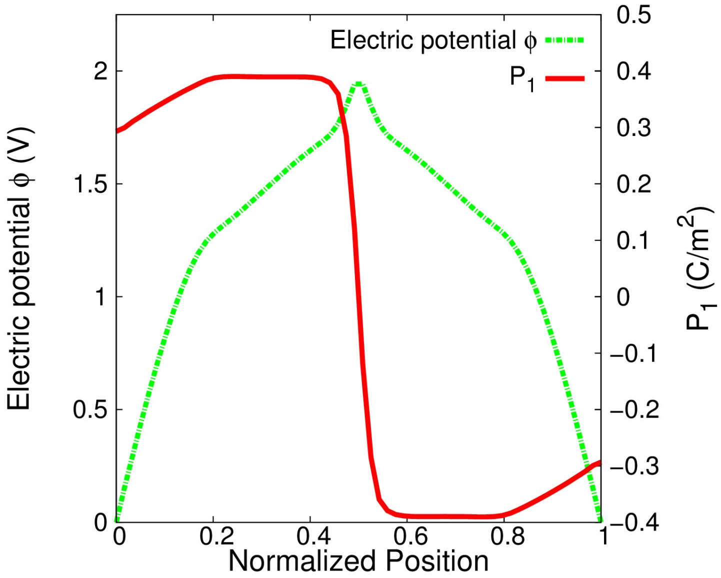

Figure 4.8: (Color online) Variation of the electric potential and of the horizontal polarization component P_1 along the cross section BB′ highlighted in Fig. 4.6. The donor concentration in this example is $N_d = 5 \cdot 10^{23}\ \mathrm{m}^{-3}$.

given by works [99, 121] as

$$G_i^I = \bigcup_{e=1}^{n_{el}} \int_{\Omega_e} \Sigma_{ij} N_{,j}^I d\Omega, \tag{4.11}$$

where the assembly operation is performed over all elements adjacent to node I, Ω_e is the element area of the e-th element, n_{el} is the number of the elements around the node I, and N^I is the shape function associated with the node I in the corresponding element. The derivative of the shape functions N^I can be computed in the same manner as for standard finite element techniques. The above mentioned approach for computing the nodal configurational force is now applied to the domain configuration shown in Fig. 4.9. In the considered head-to-head domain configuration, the domain wall orientation is characterized by the angle α with respect to the horizontal. In this simulation the mechanical aspects are neglected, since one focuses on a mechanical stress-free situation. Because the component of the configurational force tangential to the domain wall induces no motion, the normal component (the driving force) will be particularly discussed. Depending on the external loading and the charge compensation, the following four cases are studied separately.

Mokry et al derived a general formula for the local pressure on a charged domain wall considering full or partial compensation of bound polarization charges by free charges [105]. It is shown that the compensation can lead to a very strong reduction of the pressure imposed on the wall from the electric field.

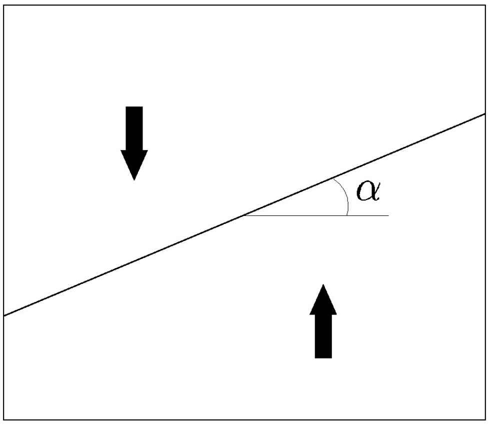

Figure 4.9: (Color online) An illustrative sketch of a head-to-head domain configuration with the domain wall angle α.

In the following it will be shown that the jump of Maxwell stress tensor across the interface equals to the driving force.

$$\begin{aligned} [\![\sigma^m_{ij} n_j]\!] &= [\![(E_i D_j - D_m E_m \delta_{ij}) n_j]\!] \\ = \langle E_i \rangle [\![D_j n_j]\!] &+ [\![E_i]\!] \langle D_j \rangle n_j - [\![D_m]\!] \langle E_m \rangle n_i - \langle D_m \rangle [\![E_m]\!] n_i \\ &= \langle E_i \rangle [\![D_j n_j]\!] - [\![D_m]\!] \langle E_m \rangle n_i. \end{aligned} \tag{4.12}$$

It is seen that the first term has $[\![D_j n_j]\!]$ which means the free charge compensation on the sharp interface. In the case without free charge compensation, the driving force reduced to

$$f_i = -[\![D_m]\!] \langle E_m \rangle n_i = 2PEn_i. \tag{4.13}$$

That is, no matter how large the tilt angle of the domain wall is, the driving force on the domain wall due to the electric field is always $2PE$ and the direction is perpendicular to the domain wall. For the case that the bound charge is totally compensated by the free charge, one has $[\![D_j n_j]\!] = 2Pcos(\theta)$ and $<E_i> = Ecos(\theta) n_i$. Then the driving force becomes

$$\begin{aligned} f_i = \langle E_i \rangle [\![D_j n_j]\!] - [\![D_m]\!] \langle E_m \rangle n_i &= 2Pcos(\theta) Ecos(\theta) n_i - 2PE \\ &= 2PE(cos^2(\theta) - 1). \end{aligned} \tag{4.14}$$

Therefore in this case the driving force varies with the tilt angle of the domain wall. It is zero at $\theta = 0, \pi$ and $2PE$ at $\theta = \pi/2$.

Case 1: Without external electric field and charge compensation. In this case the top and the bottom surfaces are set to be potential-free. For $\alpha = 0°$, the driving force is zero everywhere along the domain wall. The system resides in an equilibrium but energetically

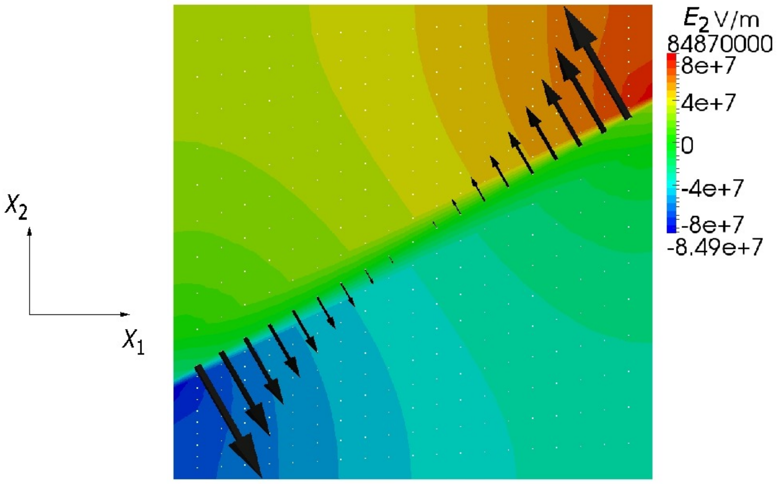

Figure 4.10: (Color online) Distribution of the vertical component of the electric field and of the configurational force vector along the domain wall with the angle $\alpha = 30°$. This plot is for Case 1, namely without applied electric field and charge compensation.

unfavorable state. Therefore it is not stable and will develop into a more stable state if the polarization is free to evolve, as the example in Section 4.3 demonstrates. For $0° < \alpha < 90°$, there is a resultant configurational moment on the interface (Fig. 4.10), due to the inhomogeneity of the electric field resulting from the uncompensated polarization charges. This moment implies that the domain wall intends to rotate to the vertical position to minimize the total energy of the system, as it will be demonstrated by the phase field simulations in the next section. The dependence of the resultant driving moment on the angle α is plotted in Fig. 4.11. This moment reaches its maximum at about $\alpha = 45°$. For $\alpha = 90°$, there is no uncompensated polarization charge and thus no inhomogeneity of the electric field. This explains that the driving force for the vertical domain wall is zero along the domain wall.

Case 2: Without external electric field but with full charge compensation. It is assumed in this case that the charges on the sharp interface due to the polarization is fully compensated, e.g. by free charge carriers available in the system. Since the domain wall is fully compensated by free charge carriers, there is no induced internal electric field for any angle α. Thus in absence of the external field, there is no driving force in the considered area.

Case 3: With external electric field but without charge compensation. When the sample is applied with an electric field of 10^7 V/m in the vertical direction, a distribution of driving force is induced along the domain wall, see Fig. 4.12. The driving force favors the growth of the domain whose polarization takes the same direction as the applied electric field. The average of the calculated driving force on the domain wall agrees with the analytical solution for the pressure on the domain wall obtained by Mokrý et al. [105]. The average driving force

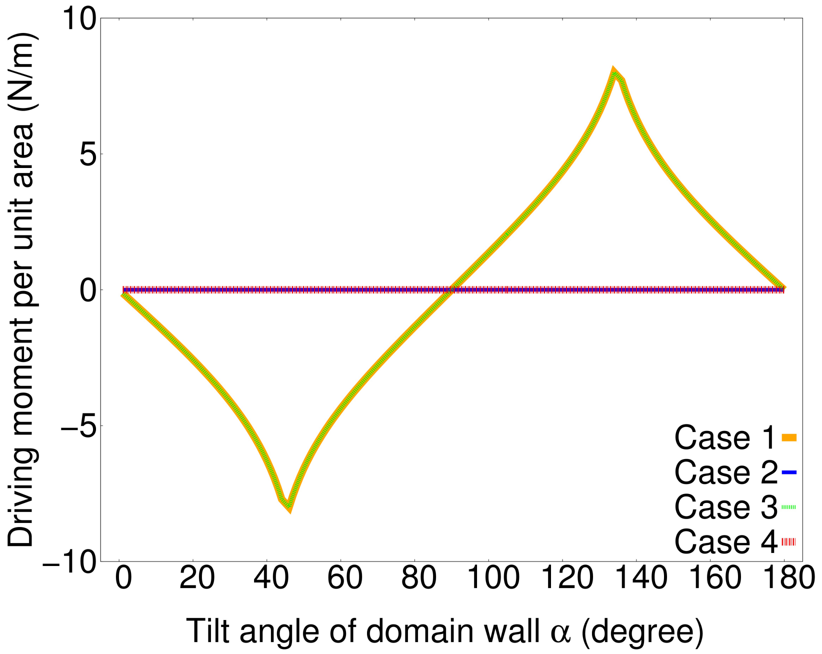

Figure 4.11: (Color online) Driving moment per unit area on the domain wall vs the domain wall tilt angle for the cases 1-4.

is also independent of the angle α (Fig. 4.13). This phenomenon was also observed in the work of Mokrý et al. [105]. On the other hand, due to the fact that the uncompensated polarization charges induce also inhomogeneous internal electric field, the driving force along the domain wall should not be homogeneous. Therefore there is a variation of the driving force along the domain wall (Fig. 4.10). Subtracting the driving force by its average value, one can obtain the variation in the same fashion as that in Fig. 4.13 for Case 1. Therefore there should exist a driving moment, which takes its maximum at the angle 45°. As it can be seen in Fig. 4.11, the dependence of the resultant moment on the angle α is exactly the same for both Case 1 and Case 3.

Case 4: With external electric field and full charge compensation. Similar to Case 2, full charge compensation implies no internal electric field. The driving force is merely due to the external electric field. In other words, the driving force remains uniform along the domain wall, and there is no driving moment. The driving force has a trigonometric dependence on the angle α, as it is shown in Fig. 4.13. If $\alpha = 0°$, there is no driving force on the interface, indicating a stable domain structure. When $\alpha = 90°$, the driving force takes the same value as the average value of the driving force in Case 3. For other angle α, besides the normal driving force there is a tangential component along the interface, which, however, does not play a role in the domain wall motion. An example of a partly compensated interface has also been studied, which appears as an intermediate situation between the case with full compensation and the

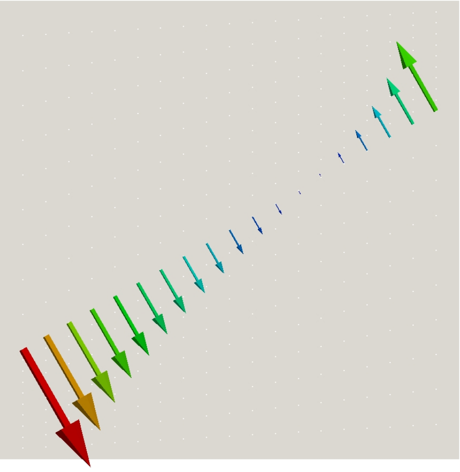

Figure 4.12: (Color online) Distribution of the configurational force vector along the domain wall with $\alpha = 30°$. This is for Case 3, namely with an applied external electric field and no charge compensation.

one without compensation. It is seen from Figs. 4.11 and 4.13 that the external electric field is responsible for the average normal driving force on the domain wall, whereas the inhomogeneity of the internal electric field induced by the uncompensated polarization charges causes the resultant driving moment on the domain wall. The situation of the driving force and moment for the four cases is summed up Table 4.4.1. The numerical solution matches the analytical solution made before, and it can further provide driving moment where the analytical method is impotent.

Table II: Summary of the results on the driving moment and the driving force for the cases 1-4.

Full charge compensation	Orientation dependent driving force, no driving moment	No driving force, no driving moment,
No charge compensation	Constant driving force, orientation dependent driving moment	No driving force, orientation dependent driving moment

Note that the force acting on the above considered charged wall is by one order of the magnitude larger than the inhomogeneous clamping pressure exerted upon an uncharged domain wall emerging due to the migration of oxygen vacancies [122, 123]. These two forces become, however, comparable for the applied electric fields of the order of the internal bias $E_{ib} \simeq 10^6$ V/m.

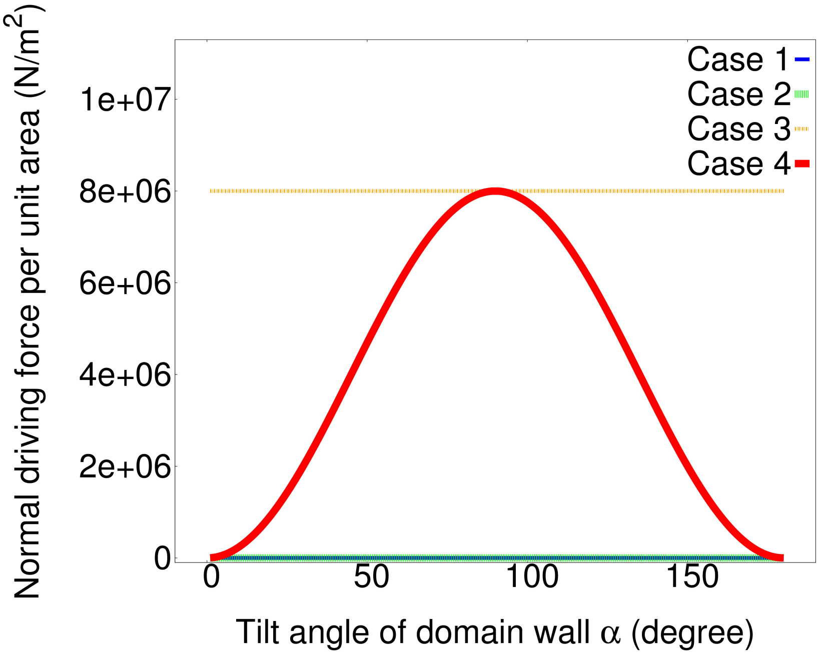

Figure 4.13: (Color online) Normal driving force per unit area vs. the domain wall tilt angle for the cases 1-4.

4.4.2 Rotational stability of domain structure in the context of phase field model

Phase field simulations based on the model presented in Section 3.1.4 are now performed to verify the predicted domain wall rotation in Section 4.4.1 and its stabilization by space charges. An initial tail-to-tail domain configuration with $\alpha = 60^\circ$ is used. Three different examples are considered: ferroelectrics free of semiconducting features, ferroelectrics with $N_d = 10^{24}\mathrm{m}^{-3}$ and $N_d = 10^{25}\mathrm{m}^{-3}$. All examples are with short circuit boundary condition, i.e., zero potential is prescribed on the top and the bottom surfaces. For dielectric ferroelectrics where no space charge is available, the domain wall is charged. The driving moment leads to rotation of the domain wall. As Fig. 4.14(a) shows, at equilibrium the domain wall reaches the vertical position, in order to avoid charged domain configuration.

For ferroelectrics with $N_d = 10^{24}\mathrm{m}^{-3}$, due to the tail-to-tail domain configuration, a low electric potential arises in the interior ($\phi < -1.3\mathrm{V}$), and thus a high positive charge density develops. As a result of evolution, the potential in the interior increases and an almost uniform charge density appears. The domain wall reaches a position between the initial one and the vertical one at equilibrium, see Fig. 4.12(b). In the case of $N_d = 10^{25}\mathrm{m}^{-3}$, an electric potential lower than that in the domain interior arises in the vicinity of the tilted domain wall together

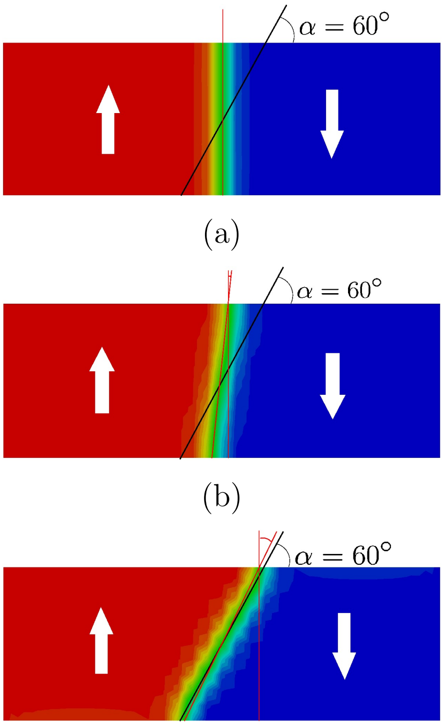

(a)

(b)

(c)

Figure 4.14: (Color online) Rotation of the domain wall as a result of the driving moment. The equilibrium domain configurations for (a) No semiconducting feature, (b) $N_d = 10^{24}$ m^{-3} and (c) $N_d = 10^{25}$ m^{-3}, respectively. The black line denotes the initial position of the domain wall.

with a high charge density, so that almost no domain wall motion occurs (Fig. 4.14(c)). Thus homogeneous distributed donors like oxygen vacancies can also hinder the domain wall rotation. This phenomenon is known as imprint [105, 124].

The rotated angle of the domain wall, from the initial configuration with α to its equilibrium state, is plotted with respect to the donor concentration in Fig. 4.15.

The variations of the total free energy and the driving moment during the domain evolution for three different examples are plotted in Figure 4.16. For the non-semiconducting case and the case of $N_d = 10^{24}\mathrm{m}^{-3}$, both the total free energy and the driving moment experience a sharp decrease at the beginning. As the evolution proceeds and the decrease of the free energy becomes slower, and the configurational moment decreases. After reaching an equilibrium, there is no configurational moment any more, and the free energy reaches its minimum. For the case of $N_d = 10^{25}\mathrm{m}^{-3}$, both quantities remain almost constant, indicating a freezing effect of domain wall by free charges. It implies that the configurational force can be correlated with the energy release rate during the evolution.

Simulations have also been performed for the corresponding cases with an initial head-to-head configuration and $\alpha = 60°$. In the case without semiconducting feature, the domain wall rotates

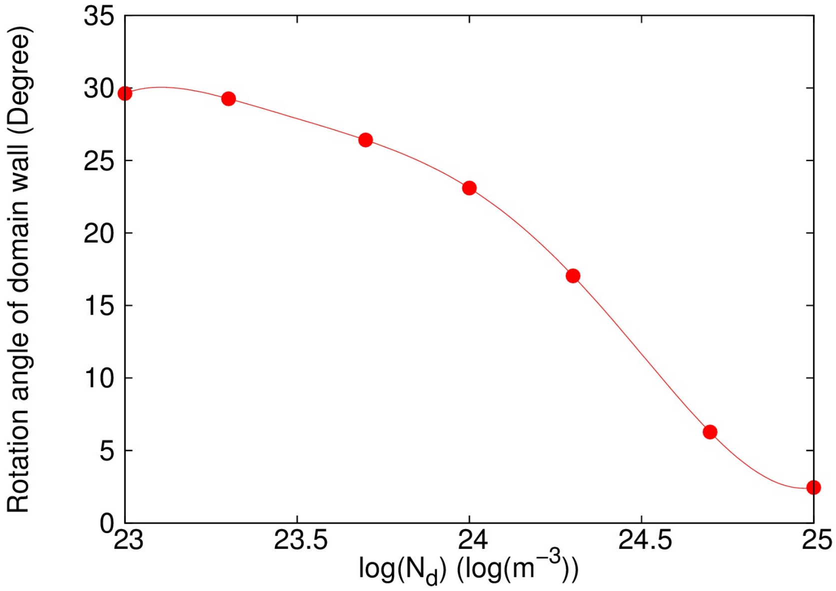

Figure 4.15: (Color online) The rotated angle of the domain wall after it reaches equilibrium.

to the vertical position after the equilibrium. Similar to the case of the corresponding tail-to-tail initial configuration, this is due to the driving moment. In the cases with semiconducting feature, the orientation of the domain wall at the equilibrium state depends on the donor concentration. In certain cases it can even evolve into a tail-to-tail structure. It should be noted that the equilibrium state can also depend on the specific choice of the Fermi level.

In this section only the self-equilibrium of the domain configuration is considered. When the external electric field is applied, the effect of the normal driving force due to the external electric field is usually more dominant than that of the driving moment. Moreover, there is a significant anisotropy of domain wall energy. Therefore the rotation motion of the domain wall is not visible. Instead, a kink-wise motion of the domain wall is observed.

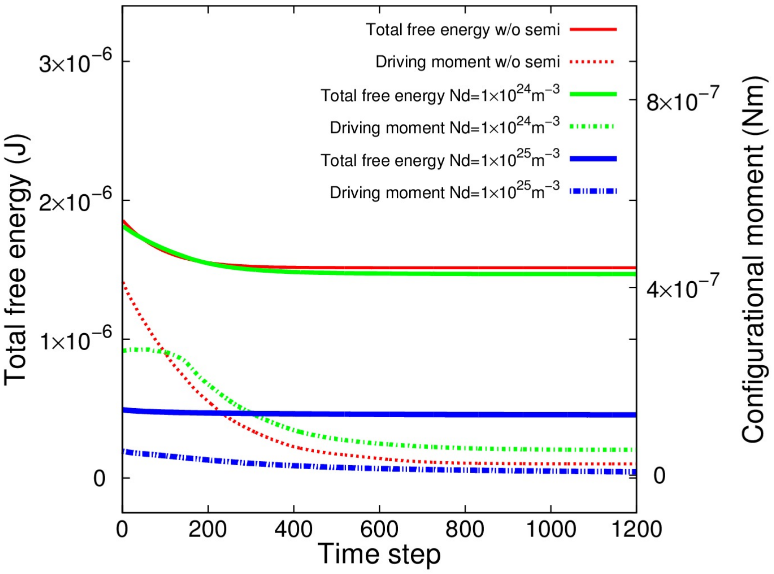

Figure 4.16: (Color online) Variation of the total free energy and of the configurational moment during the evolution of the domain structure into its equilibrium state.

Chapter 5

Conductivity of domain wall enhanced by space charge in ferroelectrics

Three kinds of 180° domain wall are ususally considered including: $'$up-down$'$, $'$head-to-head$'$ and $'$tail-to-tail$'$ which are classified as electrically neutral, positively and negatively charged respectively. Bound charges at domain walls generate large electric fields, making the domain structure unstable. However, Gureev et al. have shown that head-to-head and tail-to-tail domain configurations in electroded ferroelectric samples can be both energetically favorable and stable due to screening, if semiconducting features are taken into account [111]. Moreover, for head-to-head and tail-to-tail domain configurations, conductivity distribution across a charged domain wall was investigated and it was concluded that electrons accumulate around head-to-head domain walls [113]. Sluka et al. observed that charged domain walls become stable and conduct steadily through an electron gas [104]. It was demonstrated that the conductivity of head-to-head domain walls are much higher than that of the bulk material, whereas the tail-to-tail domain wall conductivity remains almost the same as the bulks$'$. In another study by Meier et al. [127], the tail-to-tail conductivity in $ErMnO_3$ was reported to be higher, whereas the conductivity at head-to-head domain wall experiences a drop which is in contrast to the aforementioned studies. In this work, using the phase field approach, one discusses the probable reason for this apparently inconsistent behavior of ferroelectrics.

The interplay between ferroelectric and semiconducting properties due to charge carriers in ferroelectrics has been studied extensively [130]. Semiconducting features of ferroelectrics have also been included in phase field modeling. Particularly, investigations have been made on the interaction between the oxygen vacancies and the different domain structures [100, 101, 131].

In reality, defect systems are typically much more complicated and include different vacancies and di-vacancies of constitutive elements in intentionally or unintentionally doped ferroelectrics [132]. For instance, in manganese doped barium titanate, manganese ions can occupy the titanium sites in the unit cell, thus giving rise to a defect system comprising of several point defects species. Hagemann observed enhanced aging effect in a manganese doped barium titanate related to oxygen vacancies associated with acceptor defects [133]. Lambeck and Jonker have concluded that the domain structures are stabilized due to volume effects in manganese doped barium titanate [134].

In this section, the charge compensation of charged 180° domain walls in barium titanate is studied by the phase field model and the influence on the domain wall conductivity is investigated. In contrast to Fridkin′s approach, who has previously considered similar configurations [130], the elastic variables coupled to the polarization are included consistently. The electromechanical coupling makes a difference to the similar space charge effects at grain boundaries thoroughly studied by Waser et al [135, 136].

Two defect systems are considered: a defect system where oxygen vacancies are the only point defects and a more realistic defect system where doping by manganese gives rise to several kinds of point defects. The first system allows for the comparison of our simulations with those of other groups performing modelling under similar conditions [100, 101]. The second defect system relies on density functional calculations of the defect energies [132], the concentrations of defects arising from high temperature sintering, and the subsequent quenching to normal conditions [50, 137]. These evaluations account for the temperature dependence of both the charge state and the concentration of defects. For both systems the influence of the donor or acceptor concentrations, type of domain configuration and material of electrodes on the electron or hole compensation of the polarization bound charges and, thus, on the conductivity of domain walls is established.

5.1 Domain wall conductivity of a simplified defect system

The space charge $\rho(\phi)$ can be expressed by semiconductor theory. In Mn-doped barium titanate synthesized under Ba-rich conditions, the following species commonly contribute to the local space charge: oxygen vacancies, titanium vacancies, oxygen-titanium di-vacancies, manganese-titantium substitutions, electrons and holes [132]. Oxygen vacancies act as donors, whereas titanium vacancies, oxygen-titanium di-vacancies and manganese-titanium substitution act as acceptors due to their valency. The space charge is then expressed as [59]

$$\begin{aligned}\rho(\phi) = -qN_C F_{1/2}\left(\frac{E_F - E_C + q\phi}{k_B T}\right) \\ +qN_V F_{1/2}\left(\frac{E_V - E_F - q\phi}{k_B T}\right) + qz_{V_O} N_{V_O} t_{V_O}(\phi) \\ -qz_{V_{Ti}} N_{V_{Ti}} t_{V_{Ti}}(\phi) - qz_{[V_{Ti}-V_O]} N_{[V_{Ti}-V_O]} t_{[V_{Ti}-V_O]}(\phi) \\ -qz_{Mn_{Ti}} N_{Mn_{Ti}} t_{Mn_{Ti}}(\phi).\end{aligned} \tag{5.1}$$

The Kröger−Vink notation is adopted throughout this paper, i. e., Mn_{Ti} denotes a manganese ion sitting on a titanium lattice site and V_{Ti} denotes a titanium vacancy. The electron charge is denoted by q, number of states in conduction band by N_C, valence band by N_V and Fermi level by E_F. Energy levels of the edge of the conduction band and the valence band are denoted by E_C, E_V. Valence number, concentration and ionized portion of each defect species are denoted by $z_{(\cdot)}$, $N_{(\cdot)}$ and $t_{(\cdot)}$. k is the Boltzmann constant and the absolute temperature is T. The Fermi integral $F_{1/2}$ is evaluated numerically by using the scheme suggested by van Halen et al. [98].
The 2D model described above is used to investigate charge compensation of ′head-to-head′ and ′tail-to-tail′ domain walls, and its contribution to the domain wall conductivity. In simulations, the left and right edges of a barium titanate sample are short circuited and the top and bottom edges are charge free. In a short circuited case, the Fermi level in Eq. 5.1 is determined by the type of a conductor used for the electrode. In fact, the true position of the Fermi level depends on the energy band alignment in the involved ferroelectric and electrode materials, particularly on the formation of the Schottky barrier at the interface [138]. As will be shown in the following section, the position of the Fermi level does not have a remarkable effect on the conductivity properties of the domain walls. Consequently, for simplicity, the position of the Fermi level will be assumed to coincide with that of the electrode.
The initial configuration is comprised of two domains whose polarization points towards (”head-to-head”) or opposite (”tail-to-tail”) of each other. For comparison, a semiconducting barium titanate with a defect system is first considered where only oxygen vacancies act as donors, i.e., only the first three terms on the right side of Eq. (5.1) are taken into account. In this case, electrons, holes and ionized donors can contribute to the local space charge. Simulations are conducted for samples with different oxygen vacancy concentration: 10^{24}m^{-3}, $3 \times 10^{24}\text{m}^{-3}$, $5 \times 10^{24}\text{m}^{-3}$ and $7 \times 10^{24}\text{m}^{-3}$.

For the head-to-head initial configuration, a positive electric potential is established in the middle (Fig. 5.1(b), 5.2(b)), and the free electrons in the conducting band accumulate near the domain wall (Fig. 5.1(a), 5.2(a)). As follows, the positive bound charge due to the head-to-head configuration is screened, and the initial domain configuration is stabilized. For the tail-to-tail case, from the ferroelectric-electrode interface to the interior, the electric potential increases above $1.3V$ where the material is almost free of charge such that the polarization remains relatively constant (Fig. 5.1(d), 5.2(d)). Near the domain wall, the electric potential sharply decreases below $-1.5V$ where holes begin to appear in the valence band, making the domain

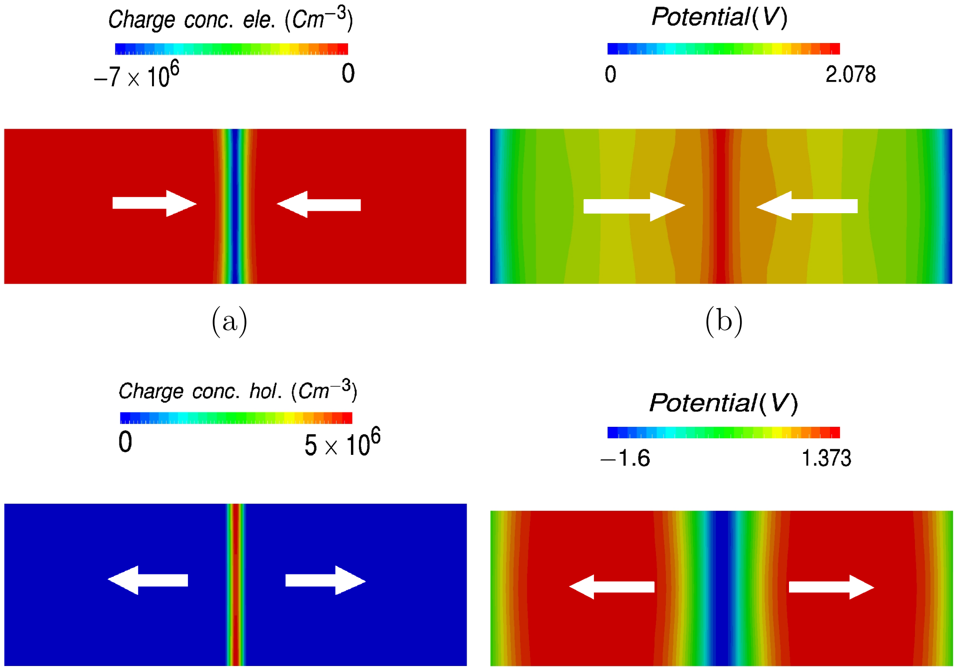

(a) (b)

(c) (d)

Figure 5.1: In a head-to-head domain configuration with a donor defect concentration of $N_{V_O} = 10^{24}\mathrm{m}^{-3}$: (a) distribution of space charge of electrons; (b) distribution of electric potential. In a tail-to-tail domain configuration with the same defect concentration: (c) distribution of space charge of holes; (d) distribution of electric potential.

wall vicinity positively charged (Fig. 5.1(c), 5.2(c)). Hence the bound charge by the tail-to-tail domain configuration is also counteracted. The otherwise unstable head-to-head and tail-to-tail domain structures are both stabilized by the semiconducting space charges. The conductivity of both the head-to-head and tail-to-tail domain walls of ferroelectrics with semiconducting features is enhanced by the accumulation mobile space charges. This conductivity is locally larger by several orders of magnitude compared to that of the bulk ferroelectrics.

The peak value of the space charge concentration at the head-to-head domain wall is larger than the one at the tail-to-tail domain wall for the case of $N_{V_O} = 10^{24}\mathrm{m}^{-3}$. Furthermore, the space charge in the head-to-head domain structure is totally attributed to electrons, while in the tail-to-tail domain structure the space charge is comprised of both holes and ionized donors. Since the mobility of the latter is much smaller than the mobility of electrons, their conductivity can be neglected. Therefore one may conclude that in the $N_{V_O} = 10^{24}\mathrm{m}^{-3}$ case the conductivity of the head-to-head domain wall is higher than that of the tail-to-tail domain wall, as it might be the case in the experimental study by Sluka et al, where, however, the density of oxygen vacancies was not evaluated [104].

For the head-to-head configuration, electrons serve as the only possible source of compensation

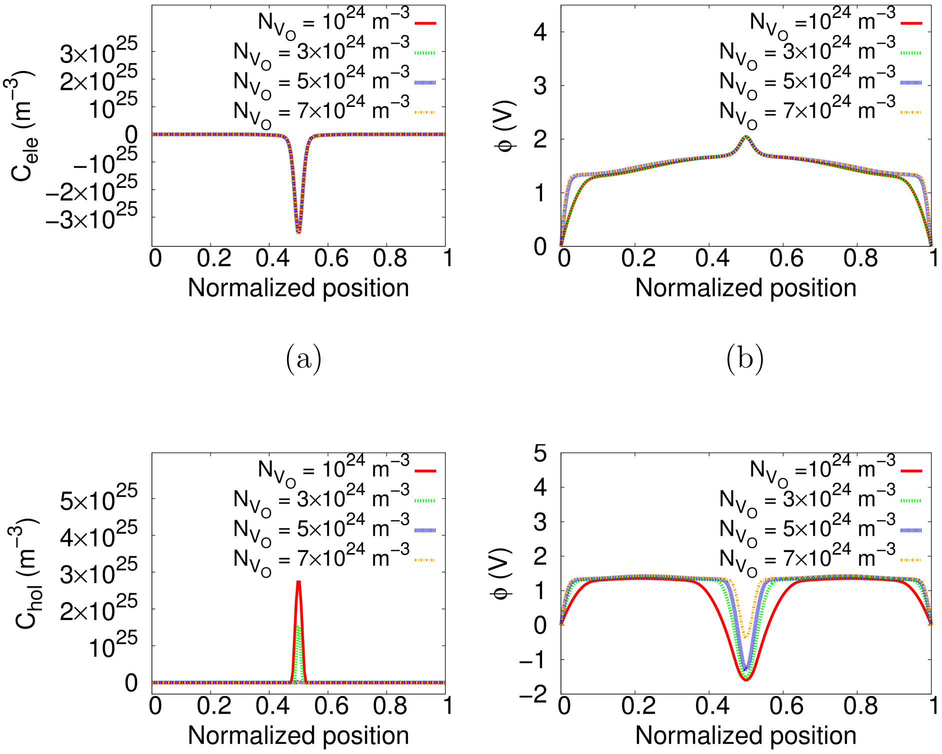

(a) (b)

(c) (d)

Figure 5.2: In the simplified system, in a head-to-head domain configuration: (a) Concentration of electrons; (b) Distribution of electric potential. In tail-to-tail domain configuration with the same defect concentration: (c) Concentration of holes; (d) Distribution of electric potential.

for the positive bound charges. No matter how large the oxygen vacancy concentration is, the electric potential in the vicinity of the domain wall maintains the same profile, and so does the space charge concentration of electrons. Therefore the donor concentration has almost no influence on the head-to-head domain wall conductivity (Fig. 5.2 (a)(b)). For the tail-to-tail configuration, in a low donor concentration case (10^{24}m^{-3}), the amount of positive charge provided by the donors is not sufficient to compensate the negative bound charges. Therefore the electric potential decreases such that enough holes are available at the domain wall (Fig. 5.2 (c)(d)). For a larger donor concentration ($3 \times 10^{24}\text{m}^{-3}$), the contribution of ionized oxygen vacancies also increases, while the proportion of holes decreases. When the donor concentration surpasses a certain threshold (approximately $5 \times 10^{24}\text{m}^{-3}$), the donors alone may provide enough positive space charges. This means that ionized donors are the sole source of compensation to the bound charge in the tail-to-tail domain structure (Fig. 5.2 (c)). Thus the conductivity of a tail-to-tail domain wall in ferroelectrics with relatively high donor concentration is very limited, which may explain the experimental results by Sluka et al. [104]

For both head-to-head and tail-to-tail domain structures, the electric potential and space charge profile from the normalized position 0.2 to 0.8 along xx′ are similar, no matter what electrode material is chosen. They differ solely in the value of the electric potential in the bulk, while the difference in potential corresponds to the difference in work function of the conductors. In this case, the type of conductors used for electrodes has limited influence on the domain wall conductivity.

5.2 Domain wall conductivity of a realistic defect system

In this section, the domain wall conductivity in a more realistic defect system is investigated, i.e. all the terms in Eq. (2.14) are included. The valency values for the first three kinds of defects are 2, 4 and 2. Electron paramagnetic resonance measurements show that Mn^{2+}, Mn^{3+} and Mn^{4+} are present in Mn-doped barium titanate [139]. In this study Mn^{3+} is taken as suggested by Zhang and Ren [140]. Barium titanate doped with 0.01mol%, 0.1mol%, 1mol% manganese is investigated by phase field simulations. The energy levels for conducting band, valence band and defect species in realistic defect system are taken from experiments and DFT calculations: $E_C = -3.2\text{eV}$, $E_V = -6.6\text{eV}$, $E_{V_O} = -3.25\text{eV}$, $E_{V_{Ti}} = -6.2\text{eV}$, $E_{[V_{Ti}-V_O]} = -6.39\text{eV}$ and $E_{Mn_{Ti}} = -5.3\text{eV}$ [132, 141, 142]. The concentration of each defect species for each doping case and the energy levels are listed in Table 5.2. It is seen that the concentration of oxygen vacancies increases with the increase of the doping concentration of manganese, whereas concentration of titanium vacancies and oxygen-titanium di-vacancies decreases. The manganese-titanium substitutions play a leading role among the defects. For the case of 1mol% manganese doping, the concentration of Mn-Ti substitutions is large enough so that the space charge provided is comparable to the holes′.

Table III: Concentration of defect species for different doping cases of manganese [137]

	0.01mol% Mn	0.1mol% Mn	1mol% Mn
N_{V_O}	$5.887 \times 10^{20}\text{m}^{-3}$	$5.811 \times 10^{21}\text{m}^{-3}$	$5.600 \times 10^{22}\text{m}^{-3}$
$N_{V_{Ti}}$	$3.612 \times 10^{20}\text{m}^{-3}$	$3.713 \times 10^{18}\text{m}^{-3}$	$4.017 \times 10^{16}\text{m}^{-3}$
$N_{[V_{Ti}-V_O]}$	$2.825 \times 10^{21}\text{m}^{-3}$	$2.863 \times 10^{20}\text{m}^{-3}$	$2.972 \times 10^{19}\text{m}^{-3}$
$N_{Mn_{Ti}}$	$1.5625 \times 10^{24}\text{m}^{-3}$	$1.5625 \times 10^{25}\text{m}^{-3}$	$1.5625 \times 10^{26}\text{m}^{-3}$

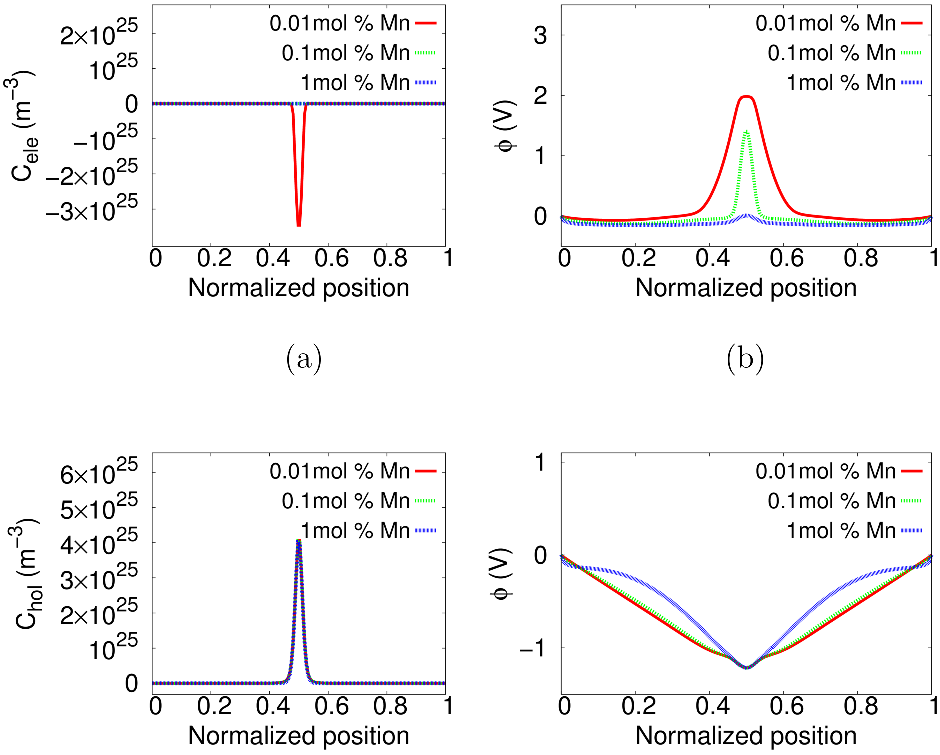

(a) (b)

(c) (d)

Figure 5.3: In the realistic system, for a head-to-head domain configuration: (a) distribution of space charge of electrons; (b) distribution electric potential. For tail-to-tail domain configuration: (c) distribution of space charge of holes; (d) distribution of electric potential.

As observed from Fig. 5.3 (b), in the head-to-head structure in a realistic defect system (0.01mol% Mn case), the electric potential at the domain wall goes to approximately 2V, where electrons begin to appear in the conduction band. This negative charge then compensates the positive bound charge due to the head-to-head configuration, like in the simplified defect system. For the 0.01mol% manganese doping case, most of the compensating charge comes from electrons while the ionized manganese-titanium substitutions also make a small contribution (Fig. 5.3 (a)). As the concentration of doping manganese increases, the proportion of compensating charge coming from ionized manganese also increases, and the proportion of compensating charge coming from electrons decreases correspondingly. The electrons at the domain wall virtually vanish as the manganese concentration reaches a certain threshold. As can be seen from Fig. 5.3 (b), for the 0.1mol% manganese doping case, electric potential rises to about 1.47V at the domain wall, no electrons longer appear at the domain wall. On the contrary, the width of the domain wall increases, so that sufficient compensating charge due to acceptors is available. For the 1mol% manganese doping case, there is a small electric potential at the domain wall in order to acquire

sufficient negative space charge from ionized manganese-titanium substitutions, since their concentration is large enough. The peak value of space charge at the domain wall gets larger and the domain wall width becomes thinner again.
As can be seen from Fig. 5.3 (c)(d), for a tail-to-tail domain wall most of the free charge compensating the charged domain wall comes from holes, and only a small portion comes from ionized oxygen vacancies. The space charge density from ionized oxygen vacancies is 188.6Cm^{-3}, 1862Cm^{-3} and 17940Cm^{-3} for 0.01mol%, 0.1mol% and 1mol% manganese doping, respectively. These values are too small in comparison to the space charge contribution from holes (approximately $6.5 \times 10^6\text{Cm}^{-3}$). The peak value of the space charge from holes increases slightly as the manganese concentration increases. Therefore it may be concluded that the concentration of manganese plays no significant role in the tail-to-tail domain wall conductivity and the domain wall width. This means that intentional or unintentional acceptor doping is in favor of higher conductivity of the tail-to-tail domain walls. Being a p-type semiconductor, ErMnO_3 studied by Meier et al. [127] is predispositioned to the compensation of tail-to-tail domain walls by holes even without doping while the positively charged head-to-head domain walls cannot be stabilized by sparse electrons.

5.3 Energy of the domain walls

The structure and properties of the tail-to-tail and head-to-head domain configurations play an important role not limited for stationary properties of ferroelectrics like conductivity but also for dynamic processes like polarization switching. During the polarization reversal such configurations inevitably emerge [143]. Thermodynamical analysis by Landauer within the classic dielectric description [143] has shown that the activation energy for the reverse domain nucleation is far too large to allow for polarization switching at realistic conditions. Account of different factors reducing this energy, e.g. ferroelectric anisotropy, electrode surface roughness, charge carrier injection [144, 145, 146], still did not solve the energy paradox. In view of the results of the actual study a possible solution to this problem might consist in the substantial reduction of the domain wall energy when considering the semiconductor features [111, 131]. This domain wall energy reduction largely originates from the strong decrease of the depolarization field which is limited by the energy gap of a semiconductor [137]. Being a phenomenological theory the phase field approach cannot deliver reliable absolute values of the domain wall energy because not all coefficients in the Gibbs energy Eq. (3.29) are known with certainty. It may, however, reveal how large the effect of the semiconducting properties on this energy is. To this end, the energy of the head-to-head and tail-to-tail domain walls was calculated for the following cases: (1) defect-free dielectric, (2) defect-free semiconductor with only electronic charge carriers

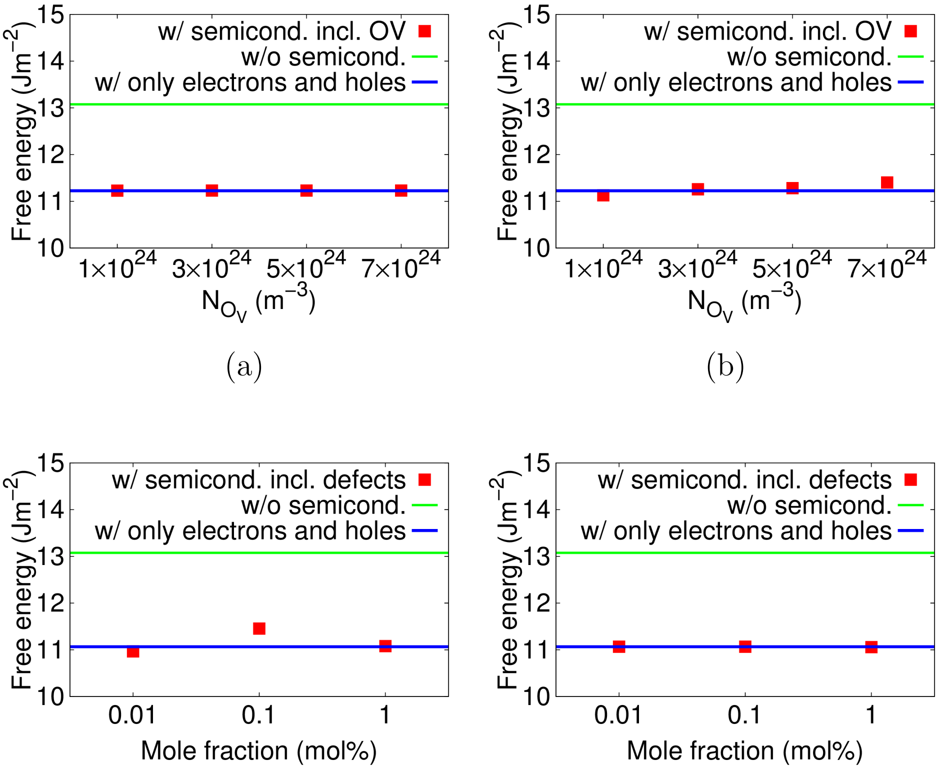

(a) (b)

(c) (d)

Figure 5.4: In the simplified system: free energy rescale to energy per unit area in (a) head-to-head configuration; (b) tail-to-tail configuration. In the realistic defect system: free energy rescale to energy per unit area in (c) head-to-head configuration; (d) tail-to-tail configuration. Red squares, green lines and blues lines denote semiconducting cases with point defects, semiconducting-free cases and semiconducting cases with only the electronic charge carriers respectively.

included, (3) semiconductor with a defect system. This is done for both domain configurations (head-to-head and tail-to-tail) and both types of defect systems (simplified and realistic). The latter two cases use the parameters described in the simulation section. In Fig. 5.4, it is shown that the domain wall energy in case (1) is always the largest (approximately 13Jm^{-1}), no matter what type of domain configuration and defect system considered. In the head-to-head simplified system configuration and in the tail-to-tail realistic defect system configuration cases, the free energy of domain wall of case (3) is almost the same as in the case (2) (Fig. 5.4 (a)(d)), since the bound charge is totally or almost totally compensated by the electronic charge carriers. In the other two, the free energy of case (3) lies above or below case (2), depending on the concentration of defect species (Fig. 5.4 (b)(c)). Thus, the screening effect due to the semiconducting features in fact reduces the energy of the domain wall but not by orders of the magnitude which is needed for solving the nucleation energy paradox.

Chapter 6

Influence of static defect dipole on behaviour of aged ferroelectrics

6.1 Introduction

In ferroelectrics, oxygen vacancies and acceptor impurities coexists. The impurity cation lies at the center of the unit cell and the oxygen vacancy lies on the one of six possible faces. Thus they form a defect dipole. This defect dipole can generate an extra electric field in addition to the depolarization field and external applied field. Among those, oxygen vacancy is a common kind of point defect that largely influences the electromechanical properties of ferroelectrics [147]. The understanding of such effect is important in explaining the mechanism of aging and fatigue of ferroelectrics.

6.2 Phase field model for ferroelectrics with static defect dipoles

For the purpose of investigating the effect of oxygen vacancy on the material behavior, several experiments have been conducted. Some researchers proposed the hypothesis from experiments that the gradual degradation is caused by the dipoles of oxygen vacancies [148]. In several experiments, aged ferroelectrics crystals exhibit large recoverable strain and double hysteresis loop

[149, 140, 150]. Theoretical and numerical methods are developed to studied the motion and distribution of oxygen vacancies. There are analytic solutions for a phenomenological model, e.g. [39]. Research has been completed by using a 2D four state Potts model [151], in which the effect of domain wall and electrostatic field was not taken into account. Phase field models have also been developed to study the interactions of oxygen vacancies with domain structures in ferroelectric single crystals [100, 101]. Those methods treat the oxygen vacancies as point defects and are not able to capture the character of the bias field caused by the oxygen vacancies and, thus, predict memory effect in the ferroelectrics. Recently a phase field model has been developed to study how oxygen vacancies influence the domain structure in ferroelectric single crystals. In this model, the oxygen vacancies are considered as defect dipoles. A finite difference scheme and a fast Fourier transformation is adopted for the computation [78]. In this chapter, the phase field model including the effect of static defect dipoles of ferroelectrics is proposed, aiming to investigate the influence of static defect dipoles on overall behaviour of aged ferroelectrics.

The pairing between the oxygen vacancy on a face of the perovskite unit cell and the impurity cation in the center form an electric dipole. Thus a defect polarization vector P_i^d appears in addition to the spontaneous one, P_i^s . Furthermore, an internal electric field will arise due to the defect dipole and it is supposed to have influence on the self organization of the spontaneous polarization. According to [101], one can assume a proportional relationship between the distance of separation and truncating lattice points, which lie out of the range of sufficient influence of the dipole. Thus an empirical relationship between local defect polarization and local defect electric field can be written as [101].

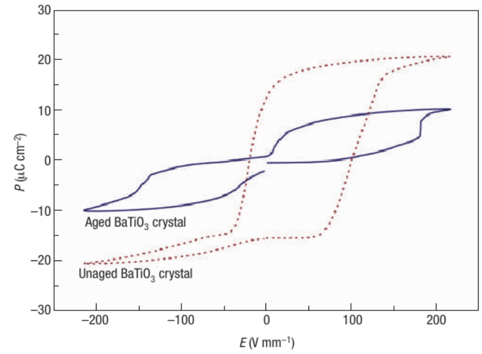

Figure 6.1: (Color online) Double hysteresis loop (P-E) of an BaTiO3 single crystal, compared with a normal hysteresis loop (dotted line) of the unaged sample (from Ren's work[149]).

$$E_i^0 = \frac{C_0 P_i^0}{\pi \kappa_0}, \tag{6.1}$$

where κ_0, C_0 are permittivity and a constant, respectively [152]. The total local polarization P_i^t and total local electric field E_i^t are then the sum of corresponding terms,

$$P_i^t = P_i^s + P_i^d, \tag{6.2}$$

$$E_i^t = E_i^e + E_i^d. \tag{6.3}$$

Then in this case Eq. (3.17) becomes

$$H^{ent}(\varepsilon_{ij}, E_i^t, P_i) = \frac{1}{2}(\varepsilon_{ij} - \varepsilon_{ij}^{\circ})[\mathbb{C}_{ijkl}(\varepsilon_{kl} - \varepsilon_{kl}^{\circ})] - (\varepsilon_{ij} - \varepsilon_{ij}^{\circ})(e_{kij}E_k^t) - \frac{1}{2}E_i^t(A_{ij}E_j^t) - P_iE_i^t. \tag{6.4}$$

After deriving the total free energy with respect to ε_{ij} and E_i^t, one gets the constitutive laws for ferroelectrics with static dipoles,

$$\sigma_{ij} = \frac{\partial H}{\partial \varepsilon_{ij}} = \mathbb{C}_{ijkl}(\varepsilon_{kl} - \varepsilon_{kl}^0) - e_{kij}E_k^t, \tag{6.5}$$

$$D_i = \frac{\partial H}{\partial E_i^t} = e_{ijk}(\varepsilon_{jk} - \varepsilon_{jk}^0) + A_{ij}E_j^t + P_i^t. \tag{6.6}$$

The evolution of spontaneous part of the polarization obeys the Landau-Ginzburg equation.

$$\dot{P}_k^s = -M_{ki}\frac{\delta H}{\delta P_i^s}. \tag{6.7}$$

More details of the numerical implementation can be found in the Appendix C.

6.3 Results

In the BaTiO$_3$ studied here, the material is supposed to have been aged for sufficient amount of time. The P_i^d is therefore parallel to the local P_i^s at the initial state [149]. The motion of oxygen vacancy is slow enough so that in the modeling the oxygen vacancy is considered to be fixed as the polarization domains evolve. Furthermore, the oxygen vacancy density is assumed to be uniform within the body studied. A BaTiO$_3$ rectangle of size $16 \times 10^{-7}m \times 8 \times 10m^{-7}$ with (001) aligned along the y axis is studied. The electric potential on the lower surface is fixed to zero and the electric potential on the upper surface varies as a triangle function with the maximum value $4 \times 10^6 Vm^{-1}$. The stress free boundary condition is assumed for the mechanical quantities ($\sigma_{ij}n_j = 0$), and flux free boundary conditions for the polarization ($P_{i,j}n_j = 0$). Two kinds of domain structures are studied: a rank-2 domain structure with 90° and 180° domains and a rank-1 domain structure with 180° domains. Both types are commonly observed in real ferroelectric crystals. As the ferroelectric ceramic ages, the spontaneous polarization configuration arrives at a rank-1 or rank-2 domain structure, and the defect polarization tend to be aligned with spontaneous ones, resulting in a minimization of electrostatic energy. Therefore, for both of the domain structures, the directions of defect dipole polarizations coincide with those of the defect spontaneous ones at the initial state.

6.3.1 Rank-2 domain structure

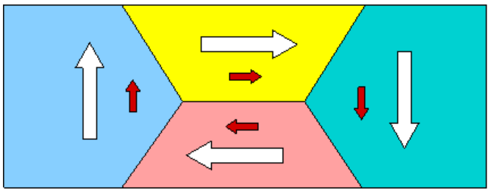

Figure 6.2: (Color online) A schematic sketch for polarization distribution of a 90° domain structure. The red arrows and white arrows denote defect dipoles and spontaneous polarization, respectively.

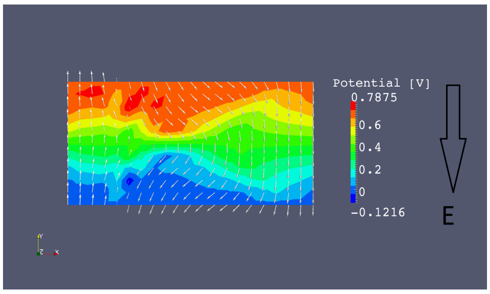

Figure 6.3: (Color online) The polarization and the electric potential distribution in BaTiO3 single crystal for a rank-2 initial domain structure during poling.

A vortex domain configuration, shown in Fig. 6.2, is taken as the initial configuration for the first example. A corresponding distribution of defect dipoles of magnitude 0.0, $2.75 \times 10^{-5}\mathrm{Cm}^{-2}$ and $6 \times 10^{-5}\mathrm{Cm}^{-2}$ is assigned. For the simulation 240000 time steps are applied, which constists of two cycling periods of electric fields. As the exterior electric field increases, domains favored by the electric field grow at the expense of other decreasing domains. The domain favored by the exterior field grows and the two domains lying perpendicular to the field shrink (Fig. 6.3). After the electric field reaches a certain threshold, the domain against the field switches and a single domain arises. After further loading the polarization increases only linearly, which corresponds to the saturation point on the hysteresis curve. This is plotted with electric field against polarization (Fig. 6.4). The electric field returns to zero. This can be seen from the hysteresis curve, when the defect dipoles are large enough (about $4.5 \times 10^{-5}\mathrm{Cm}^{-2}$). The spontaneous polarization tends to follow the defect polarization in favor of a minimization of total energy of the depolarization and inner defect field, and the overall polarization again becomes nearly zero, which is commonly called the ′memory effect′ (Fig. 6.5). As the magnitude of defect dipoles increases, the required electric field for saturation of polarization increases too, resulting in a shift of the saturation point. Meanwhile, the double loop becomes more significant, and the accessible recoverable strain available is larger than the defect free case (Fig. 6.6). For large

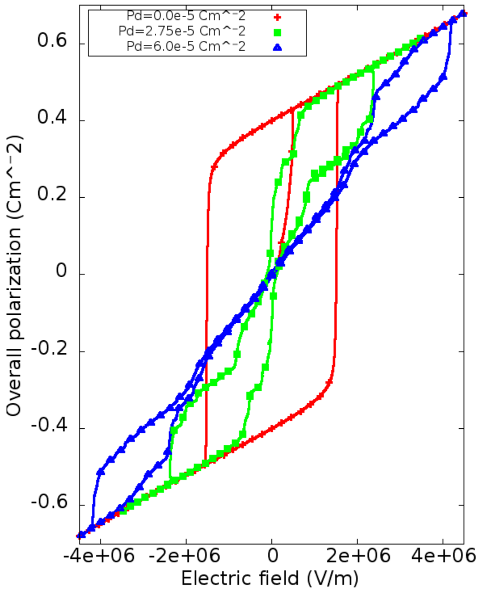

Figure 6.4: (Color online) The polarization hysteresis loop for a rank-2 domain structure of different defect dipole magnitude.

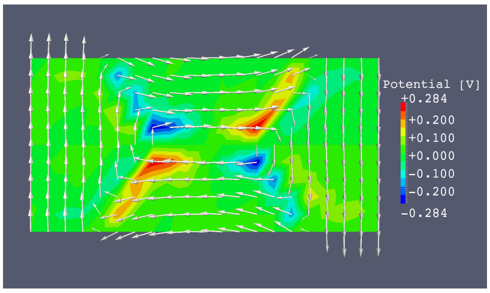

Figure 6.5: (Color online) The polarization and electric potential distribution for a rank-2 initial domain structure after removal of external electric field.

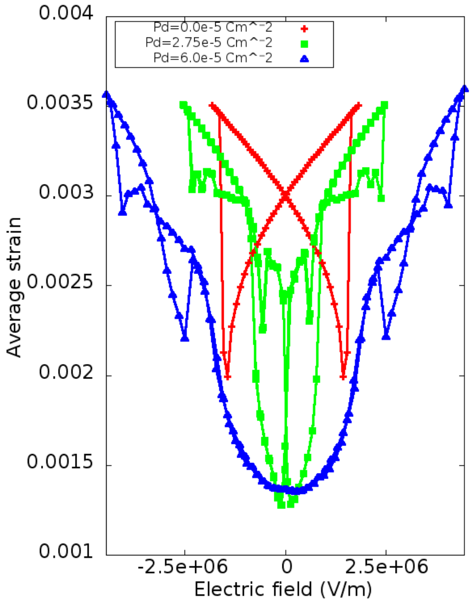

Figure 6.6: (Color online) The strain butterfly loop for a rank-2 domain structure of different defect dipole magnitude.

defect dipoles, the overall behavior of the ferroelectrics is almost becoming linear, as seen from Fig. 6.4. Such double loop effect is also experimentally verified from the ferroelectric single crystals [149, 140, 150].

6.3.2 Rank-1 domain structure

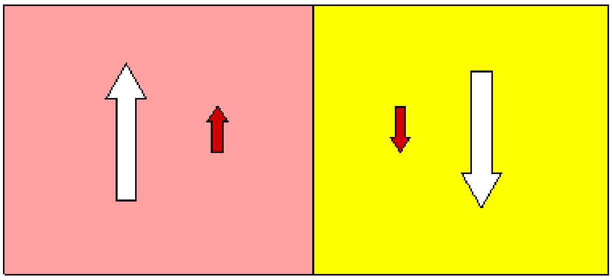

Figure 6.7: (Color online) A schematic sketch for polarization distribution of a 180° domain structure. The red arrows and white arrows denote defect dipoles and spontaneous polarization, respectively.

In the simulation, defect dipoles with values of 0.0, $2.75 \times 10^{-5}\mathrm{Cm}^{-2}$ and $6 \times 10^{-5}\mathrm{Cm}^{-2}$ are

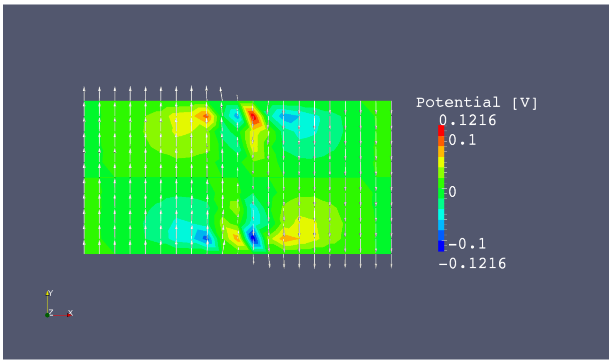

Figure 6.8: (Color online) The polarization and electric potential distribution for a rank-2 initial domain structure after removal of external electric field.

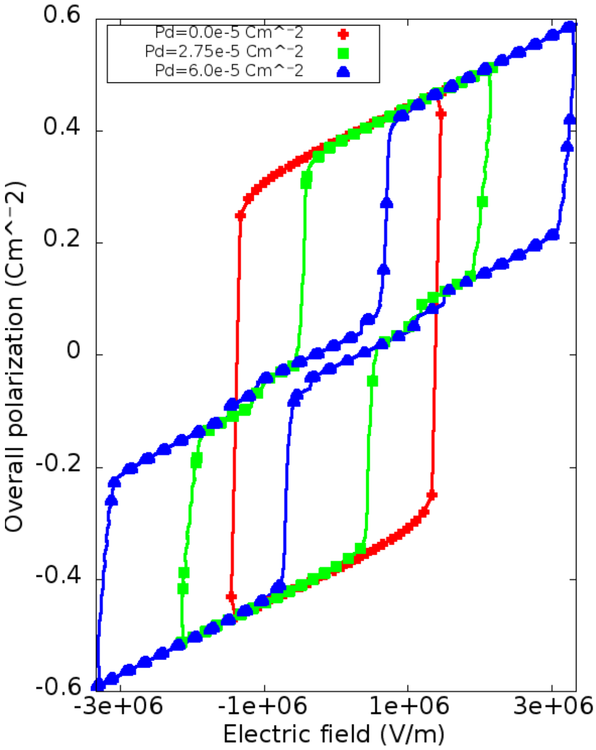

Figure 6.9: (Color online) The polarization hysteresis loop for a rank-1 domain structure of different defect dipole magnitude.

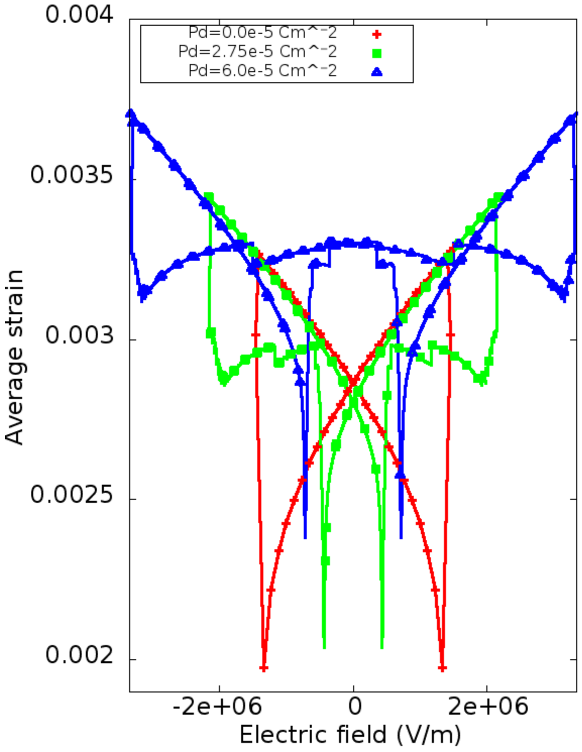

Figure 6.10: (Color online) The strain butterfly loop for a rank-1 domain structure of different defect dipole magnitude.

studied, respectively. The initial domain configuration is depicted as in Fig. 6.7. The spontaneous polarization follows the defect dipoles after unloading (Fig. 6.8) and thus a double loop is observed from the hysteresis curve (Fig. 6.9). As displayed in the Fig. 6.9, the coercive field for realizing the switching is smaller than the rank-2 domain structure case. However, compared with the rank-2 domain structure, the area encircled by the hysteresis curve is larger, indicating a larger energy cost for the switching process. The hysteresis loop retains its shape as in the defect free case in some way, only having both parts dislocated, which shows a ′deferring′ effect of defect dipoles in hindering the domains from getting poled. Unlike in the case of 90° defect dipoles, even for very large defect dipoles, the overall polarization does not come so close to zero after electric unloading (Fig. 6.9), displaying a weaker memory effect. From the ′butterfly′ curve plotted using electric field versus strain, it is seen that in the rank-1 domain configuration case, the recoverable strain by the electric field is less significant than in the rank-2 domain configuration case, but still larger than the defect free one (Fig. 6.10). This leads to the conclusion that 90° domain structure is the main factor for the large recoverable strain in a multi-domain system. The result is consistent with previous experiment [140].

Chapter 7

Influence of switchable defect dipole on behaviour of aged ferroelectrics

7.1 Introduction

Defect dipoles of different orientation are equivalent in energy in the paraelectric state. But they have a preferred orientation in a polarized media. The occurrence of internal bias fields has been attributed to the switching of defect dipoles, and the transient orientation of dipoles is described by a kinetic model by Arlt and Neumann [148].
Recently, it is shown that in Fe-doped lead titanate, there is a large dependence of the barrier for reorientation on the position of the oxygen vacancy with respect to the Fe atom and also the spontaneous polarization [153]. Zhang et al. studied the dynamics of defect dipoles in barium titanate experimentally. Support is found for the ′defect symmetry principle′. It is assumed that nonswitching defect dipoles provide a restoring force for switching of spontaneous polarization [154]. Jakes et al. [155] have shown that defect dipoles are not located at domain walls preferentially but within the domains in Fe3+ doped PZT. Morozov et al. investigated aging-deaging process taking place in PZT ceramics under switching conditions. They concluded that two or more mechanisms are possible for domain stabilization [156]. Erhart et al. [157] have described the formation and switching of defect dipoles in acceptor doped lead titanate by a kinetic model which is an extension of the existing Arlt-Neumann model. The chapter aims to develop a kinetic model together with the phase field model in order to capture the reorientation of defect dipoles in the presence of electric fields. Cu-doped lead titanate are considered as examples. After getting the energy landscape for oxygen vacancy migration, the evolution equation is obtained. The exact behavior for these defect dipole switching processes

depend largely on dopant type, concentration, and temperature. Simulations are done for a PZT sample at 450K, because at the temperature the motion of defect dipoles is much quicker. The original PZT sample can be considered as being $'$aged$'$. Under an alternating external field the current model can depict the interaction of switching of spontaneous polarization and evolution of defect dipoles.

7.2 Phase field model for ferroelectrics coupled with kinetic model of switchable defect dipoles

In treating the jumping phenomenon of atoms or vacancies, it is assumed that each step they experience is a independent event which is irrelevant to the steps before it. The position at which an atom or a vacancy resides is equilibrium with lower energy compared to the vicinity. Therefore, the atoms or vacancies can jump onto the nearby positions only if they are provided with suffient energy to overcome the energy barrier. Normally the average vibration energy each atom or vacancy possesses is far less than the energy needed to jump onto the neighborhood position. One defines the energy a vacancy has at equilibrium position as G_1 and the energy at the peak of the barrier as G_2. According to statistical mechanics, the distribution of free energy of atoms is described by Maxwell-Boltzmann distribution. If the total number of atoms is N. One denotes the number of atoms which has higher energy than G_1 and G_2 by n_1 and n_2, respectively. Then, one has

$$\frac{n_1}{N} = exp(-\frac{G_1}{k_B T}), \tag{7.1}$$

$$\frac{n_2}{N} = exp(-\frac{G_2}{k_B T}). \tag{7.2}$$

Therefore, after dividing Eq. (7.2) by Eq. (7.1), one obtains

$$\frac{n_2}{n_1} = exp(-\frac{G_2 - G_1}{k_B T}) = exp(-\frac{\Delta G}{k_B T}). \tag{7.3}$$

Since most of vacancies are at equilibrium position, therefore one has $n_1 \approx N$. Then it can be derived that the proportion of vacancies that have suffient energy to jump to the neighborhood position is

$$p = \frac{n_2}{N} \approx exp(-\frac{\Delta G}{k_B T}). \tag{7.4}$$

It is seen that the lower ΔG is and the higher the temperature T becomes, the more probable a vacancy can jump to a neighboring position. Then the rate of flow of vacancies from position i to j is

$$\frac{1}{M}\nu_0 exp(-\frac{\Delta E^{i-j}}{k_B T})c_i, \tag{7.5}$$

where M is the number of choices of jumping from position i, ν_0 is the frequency of vibration, E^{i-j} the energy barrier from position i to j, and c_i is the concentration of vacancies at position i. Then for the studied case in 2D where an oxygen vacancy is bounded to a foreign atom (Fig. 7.1), the jumping of vacancies out of position i will cause the increase of concentration of vacancies at position $i-1$ and $i+1$ (or +/- 4), and vice versa. Therefore the equations for the evolution are

$$\dot{c}_1 = -\frac{1}{2}K_{12}c_1 - \frac{1}{2}K_{14}c_1 + \frac{1}{2}K_{21}c_2 + \frac{1}{2}K_{41}c_4, \tag{7.6}$$

$$\dot{c}_2 = -\frac{1}{2}K_{23}c_2 - \frac{1}{2}K_{21}c_2 + \frac{1}{2}K_{32}c_3 + \frac{1}{2}K_{12}c_1, \tag{7.7}$$

$$\dot{c}_3 = -\frac{1}{2}K_{34}c_3 - \frac{1}{2}K_{32}c_3 + \frac{1}{2}K_{43}c_4 + \frac{1}{2}K_{23}c_2, \tag{7.8}$$

$$\dot{c}_4 = -\frac{1}{2}K_{41}c_4 - \frac{1}{2}K_{43}c_4 + \frac{1}{2}K_{14}c_1 + \frac{1}{2}K_{34}c_3, \tag{7.9}$$

where the negative terms on the right side stand for the jumping out from the position and the positive terms stand for the jumping in onto the position. Fig. 7.2 schematically shows the kinetic model explained here. The coefficients K_{ij} are expressed as

$$K_{ij} = \nu_0 exp(-\frac{\mathit{\Delta} E_m^{i-j}}{k_B T}), \tag{7.10}$$

where ΔE_m^{i-j} is the migration energy of an oxygen vacancy from position i onto position j. The values of E_m^{i-j} are shown in Fig. 7.3. The local defect polarization P_i^d and the concentration of oxygen vacancies at the four possible positions is derived as

$$P_i^d = (c_{i+2} - c_i)V_0 P_0^d, \quad i = 1, 2. \tag{7.11}$$

This defect polarization makes a contribution to the total polarization, and this exerts an internal bias field according to Eq. (6.2) and (6.3). For the frequency of attempting, an approximated value is taken $\nu_0 = 2Thz$. Details of the implementation in Fortran can be found in Appendix C.

7.3 Simulation example: Switching of defect dipoles at high temperature and deaging

At room temperature, the switching of the defect dipoles takes several days, whereas at the temperature of 450K, the switching can be achieved within a minute. $BaTiO_3$ has a Curie temperature of 393K, therefore at 450K it loses the ferroelectricity. PZT has a Curie temperature of over 500K, therefore 450K well below the Curie temperature of PZT. As shown by Erhart

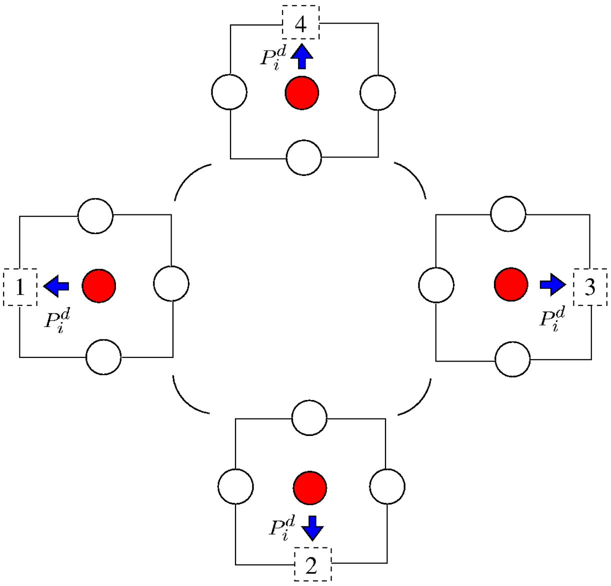

Figure 7.1: (Color online) Four possible positions of a oxygen vacancy bound to a B-site substitution and the energy barriers.

et al. [157], the external electric field has almost no inluence on the redistribution of oxygen vacancies.

Table IV: Parameters used in the simulation

C_{11}	$14 \cdot 10.76^{10}\mathrm{Nm}^{-2}$	A_{12}	0.0	ϵ	$1.2834 \cdot 10^{-7}\mathrm{m}$
C_{12}	$1.4 \cdot 6.31^{10}\mathrm{Nm}^{-2}$	A_{21}	0.0	γ	$1.8334\mathrm{Jm}^{-2}$
C_{13}	0.0	A_{22}	$2.124 \cdot 10^{-8}\mathrm{CV}^{-1}\mathrm{m}^{-1}$	κ_s	0.70
C_{21}	$1.4 \cdot 6.31^{10}\mathrm{Nm}^{-2}$	A_{11}	$2.124 \cdot 10^{-8}\mathrm{CV}^{-1}\mathrm{m}^{-1}$	κ_i	0.17
C_{22}	$34 \cdot 10.04^{10}\mathrm{Nm}^{-2}$	b_{11}	0.0	a_1	1.0
C_{23}	0.0	b_{12}	0.0	a_2	$-8.125\mathrm{m}^4\mathrm{C}^{-2}$
C_{31}	0.0	b_{13}	$12.0\mathrm{Cm}^{-2}$	a_3	$-15.82\mathrm{m}^8\mathrm{C}^{-4}$
C_{32}	0.0	b_{21}	$-9.6\mathrm{Cm}^{-2}$	a_4	$142.79\mathrm{m}^8\mathrm{C}^{-4}$
C_{33}	$1.96 \cdot 10^{10}\mathrm{Nm}^{-2}$	b_{22}	$15.1\mathrm{Cm}^{-2}$	a_5	$171.41\mathrm{m}^{12}\mathrm{C}^{-6}$
P_0	$0.4\mathrm{Cm}^{-2}$	b_{23}	0.0	G	$1.8334\mathrm{Jm}^{-2}$
S_0	0.003	V_0	6.4^{-29}		
C_0	1.02	ν_0	2THz		

However, for the case of alternating external field, the reversal of the spontaneous polarization modifies energy landscape for the redistribution of the oxygen vacancies, and the coefficients

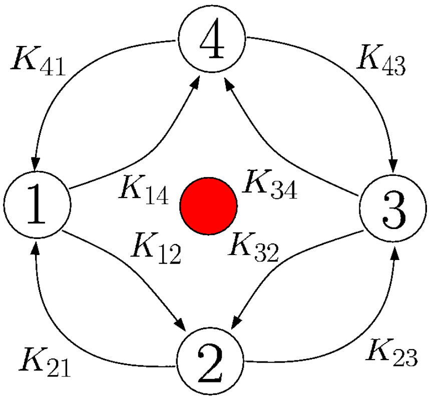

Figure 7.2: (Color online) The coefficients for jumping of oxygen vacancies between the four positions.

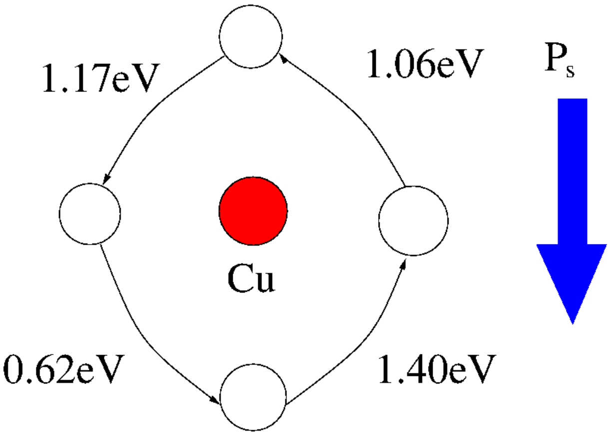

Figure 7.3: (Color online) The energy barriers for jumping of oxygen vacancies between the four positions.

K_{ij} get modified. Since for the 2D case there are four possible polarization directions, one can simply conceive that the numbering of the four possible position of oxygen vacancies is only shifted clockwise after each polarization switching (Fig. 7.3).

In the simulation of the ferroelectric polarization switching and defect dipole reversal, one confronts problems in terms of time scale. Ferroelectric polarization reversal is generally very fast.

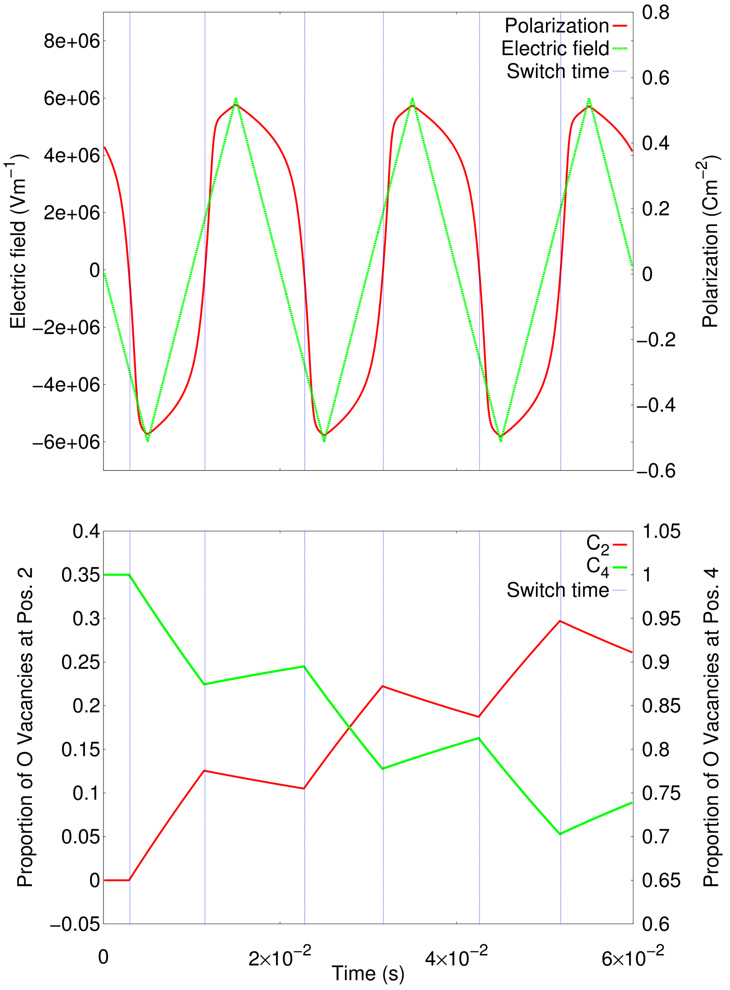

Figure 7.4: (Color online) The evolution of the electric loading, the evolution of spontaneous polarization, c_2 and c_4 for loading cycle $T = 2 \times 10^{-2}$

However defect pole reversal is very slow, as mentioned above, at room temperature the defect dipole reversal can take several days. The length of cycling loading will take in the order of $10^{-4}s$. Such ferroelectric polarization reversal and length of loading is not on the same time scale. To solve this problem, one takes the following approach. One chooses a much smaller value for the domain mobility coefficient and thus the switching of ferroelectric polarization can be accomplished within each time step applied.

In the simulation, a PZT sample of size as studied in Chapter 6 is used. The material parameters are listed in Table 7.3. As initial condition a uniform spontaneous polarization is set and the defect dipoles are coaligned with the spontaneous ones. The magnitude of defect dipole is $P^d = 3.296 \times 10^{-5} Cm^{-2}$.

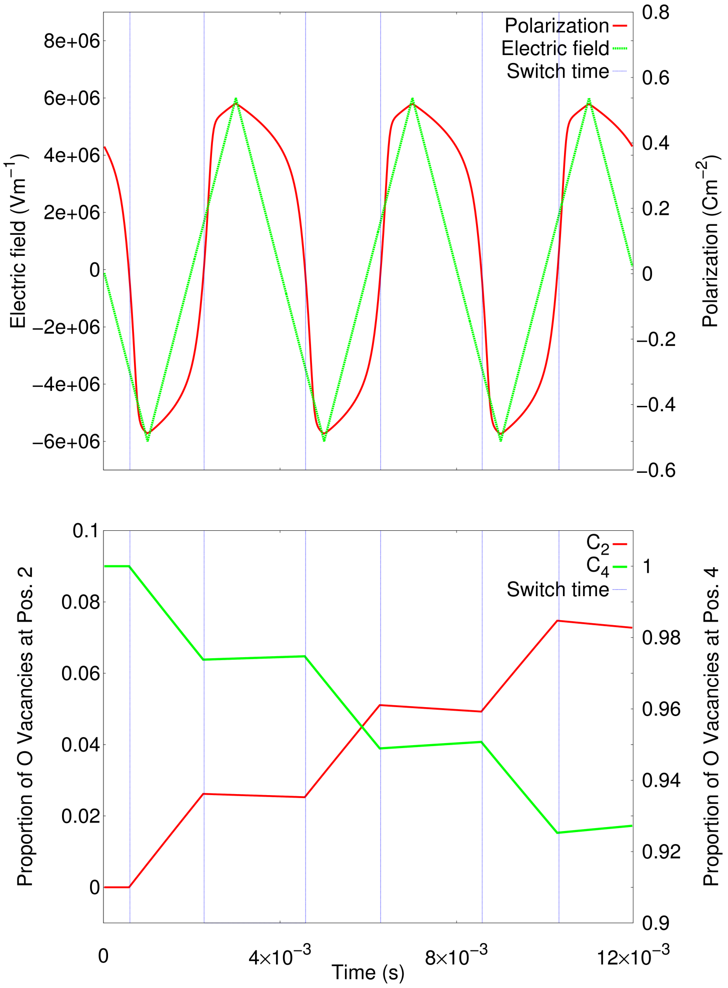

Figure 7.5: (Color online) The evolution of the electric loading, the evolution of spontaneous polarization, c_2 and c_4 for loading cycle $T = 4 \times 10^{-3}$

In this part, numerical simulations are conducted to show how the concentrations of oxygen vacancies at four positions around the $Cu - Ti$ substitutions develop. The initial spontaneous polarization is pointing upwards and all the oxygen vacancies are at position four. Three bipolar triangular electric field signals are applied with different period T. Firstly, the electric field downwards increases from zero. As the field exceeds certain coercive field value, the spontaneous polarization switches. Meanwhile, the oxygen vacancies begin to jump from position four to two via position one and three. Because of the magnitude of energy barriers, only very tiny portion of oxygen vacancies stay at position one or three. As shown by the simulation results, they are almost either at position two or four. After reaching the peak value, the electric field amplitude all in the negative direction decreases and increases in the positive direction. As the electric field

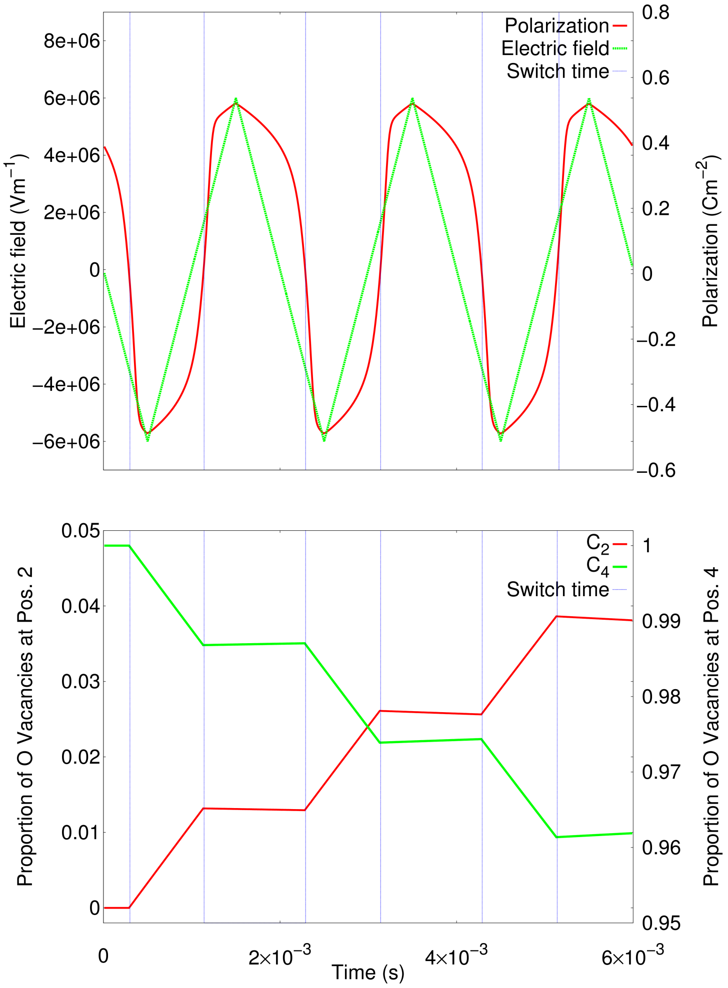

Figure 7.6: (Color online) The evolution of the electric loading, the evolution of spontaneous polarization, c_2 and c_4 for loading cycle $T = 2 \times 10^{-3}$

again reaches the coercive value in the positive direction the spontaneous polarization switches again upwards. The oxygen vacancies also turn around to jump back from position two to four. As can be seen from the evolution equation of the oxygen vacancies, the rate of those oxygen vacancies jumping from certain position is proportional to the concentration of those at that position. Therefore, since after the second switching the concentration of oxygen vacancies at position two is much smaller than those as position four, the rate of the vacancies jumping back is also much lower than the rate of jumping from position four to two. As can be seen in Fig. 7.4,7.5,7.6, the concentration of oxygen vacancies at position two and four develops in a $'$zig-zag$'$ way, and there is a netto increase of oxygen vacancies at position two. Simulation result show that after sufficient cycling the $'$zig-zag$'$ curve will rise until the concentrations of oxygen vacan-

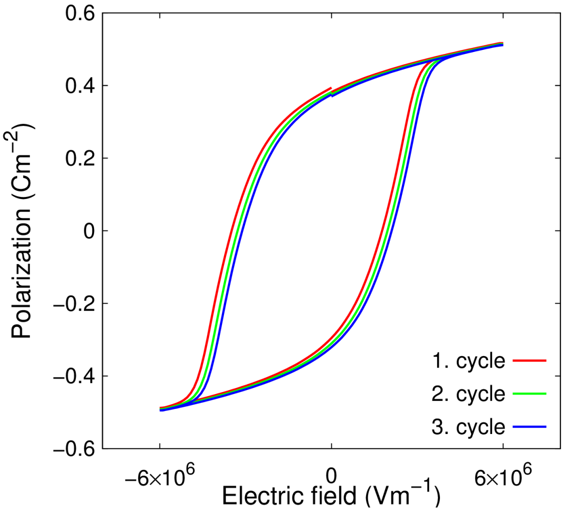

Figure 7.7: (Color online) The hysteresis loop under cyclic loading for $T = 20 \times 10^{-3}$

cies at position two and four are almost the same, whose number of oxygen vacancies reach a dynamic eqiulibrium with each other and both alternate around 0.5 (Fig. 7.8).

As initially an internal bias field exists, the hysteresis loop is not symmetric about the origin point where electric field is zero. It is displaced by E_d to the right. As the number of cycling load increases, the number of vacancies at position two and four gets its new equilibrium. The internal bias field is eliminated and the hysteresis loop is again symmetric about the E axis (Fig. 7.7). Therefore a deaging phenomenon by cyclic electric field is then verified. It is shown that for higher temperature the deaging is achieved in a shorter time.

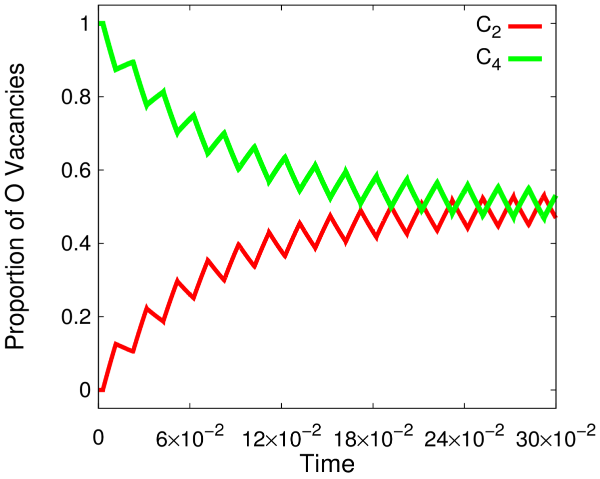

Figure 7.8: (Color online) The evolution of c_2 and c_4 under cyclic loading until they reach a dynamic eqiulibrium with each other and both alternate around 0.5

Chapter 8

Conclusion and outlook

The ferroelectrics which possess switchable polarization below the Curie temperature can be applied as actuators and memory storage devices. Oxygen vacancies are commonly present in perovskite ferroelectrics and they are mobile at high temperatures. Besides that, in order to enhance certain properties, perovskite ferroelectrics are doped with foreign atoms (e.g. iron, copper, manganese, etc) which again results in the appearance of certain kinds of point defects. Those point defects may bring about semiconducting features and induces space charges in ferroelectric cystals. Beyond that, an oxygen vacancy on a face of the perovskite unit cell and the impurity cation center may form a complex and an electric dipole. This electric dipoles have an elecrtric field and the switching behaviour of ferroelectrics can be modified. In this thesis, the model has been set up to investigate those two effects: a model that incorporates the ferroelectric and semiconducting feature of ferroelectric perovskites at the same time and a model taking the internal bias field due to the defect dipole into account. Both models are built on the phase field model of ferroelectrics.

In Chapter 1, a introduction is made on the concise history, fundamental physics and behaviour of ferroelectrics.

In Chapter 2, in order to set up the phenomenological theory, one discussed basics of continuum mechanics, where the deformation was treated as a mapping from the reference configuration onto the current configuration. For the electric properties, one started from the microscopic perspective. Electrostatic energy of many charge particles and the power of external electric field were derived, as well as the balance laws. After introducing the electric enthalpy as free energy, a variational principle was shown.

In Chapter 3, some basics of phase field methods are discussed and the Landau-Ginzburg equation was derived in a thermodynamically consistent way based on the microforce theory by Gurtin. The meaning of each parameter was also explained. The phase field modeling was numerically realized by finite element method using FEAP, for which some details were provided. Since the domain structure evolution is certain change in the ′material′ or ′reference′ configuration, one is interested in the driving force or tendency of such change by making use of the concept ′configurational force′ from Eshelby. The configurational stress tensor was obtained by variational calculation.

In Chapter 4, the semiconducting feature of ferroelectrics with point defects was studied. the role of donors and electronic charge carriers in the domain structure stabilization was studied in a quantitative way. By accounting for semiconducting properties of barium titanate, the appearance of depletion layers near the electrodes was predicted. The stabilization of the head-to-head and tail-to-tail domain structures through the space charge was also demonstrated.

As an indication of the stability, the driving force on the domain wall in the head-to-head domain structure was quantitatively investigated by the configurational force theory. The effects of an applied electric field and space charge compensation on the driving force and the driving moment were discussed, as well as the influence of the domain wall orientation. In particular, the results show that the considered domain wall should rotate due to the driving moment, which results from the inhomogeneous internal electric field due to the uncompensated polarization charge.

The effect of the predicted driving moment was then visualized by phase field simulations. It can be seen that the equilibrium position of the domain wall in a head-to-head or tail-to-tail domain configuration depends on the compensation situation. When semiconducting features are included, the equilibrium position is related to the position of the Fermi level and the donor/acceptor concentration. Depending on these circumstances one of the above two configurations becomes more favorable. It is interesting that both head-to-head and tail-to-tail configurations were in fact observed experimentally revealing enhanced electrical conductivity through domain walls.

In the mentioned study only donors were considered in the system, with the purpose of identifying their role in domain wall stabilization. This choice of the model defect system was also adopted in the studies by Xiao et al. [100] and Hong et al. [101] It should be noted that the strong compensation of the charged domain wall by the semiconducting effect requires rather high donor doping of $N_d = 10^{25} m^{-3}$ as is seen in Fig. 4.14 (c). Typical intrinsic concentrations of the oxygen vacancies emerging due to sintering of ferroelectric ceramics at high temperature are of the order of $10^{20} m^{-3}$ as evaluated by Erhart and Albe [50]. Due to acceptor doping of about 1 mol, the test value used in this paper was enhanced up to $N_d = 5 \times 10^{22} m^{-3}$ ([137]). In any case, Fig. 4.15 exhibits a rather slow logarithmic dependence of the equilibrium rotation angle on the donor density, which means that even the effect of the intrinsic donor defects should be remarkable. However, an apparent saturation of the rotation angle at low donor densities might also mean the stabilization of the charged domain wall by electronic carriers alone. In the further study, a defect system obtained by the first principle calculations by Erhart and Albe will be included in the phase field simulations [50]. In the future work, the diffusion of the oxygen vacancies will also be incorporated, and their interaction with the domain structure will be further studied. In doing so, the formulation of the configurational force should also be modified correspondingly so that the additional contribution by the diffusion into the driving force can be taken into account.

In Chapter 5, the study of the domain wall conductivity has shown that in both the simplified and the realistic defect systems in barium titanate, head-to-head, and tail-to-tail domain configurations may be stabilized by the space charge which screens the bound charge. The conductivity of the head-to-head domain wall in the simplified defect system and of the tail-to-tail domain wall in the more realistic defect system is almost independent of the concentrations of the oxygen vacancies and manganese-titanium substitutions, respectively. On the contrary, conductivity of the tail-to-tail domain wall in the simplified defect system and of the head-to-head domain wall in the realistic defect system depends strongly on the concentration of the corresponding leading defect species. The higher the concentration, the lower the conductivity becomes. As the concentration surpasses a threshold value, the domain wall conductivity becomes as low as the bulks. Thus, stabilization and conductivity of charged domain walls of either type in ferroelectrics can be effectively tuned by medium acceptors or donor doping. Semiconducting features has also a reducing effect on the energy of the domain walls in charged configurations but not to the extent which would allow one to solve the Landauer paradox.

The phase field modeling of ferroelectrics with static defect dipole is developed in Chapter 6 and computation is conducted in order to study the dipole effect of oxygen vacancies on the different domain structures. In the model, the oxygen vacancies are treated as electric dipoles and the ensuing interior electric field is taken into account as well. The numerical simulations demonstrate that the internal bias electric field caused by the oxygen vacancies does play a notable role in modifying the overall domain switching behavior of ferroelectric single crystals. The domain memory effect, in which the zero overall polarization and the initial domain patterns are recovered after electric unloading and thus the double hysteresis loops take place, are well reproduced in the modeling. Calculation shows that the recoverable strain in the rank-2 domain structure is more significant than that in the rank-1 domastructure, and thus one is led to the conclusion that the former is the main factor for the effect. The phenomenological frame has limitations because it is unable to capture all the mechanisms in the structural inhomogeneities, thus neglecting some details of the interactions between defects and domain walls in ferroelectrics.

In Chapter 7, a kinetic model is derived that enables investigation of the time evolution of defect dipoles in the presence of electric fields in PZT. The most important input parameter is the energy barriers for oxygen vacancy migration which is obtained from density functional theory calculations. As a result, at room temperature the migration of oxygen vacancies is quite slow. The simulations were conducted at 450K, which is also well below the Curie temperature, where the material possesses its ferroelectricity. The simulation shows that after each switching of spontaneous polarization, the migration of oxygen vacancies also change their migration direction due to the change of energy landscape. For a initially aged material in which the defect dipoles formed by Cu-substitutes and oxygen vacancies are coaligned with the spontaneous polarization, the simulations show that, after sufficient loading cycles, the number of oxygen vacancies which form defect dipoles with the Cu-substitution which are parallel and antiparallel to the spontaneous polarization is the same. The hysterresis loops which were not symmetric about the E axis can be displaced to the position so that they become symmetric about the E axis. That is, after sufficient time of cyclic loading, the sample can be ′deaged′ in the sense of defect dipole reorientation.

Studying this problem will give a good perspective and understanding of the evolution of fatigue and aging in ferroelectrics. Some results will motivate experiments on the stability of domain walls and on aging. The study also provides a motivation for a detailed theoretical investigation of interaction of the domain structure with point defects and issues related to charges due to semiconducting feature. A suggestion for future work would be to investigate the motion of oxygen vacancies and their role in fatigue and aging. Fatigue is a phenomenon after million times of cyclic loading, which is too difficult to simulate using the current phase field model. Hence, certain acceleration approaches are necessary. The polycrystalline ferroelectrics are also of interest, as polycrystalline solids are mostly applied in the actual industry application instead of single crystal. The incorporation of diffusion of oxygen vacancies is a possibility for investigation. Additionally, a combination of the defect dipole model and semiconducting model may also be of interest.

List of Figures

Chapter 9

Appendix

9.1 Appendix A: The thermodynamic characteristic functions

The state of the system can be definitely determined by (σ_{ij}, E_i, T). One from the three pairs each $(\sigma_{ij}, \varepsilon_{ij}), (E_i, D_i)$ and (T, S) can be chosen as independent variable, the other as dependent variable and a characteristic energy function can be defined. Therefore, eight energy functions can be formed:

internal energy,

$$dU = \sigma_{ij} d\varepsilon_{ij} + E_i dD_i + TdS, \tag{9.1}$$

free energy,

$$F = U - TS, df = \sigma_{ij} d\varepsilon_{ij} + E_i dD_i - SdT, \tag{9.2}$$

Gibbs energy,

$$G = U - \sigma_{ij}\varepsilon_{ij} - E_iD_i - TS, dG = -\varepsilon_{ij}d\sigma_{ij} - D_idE_i - SdT, \tag{9.3}$$

Electric Gibbs energy,

$$G^{ele} = U - E_iD_i - TS, dG = \sigma_{ij}d\varepsilon_{ij} - D_idE_i - SdT, \tag{9.4}$$

Elastic Gibbs energy,

$$G^{elast} = U - \sigma_{ij}\varepsilon_{ij} - TS, dG = -\varepsilon_{ij}d\sigma_{ij} + E_idD_i - SdT, \tag{9.5}$$

Heat enthalpy,

$$H^{heat} = U - \sigma_{ij}\varepsilon_{ij} - E_iD_i, dH = -\varepsilon_{ij}d\sigma_{ij} - D_idE_i + TdS, \tag{9.6}$$

Electric enthalpy,

$$H^{ele} = u - E_iD_i, dH = \sigma_{ij}d\varepsilon_{ij} - D_idE_i + TdS, \tag{9.7}$$

Elastic enthalpy,

$$H^{elast} = U - \sigma_{ij}\varepsilon_{ij}, dH = -\varepsilon_{ij}d\sigma_{ij} + E_idD_i + TdS. \tag{9.8}$$

In this dissertation one uses electric Gibbs energy. For the isothermal case, electric Gibbs energy is equivalent to electric enthalpy.

9.2 Appendix B: Stiffness matrices

$$ {}^{\sigma\sigma}K^{IJ}_{ij} = -\int {}^{u}B^{I}_{mi}\mathbb{C}_{mn}{}^{u}B^{J}_{nj}dV. \tag{9.9} $$

$$ {}^{\sigma D}K^{IJ}_{ij} = -\int {}^{u}B^{I}_{mi}b_{nm}{}^{\phi}B^{J}_{nj}dV. \tag{9.10} $$

$$ {}^{\sigma P}K^{IJ}_{ij} = -\int {}^{u}B^{I}_{mi}(\mathbb{C}_{mk}\frac{\partial \varepsilon^{0}_{k}}{\partial P_n} + \frac{\partial b_{km}}{\partial P_n}E_k)^{P}N^{J}_{nj}dV. \tag{9.11} $$

$$ {}^{D\sigma}K^{IJ}_{ij} = -\int {}^{\phi}B^{I}_{mi}b_{mn}{}^{u}B^{J}_{nj}dV. \tag{9.12} $$

$$ {}^{DD}K^{IJ}_{ij} = -\int {}^{\phi}B^{I}_{mi}\epsilon_{mn}{}^{\phi}B^{J}_{nj}dV. \tag{9.13} $$

$$ {}^{DP}K^{IJ}_{ij} = -\int {}^{\phi}B^{I}_{mi}(\frac{\partial b_{mk}}{\partial P_n}(\varepsilon_k - \varepsilon^{0}_{k}) - b_{mk}\frac{\partial \varepsilon^{0}_{k}}{\partial P_n} + \delta_{mn})^{P}N^{J}_{nj}dV. \tag{9.14} $$

$$ {}^{P\sigma}K^{IJ}_{ij} = -\int {}^{\phi}N^{I}_{mi}(\frac{\partial \varepsilon^{0}_{k}}{\partial P_m}\mathbb{C}_{kn} + E_k\frac{\partial b_{kn}}{\partial P_m})^{P}B^{J}_{nj}dV. \tag{9.15} $$

$$ {}^{PD}K^{IJ}_{ij} = -\int {}^{P}N^{I}_{mi}(-\frac{\partial \varepsilon_k}{\partial P_m}b_{nk} + (\varepsilon_k - \varepsilon^{0}_{k})\frac{\partial b_{nk}}{\partial P_m} + \delta_{mn})^{\phi}B^{J}_{nj}dV. \tag{9.16} $$

$$ {}^{PP}K^{IJ}_{ij} = -\int -{}^{P}N^{I}_{mi}(\frac{\partial \varepsilon^{2}_{k}}{\partial P_m \partial P_n}\sigma_k - \frac{\partial \varepsilon_k}{\partial P_m}(\mathbb{C}_{kl}\frac{\partial \varepsilon_l}{\partial P_n} + \frac{\partial b_{kl}}{\partial P_n}E_k))^{P}N^{J}_{nj} - {}^{P}N^{I}_{mi}. \tag{9.17} $$

$$ (-\frac{\partial \varepsilon^{0}_{l}}{\partial P_m}\frac{\partial b_{kl}}{\partial P_n}E_k + (\varepsilon_l - \varepsilon^{0}_{l})\frac{\partial^2 b_{kl}}{\partial P_m \partial P_n}E_k)^{P}N^{J}_{nj}dV. \tag{9.18} $$

$$ {}^{P}N^{J}_{mi}\kappa_s\frac{G}{\epsilon}\frac{\partial^2 \psi}{\partial P_m \partial P_n}{}^{P}N^{J}_{nj} + {}^{P}B^{J}_{mi}\kappa_i\frac{G\epsilon}{P^{2}_{0}}{}^{P}B^{J}_{mj}dV. \tag{9.19} $$

9.3 Appendix C: The FEAP code for the phase field model

```
         subroutine elmt36(d,ul,xl,ix,tl,s,p,ndf,ndm,nst,isw)
c
c     FEM Dom nenw nde mit Ordnungsparameter, rein elektrisch DaS & RaM
c
c     4 Knoten Element 2D / 4 Gau -Punkte
c
c     Implementierte Konstitutivgleichungen (in Vektor-/Voigtnotation)
c
c     dP_i/dt = - alpha vardPsi/vardP
c       D_i = B_ij (eps_j-eps^0_j) +  A_ij E_j   + P_i
c     sig_i = C_ij (eps_j-eps_j^0) - B_ij E_i
c
c     Eingabedaten:
c
c     C rein elast.    Materialverhalten (3x3)
c     B elast. elektr. Kopplung          (2x3)
c     A rein elektr.   Materialverhalten (2x2)
c     P0 spontane Polarisation, eps0 spontane Verzerrung
c     alpha, G, epsil     f r Evolutionsgleichung
c     theta: Winkel f r P_0
c     psi1:  parameter fuer H^sep
c
c
      !implicit double precision (a-h,o-z)
      implicit none
c
      include   'cdata.h'      ! numnp,numel,nummat,nen,neq,ipr
      include   'tdata.h'
      include   'eltran.h'
      include   'iofile.h'
      include   'prstrs.h'
      include   'comblk.h'

      real*8 d(*),ul(ndf,nen,*),xl(ndm,*),tl(*),s(nst,*),p(*)
      integer ix(*)
      integer ndf,ndm,nst,isw

c

      real*8      a(5)
```

```
      real*8    cc(3,3),bb(2,3),aa(2,2),pol0,ep0,alpha,G,epsil
      real*8    psi1,theta,rho,dRho_dPhi

      real*8    drittel,pi,fakt,pol0q,kaps,kapi,b33,b31,b15
      real*8    costh,sinth,Q(2,2),QT(2,2)
      real*8    xl_r(2,4),ul_r(5,4,4),p_r(20)
      real*8    kmat(20,20),dmat(20,20)
      real*8    kron(2,2)

      real*8    shp(3,4),sg(3,16),ss(2),xsj
      real*8    shp_gl(3,4),xsj_gl

      real*8    u(2),eps(3)
      real*8    phiel,eel(2)
      real*8    pol(2),poldot(2),gradpol(4)
      real*8    eel_gl(2),pol_gl(2)


      real*8    abspol,abspol2,abspoli,apoldp0
      real*8    pol1q,pol2q
      real*8    nvec(2),nn(2,2),nnn(2,2,2)
      real*8    dnvecdpol(2,2),d2nvecdpol(2,2,2)
      real*8    dndpn(2,2,2),dndpnn(2,2,2,2)

      real*8    eps0(3),deps0dpol(3,2),d2eps0dpol(3,2,2)
      real*8    brot(2,2,2),dbrotdpol(2,2,2,2),d2brotdpol(2,2,2,2,2)

      real*8    krnn(2,2),krpp(2,2),krdndp(2,2,2,2)
      real*8    dnnndpol(2,2,2,2),d2nnndpol(2,2,2,2,2)

      real*8    bbb(2,3),dbdpol(2,3,2),d2bdpol(2,3,2,2)


      real*8    del(2),sig(3)
      real*8    Hent,Hint,Hsep
      real*8    dsigdu(3,2),dsigde(3),dsigdp(3,2)
      real*8    ddeldu(2,2),ddelde(2),ddeldp(2,2)

      real*8    hilfep(2)
      real*8    hilfpu(2,2),hilfpu2(3,2)
      real*8    hilfpe(2),hilfpe2(3,2)
      real*8    hilfpp(2,2),hilfpp2(2,2),hilfpp3(2,2)

      real*8    dpsidpol(2),dpsidpol2(2,2)
```

```

      real*8       hilfres1(2),hilfres2(2)
      real*8       dpsidp(2)

      real*8       angle
      real*8       sig_gl(3),del_gl(2)

      real*8       s_r(20,20),s_q(20,20)


      real*8       Biel(2),Bjel(2),Bi(4,2),Bj(4,2)
      real*8       Biu(3,2),Bju(3,2)

      real*8       valp(9)

      integer      i,j,k,i1,j1,k1,k2,lint,l,m,n
      real*8      rho_ele,rho_hol,rho_don,rho_acc

      real*8       parms(16)

      save a

c       print*,'called with isw=',isw

c
c.... go to correct array processor
c                              1 1 1 1 1 1
c           1 2 3 4 5 6 7 8 9 0 1 2 3 4 5
      go to(1,2,3,3,2,3,2,3,2,2,2,2,2,3,3), isw
      return

c.... input material properties

1     continue

      call dinput(d(1),3)
      cc(1,1) = d(1)
      cc(1,2) = d(2)
      cc(1,3) = d(3)
      call dinput(d(4),3)
      cc(2,1) = cc(1,2)
      cc(2,2) = d(5)
      cc(2,3) = d(6)
      call dinput(d(7),3)
```

```
      cc(3,1) = cc(1,3)
      cc(3,2) = cc(2,3)
      cc(3,3) = d(9)
      call dinput(d(10),3)
      bb(1,1) = d(10)
      bb(1,2) = d(11)
      bb(1,3) = d(12)
      call dinput(d(13),3)
      bb(2,1) = d(13)
      bb(2,2) = d(14)
      bb(2,3) = d(15)
      call dinput(d(16),2)
      aa(1,1) = d(16)
      aa(1,2) = d(17)
      call dinput(d(18),2)
      aa(2,1) = aa(1,2)
      aa(2,2) = d(19)
      call dinput(d(20),2)
      pol0 = d(20) ! equilibrium (spontaneous) polarization
      ep0 = d(21) ! eigenstrain due to polarization change
      call dinput(d(22),3)
      alpha = d(22) ! mobility of the domain wall
     G = d(23) ! domain wall energy per area
      epsil = d(24) ! domain wall thickness
      call dinput(d(25),1)
      psi1 = d(25)  ! energy barrier for 180  domain switching
      call dinput(d(26),1)
      theta = d(26) ! domain orientation angle
      call dinput(d(27),4)
      parms(1) = d(27)  !Ef .. Fermi level
      parms(2) = d(28)  !Ec .. bottom of the conduction band
      parms(3) = d(29)  !Ev .. top of the valence band
      parms(4) = d(30)  !Ed .. donor level
      call dinput(d(31),4)
      parms(5) = d(31)  !Ea .. acceptor level
      parms(6) = d(32)  !Nc .. Effective density state in the conductive band
      parms(7) = d(33)  !Nv .. Effective density state in the valence band
      parms(8) = d(34)  !Nd .. donor density
      call dinput(d(35),4)
      parms(9)  = d(35) !Na .. acceptor density
      parms(10) = d(36) !za .. acceptor valence
      parms(11) = d(37) !zd .. donor valence
      !gd .. ground state degeneracy of the donor impurity level
```

```
      parms(12) = d(38)
      call dinput(d(39),4)
      parms(13) = d(39) !ga .. degeneracy of acceptor level
      parms(14) = d(40) !q  .. absolute value of the electron charge
      parms(15) = d(41) !k  .. Boltzmann constant
      parms(16) = d(42) !T  .. absolute temperature

      write(iow,2000) ((cc(i,j),j=1,3),i=1,3),((bb(i,j),j=1,3),i=1,2),
     x           ((aa(i,j),j=1,2),i=1,2),pol0,ep0,alpha,G,epsil,
     x           psi1,theta,(parms(i),i=1,16)

      return

2     continue
      return

3     continue

      cc(1,1) = d(1)
      cc(1,2) = d(2)
      cc(1,3) = d(3)
      cc(2,1) = cc(1,2)
      cc(2,2) = d(5)
      cc(2,3) = d(6)
      cc(3,1) = cc(1,3)
      cc(3,2) = cc(2,3)
      cc(3,3) = d(9)
      bb(1,1) = d(10)
      bb(1,2) = d(11)
      bb(1,3) = d(12)
      bb(2,1) = d(13)
      bb(2,2) = d(14)
      bb(2,3) = d(15)
      aa(1,1) = d(16)
      aa(1,2) = d(17)
      aa(2,1) = aa(1,2)
      aa(2,2) = d(19)
      pol0    = d(20)
      ep0     = d(21)
      alpha   = d(22)
     G        = d(23)
      epsil   = d(24)
      psi1    = d(25)
      theta   = d(26)
```

```
      parms(1) = d(27)  !Ef .. Fermi level
      parms(2) = d(28)  !Ec .. bottom of the conduction band
      parms(3) = d(29)  !Ev .. top of the valence band
      parms(4) = d(30)  !Ed .. donor level
      parms(5) = d(31)  !Ea .. acceptor level
      parms(6) = d(32)  !Nc .. Effective density state in the conductive
   band
      parms(7) = d(33)  !Nv .. Effective density state in the valence band
      parms(8) = d(34)  !Nd .. density of negative ion defect
      parms(9)  = d(35) !Na .. density of positive ion defect
      parms(10) = d(36) !za .. acceptor valence
      parms(11) = d(37) !zd .. donor valence
      !gd .. ground state degeneracy of the donor impurity level
      parms(12) = d(38)
      parms(13) = d(39) !ga .. degeneracy of acceptor level
      parms(14) = d(40) !q  .. absolute value of the electron charge
      parms(15) = d(41) !k  .. Boltzmann constant
      parms(16) = d(42) !T  .. absolute temperature

      drittel=1.d0/3.d0
      pi=3.1415926536d0
      theta=theta*pi/180.d0

      fakt=1.5d0*ep0/pol0
      pol0q=pol0**2.d0

      kaps=0.70d0
      kapi=0.17d0

      b33=bb(2,2)
      b31=bb(2,1)
      b15=2.d0*bb(1,3)

      costh=dcos(theta)
      sinth=dsin(theta)

      Q(1,1)=costh
      Q(1,2)=sinth
      Q(2,1)=-Q(1,2)
      Q(2,2)=costh

      QT(1,1)=costh
      QT(1,2)=-sinth
      QT(2,1)=-QT(1,2)
```

```
      QT(2,2)=costh

      if(a(1).ne.1.d0) then
        call getacoef36(a,psi1,pol0)
        print*,"coeff.:",a
      endif

      do i=1,4
        xl_r(1,i)=Q(1,1)*xl(1,i)+Q(1,2)*xl(2,i)
        xl_r(2,i)=Q(2,1)*xl(1,i)+Q(2,2)*xl(2,i)
        ul_r(1,i,1)=Q(1,1)*ul(1,i,1)+Q(1,2)*ul(2,i,1)
        ul_r(2,i,1)=Q(2,1)*ul(1,i,1)+Q(2,2)*ul(2,i,1)
        ul_r(3,i,1)=ul(3,i,1)
        ul_r(4,i,1)=Q(1,1)*ul(4,i,1)+Q(1,2)*ul(5,i,1)
        ul_r(5,i,1)=Q(2,1)*ul(4,i,1)+Q(2,2)*ul(5,i,1)
        ul_r(1,i,4)=Q(1,1)*ul(1,i,4)+Q(1,2)*ul(2,i,4)
        ul_r(2,i,4)=Q(2,1)*ul(1,i,4)+Q(2,2)*ul(2,i,4)
      enddo

      call int2d(2,lint,sg)

      do i=1,20
        p_r(i)=0.d0
        do j=1,20
          kmat(i,j)=0.d0
          dmat(i,j)=0.d0
        enddo
      enddo
      kron(1,1)=1.d0
      kron(1,2)=0.d0
      kron(2,1)=0.d0
      kron(2,2)=1.d0

      do 320 l = 1,lint
        ss(1)=sg(1,l)
        ss(2)=sg(2,l)
        call shp2d(ss,xl_r,shp,xsj,ndm,4,ix,.false.)
        xsj = xsj*sg(3,l)
        call shp2d(ss,xl,shp_gl,xsj_gl,ndm,4,ix,.false.)
        xsj_gl = xsj_gl*sg(3,l)

        phiel=0.d0
        eps(1)=0.d0
        eps(2)=0.d0
```

```
        eps(3)=0.d0
        Hent=0.d0
        Hint=0.d0
        Hsep=0.d0

        do i=1,2
          u(i)=0.d0
          eel(i)=0.d0
          eel_gl(i)=0.d0
          pol(i)=0.d0
          poldot(i)=0.d0
          gradpol(2*(i-1)+1)=0.d0
          gradpol(2*(i-1)+2)=0.d0
        enddo

        do j=1,4
          phiel = phiel + shp(3,j)*ul_r(3,j,1)
          pol(1) = pol(1) + shp(3,j)*ul_r(1,j,1)
          pol(2) = pol(2) + shp(3,j)*ul_r(2,j,1)
          poldot(1) = poldot(1) + shp(3,j)*ul_r(1,j,4)
          poldot(2) = poldot(2) + shp(3,j)*ul_r(2,j,4)
          u(1) = u(1) + shp(3,j)*ul_r(4,j,1)
          u(2) = u(2) + shp(3,j)*ul_r(5,j,1)
          eps(1) = eps(1) + shp(1,j)*ul_r(4,j,1)
          eps(2) = eps(2) + shp(2,j)*ul_r(5,j,1)
          eps(3) = eps(3) + shp(1,j)*ul_r(5,j,1) + shp(2,j)*ul_r(4,j,1)
          eel(1) = eel(1) - shp(1,j)*ul_r(3,j,1)
          eel(2) = eel(2) - shp(2,j)*ul_r(3,j,1)
          eel_gl(1) = eel_gl(1) - shp_gl(1,j)*ul(3,j,1)
          eel_gl(2) = eel_gl(2) - shp_gl(2,j)*ul(3,j,1)
          gradpol(1) = gradpol(1) + shp(1,j)*ul_r(1,j,1)
          gradpol(2) = gradpol(2) + shp(2,j)*ul_r(2,j,1)
          gradpol(3) = gradpol(3) + shp(2,j)*ul_r(1,j,1)
          gradpol(4) = gradpol(4) + shp(1,j)*ul_r(2,j,1)
        enddo

        abspol=dsqrt(pol(1)*pol(1)+pol(2)*pol(2))
        abspol2=abspol**2.d0
        abspoli=1.d0/abspol
        apoldp0=abspol/pol0
        pol1q=pol(1)**2.d0
        pol2q=pol(2)**2.d0

        if(abspol.ne.0.d0) then
```

```
            nvec(1)=pol(1)/abspol
            nvec(2)=pol(2)/abspol
            nn(1,1)=nvec(1)*nvec(1)
            nn(1,2)=nvec(1)*nvec(2)
            nn(2,1)=nn(1,2)
            nn(2,2)=nvec(2)*nvec(2)
            nnn(1,1,1)=nn(1,1)*nvec(1)
            nnn(1,1,2)=nn(1,1)*nvec(2)
            nnn(1,2,1)=nnn(1,1,2)
            nnn(1,2,2)=nn(1,2)*nvec(2)
            nnn(2,1,1)=nnn(1,1,2)
            nnn(2,1,2)=nnn(1,2,2)
            nnn(2,2,1)=nnn(1,2,2)
            nnn(2,2,2)=nn(2,2)*nvec(2)
            dnvecdpol(1,1)=abspoli*(1.d0-nn(1,1))
            dnvecdpol(1,2)=-abspoli*nn(1,2)
            dnvecdpol(2,1)=dnvecdpol(1,2)
            dnvecdpol(2,2)=abspoli*(1.d0-nn(2,2))
            dndpn(1,1,1)=dnvecdpol(1,1)*nvec(1)
            dndpn(1,1,2)=dnvecdpol(1,1)*nvec(2)
            dndpn(1,2,1)=dnvecdpol(1,2)*nvec(1)
            dndpn(1,2,2)=dnvecdpol(1,2)*nvec(2)
            dndpn(2,1,1)=dndpn(1,2,1)
            dndpn(2,1,2)=dndpn(1,2,2)
            dndpn(2,2,1)=dnvecdpol(2,2)*nvec(1)
            dndpn(2,2,2)=dnvecdpol(2,2)*nvec(2)
            dndpnn(1,1,1,1)=dnvecdpol(1,1)*nn(1,1)
            dndpnn(1,1,1,2)=dnvecdpol(1,1)*nn(1,2)
            dndpnn(1,1,2,1)=dndpnn(1,1,1,2)
            dndpnn(1,1,2,2)=dnvecdpol(1,1)*nn(2,2)
            dndpnn(1,2,1,1)=dnvecdpol(1,2)*nn(1,1)
            dndpnn(1,2,1,2)=dnvecdpol(1,2)*nn(1,2)
            dndpnn(1,2,2,1)=dndpnn(1,2,1,2)
            dndpnn(1,2,2,2)=dnvecdpol(1,2)*nn(2,2)
            dndpnn(2,1,1,1)=dndpnn(1,2,1,1)
            dndpnn(2,1,1,2)=dndpnn(1,2,1,2)
            dndpnn(2,1,2,1)=dndpnn(1,2,1,2)
            dndpnn(2,1,2,2)=dndpnn(1,2,2,2)
            dndpnn(2,2,1,1)=dnvecdpol(2,2)*nn(1,1)
            dndpnn(2,2,1,2)=dnvecdpol(2,2)*nn(1,2)
            dndpnn(2,2,2,1)=dndpnn(2,2,1,2)
            dndpnn(2,2,2,2)=dnvecdpol(2,2)*nn(2,2)

            d2nvecdpol(1,1,1)=-abspoli*
```

```
     x       ((nvec(1)-nnn(1,1,1))/abspol+2.d0*dndpn(1,1,1))
          d2nvecdpol(1,1,2)=-abspoli*
     x       ((nvec(2)-nnn(1,1,2))/abspol+2.d0*dndpn(1,2,1))
          d2nvecdpol(1,2,1)=-abspoli*
     x       ((-nnn(1,2,1))/abspol+dndpn(1,1,2)+dndpn(2,1,1))
          d2nvecdpol(1,2,2)=-abspoli*
     x       ((-nnn(1,2,2))/abspol+dndpn(1,2,2)+dndpn(2,2,1))
          d2nvecdpol(2,1,1)=-abspoli*
     x       ((-nnn(2,1,1))/abspol+dndpn(2,1,1)+dndpn(1,1,2))
          d2nvecdpol(2,1,2)=-abspoli*
     x       ((-nnn(2,1,2))/abspol+dndpn(2,2,1)+dndpn(1,2,2))
          d2nvecdpol(2,2,1)=-abspoli*
     x       ((nvec(1)-nnn(2,2,1))/abspol+2.d0*dndpn(2,1,2))
          d2nvecdpol(2,2,2)=-abspoli*
     x       ((nvec(2)-nnn(2,2,2))/abspol+2.d0*dndpn(2,2,2))

          eps0(1)=fakt*abspol*(nn(1,1)-drittel)
          eps0(2)=fakt*abspol*(nn(2,2)-drittel)
          eps0(3)=fakt*abspol*2.d0*nn(1,2)
          deps0dpol(1,1)=fakt*(2.d0*nvec(1)-nnn(1,1,1)-drittel*nvec(1))
          deps0dpol(2,1)=fakt*(-nnn(2,2,1)-drittel*nvec(1))
          deps0dpol(3,1)=fakt*2.d0*(nvec(2)-nnn(1,2,1))
          deps0dpol(1,2)=fakt*(-nnn(1,1,2)-drittel*nvec(2))
          deps0dpol(2,2)=fakt*(2.d0*nvec(2)-nnn(2,2,2)-drittel*nvec(2))
          deps0dpol(3,2)=fakt*2.d0*(nvec(1)-nnn(1,2,2))

          d2eps0dpol(1,1,1)=fakt*(2.d0*dnvecdpol(1,1)
     x                           -3.d0*dndpnn(1,1,1,1)
     x                           -drittel*dnvecdpol(1,1))
          d2eps0dpol(1,1,2)=fakt*(2.d0*dnvecdpol(1,2)
     x                           -3.d0*dndpnn(1,2,1,1)
     x                           -drittel*dnvecdpol(1,2))
          d2eps0dpol(2,1,1)=fakt*(-2.d0*dndpnn(2,1,2,1)-dndpnn(1,1,2,2)
     x                            -drittel*dnvecdpol(1,1))
          d2eps0dpol(2,1,2)=fakt*(-2.d0*dndpnn(2,2,2,1)-dndpnn(1,2,2,2)
     x                            -drittel*dnvecdpol(1,2))
          d2eps0dpol(3,1,1)=fakt*2.d0*(dnvecdpol(2,1)
     x                                -2.d0*dndpnn(1,1,1,2)
     x                                -dndpnn(2,1,1,1))
          d2eps0dpol(3,1,2)=fakt*2.d0*(dnvecdpol(2,2)
     x                                -2.d0*dndpnn(1,2,1,2)
     x                                -dndpnn(2,2,1,1))
          d2eps0dpol(1,2,1)=fakt*(-2.d0*dndpnn(1,1,1,2)-dndpnn(2,1,1,1)
     x                            -drittel*dnvecdpol(2,1))
```

```
          d2eps0dpol(1,2,2)=fakt*(-2.d0*dndpnn(1,2,1,2)-dndpnn(2,2,1,1)
     x                                  -drittel*dnvecdpol(2,2))
          d2eps0dpol(2,2,1)=fakt*(2.d0*dnvecdpol(2,1)
     x                                 -3.d0*dndpnn(2,1,2,2)
     x                                -drittel*dnvecdpol(2,1))
          d2eps0dpol(2,2,2)=fakt*(2.d0*dnvecdpol(2,2)
     x                                 -3.d0*dndpnn(2,2,2,2)
     x                                -drittel*dnvecdpol(2,2))
          d2eps0dpol(3,2,1)=fakt*2.d0*(dnvecdpol(1,1)
     x                                      -2.d0*dndpnn(2,1,2,1)
     x                                      -dndpnn(1,1,2,2))
          d2eps0dpol(3,2,2)=fakt*2.d0*(dnvecdpol(1,2)
     x                                      -2.d0*dndpnn(2,2,2,1)
     x                                      -dndpnn(1,2,2,2))

          krnn(1,1)=1.d0-nn(1,1)
          krnn(1,2)=-nn(1,2)
          krnn(2,1)=-nn(2,1)
          krnn(2,2)=1.d0-nn(2,2)

          do k=1,2
            do i=1,2
              do j=1,2
                brot(k,i,j)=(b33*nnn(i,j,k)+b31*krnn(i,j)*nvec(k)
     x                      +b15*.5d0*(krnn(k,i)*nvec(j)
     x                      +krnn(k,j)*nvec(i)))*apoldp0
                do k1=1,2
                  dnnndpol(k,i,j,k1)=dnvecdpol(i,k1)*nn(j,k)
     x                               +nn(i,k)*dnvecdpol(j,k1)
     x                               +nn(i,j)*dnvecdpol(k,k1)
                enddo
                do k1=1,2
                  do k2=1,2
                    d2nnndpol(k,i,j,k1,k2)=
     x                       d2nvecdpol(k,k1,k2)*nn(i,j)
     x                      +dnvecdpol(k,k1)*dndpn(i,k2,j)
     x                      +dnvecdpol(k,k1)*dndpn(j,k2,i)
     x                      +dnvecdpol(k,k2)*dndpn(i,k1,j)
     x                      +d2nvecdpol(i,k1,k2)*nn(k,j)
     x                      +dnvecdpol(i,k2)*dndpn(j,k1,k)
     x                      +dnvecdpol(k,k1)*dndpn(j,k2,i)
     x                      +dnvecdpol(i,k1)*dndpn(j,k2,k)
     x                      +d2nvecdpol(j,k1,k2)*nn(k,i)
                  enddo
```

```
                enddo
              enddo
            enddo
          enddo

          krpp(1,1)=1.d0-2.d0*pol1q/abspol2
          krpp(1,2)=-2.d0*pol(1)*pol(2)/abspol2
          krpp(2,1)=krpp(1,2)
          krpp(2,2)=1.d0-2.d0*pol2q/abspol2

          krdndp(1,1,1,1)=dnvecdpol(1,1)
          krdndp(1,1,1,2)=dnvecdpol(1,2)
          krdndp(1,1,2,1)=krdndp(1,1,1,2)
          krdndp(1,1,2,2)=dnvecdpol(2,2)
          krdndp(1,2,1,1)=0.d0
          krdndp(1,2,1,2)=0.d0
          krdndp(1,2,2,1)=0.d0
          krdndp(1,2,2,2)=0.d0
          krdndp(2,1,1,1)=0.d0
          krdndp(2,1,1,2)=0.d0
          krdndp(2,1,2,1)=0.d0
          krdndp(2,1,2,2)=0.d0
          krdndp(2,2,1,1)=dnvecdpol(1,1)
          krdndp(2,2,1,2)=dnvecdpol(1,2)
          krdndp(2,2,2,1)=dnvecdpol(2,1)
          krdndp(2,2,2,2)=dnvecdpol(2,2)

          do k=1,2
            do i=1,2
              do j=1,2
                do k1=1,2
                      dbrotdpol(k,i,j,k1)=pol(k1)/abspol2*brot(k,i,j)
     x                 +apoldp0*(dnnndpol(k,i,j,k1)*(b33-b31-b15)
     x                              +b31*krdndp(i,j,k,k1)
     x                     +.5d0*b15*(krdndp(k,i,j,k1)
     x                               +krdndp(k,j,i,k1)))
                enddo
                do k1=1,2
                  do k2=1,2
                    d2brotdpol(k,i,j,k1,k2)=1.d0/abspol2*(krpp(k1,k2)
     x                       *brot(k,i,j)+pol(k1)*dbrotdpol(k,i,j,k2))
     x         +nvec(k2)/pol0*(dnnndpol(k,i,j,k1)*(b33-b31-b15)
     x                           +b31*krdndp(i,j,k,k1)
     x                     +.5d0*b15*(krdndp(k,i,j,k1)
```

```
     x                                    +krdndp(k,j,i,k1)))
     x          +apoldp0*(d2nnndpol(k,i,j,k1,k2)*(b33-b31-b15)
     x                           +b31*kron(i,j)*d2nvecdpol(k,k1,k2)
     x                           +.5d0*b15*(kron(k,i)*d2nvecdpol(j,k1,k2)
     x                                     +kron(k,j)*d2nvecdpol(i,k1,k2)))
                  enddo
                enddo
              enddo
            enddo
          enddo
          call voigt_b36(bbb,brot,dbdpol,dbrotdpol,d2bdpol,d2brotdpol)
        else
          call setzero36(eps0,deps0dpol,d2eps0dpol,bbb,dbdpol,d2bdpol)
        endif ! if(abspol.ne.0.d0) then; LINE 314

        do j=1,2
          del(j)=0.d0
          do k=1,2
            del(j)=del(j)+aa(j,k)*eel(k)
          enddo
          do k=1,3
            del(j)=del(j)+bbb(j,k)*(eps(k)-eps0(k))
          enddo
          del(j)=del(j)+pol(j)
        enddo

        do j=1,3
          sig(j)=0.d0
          do k=1,3
            sig(j)=sig(j)+cc(j,k)*(eps(k)-eps0(k))
          enddo
          do k=1,2
            sig(j)=sig(j)-bbb(k,j)*eel(k)
          enddo
        enddo

        do j=1,3
          Hent=Hent+0.5d0*sig(j)*(eps(j)-eps0(j))
        enddo
        do j=1,2
          Hent=Hent-0.5d0*del(j)*eel(j)-0.5d0*pol(j)*eel(j)
        enddo

        Hsep=kaps*G/epsil*(a(1)+a(2)*(pol1q+pol2q)
```

```
     x               +a(3)*(pol(1)**4.d0+pol(2)**4.d0)
     x               +a(4)*pol1q*pol2q
     x               +a(5)*(pol(1)**6.d0+pol(2)**6.d0))

        Hint=kapi*G*epsil/pol0q*(gradpol(1)**2.d0
     x  +gradpol(2)**2.d0+gradpol(3)**2.d0+gradpol(4)**2.d0)

c       Berechnung einiger Hilfgroessen fuer Tangente vorziehen

c       compute the free charge density and its derivative; routines are
c       provided in ”free_charge_density.f”
        call getFreeChargeDensity(phiel,parms,rho
     x    ,rho_ele,rho_hol,rho_don,rho_acc )
        call getTangentFreeChargeDensity(phiel,parms,dRho_dPhi)



        if(isw.eq.3) then
          do i1=1,3
            do j1=1,2
              dsigdp(i1,j1)=0.d0
              do k1=1,3
                dsigdp(i1,j1)=dsigdp(i1,j1)-cc(i1,k1)*deps0dpol(k1,j1)
              enddo
              do k1=1,2
                dsigdp(i1,j1)=dsigdp(i1,j1)-dbdpol(k1,i1,j1)*eel(k1)
              enddo
            enddo
          enddo

          do i1=1,2
            do j1=1,2
              ddeldp(i1,j1)=0.d0
              do k1=1,3
                ddeldp(i1,j1)=ddeldp(i1,j1)
     x                     +dbdpol(i1,k1,j1)*(eps(k1)-eps0(k1))
     x                     -bbb(i1,k1)*deps0dpol(k1,j1)
              enddo
              ddeldp(i1,j1)=ddeldp(i1,j1)+kron(i1,j1)
            enddo
          enddo

          do i1=1,3
            do j1=1,2
```

```
              hilfpu2(i1,j1)=0.d0
              do k1=1,2
                hilfpu2(i1,j1)=hilfpu2(i1,j1)+dbdpol(k1,i1,j1)*eel(k1)
              enddo
            enddo
          enddo

          dpsidpol2(1,1)=2.d0*a(2)+12.d0*a(3)*pol1q+
     x                 2.d0*a(4)*pol2q+30.d0*a(5)*pol(1)**4.d0
          dpsidpol2(1,2)=4.d0*a(4)*pol(1)*pol(2)
          dpsidpol2(2,1)=dpsidpol2(1,2)
          dpsidpol2(2,2)=2.d0*a(2)+12.d0*a(3)*pol2q+
     x                 2.d0*a(4)*pol1q+30.d0*a(5)*pol(2)**4.d0


          do i1=1,2
            do j1=1,2
              hilfpp3(i1,j1)=0.d0
              do k1=1,3
                do k2=1,2
                  hilfpp3(i1,j1)=hilfpp3(i1,j1)
     x             -deps0dpol(k1,j1)*dbdpol(k2,k1,i1)*eel(k2)
     x             +(eps(k1)-eps0(k1))*d2bdpol(k2,k1,i1,j1)*eel(k2)
                enddo
              enddo
            enddo
          enddo

          do i1=1,2
            do j1=1,2
              hilfpp2(i1,j1)=0.d0
              do k1=1,3
                hilfpp2(i1,j1)=hilfpp2(i1,j1)
     x            +d2eps0dpol(k1,i1,j1)*sig(k1)
     x            +deps0dpol(k1,i1)*dsigdp(k1,j1)
              enddo
            enddo
          enddo

        endif ! if(isw.eq.3) then; LINE 540


        if(mod(isw,3).eq.0) then
          do 300 i=1,4
```

```
              Biel(1)=shp(1,i)
              Biel(2)=shp(2,i)

              Bi(1,1)=shp(1,i)
              Bi(1,2)=0.d0
              Bi(2,1)=0.d0
              Bi(2,2)=shp(2,i)
              Bi(3,1)=shp(2,i)
              Bi(3,2)=0.d0
              Bi(4,1)=0.d0
              Bi(4,2)=shp(1,i)

              Biu(1,1)=shp(1,i)
              Biu(1,2)=0.d0
              Biu(2,1)=0.d0
              Biu(2,2)=shp(2,i)
              Biu(3,1)=shp(2,i)
              Biu(3,2)=shp(1,i)

              if(isw.eq.3) then
                do 310 j=1,4
                  Bjel(1)=shp(1,j)
                  Bjel(2)=shp(2,j)

                  Bj(1,1)=shp(1,j)
                  Bj(1,2)=0.d0
                  Bj(2,1)=0.d0
                  Bj(2,2)=shp(2,j)
                  Bj(3,1)=shp(2,j)
                  Bj(3,2)=0.d0
                  Bj(4,1)=0.d0
                  Bj(4,2)=shp(1,j)

                  Bju(1,1)=shp(1,j)
                  Bju(1,2)=0.d0
                  Bju(2,1)=0.d0
                  Bju(2,2)=shp(2,j)
                  Bju(3,1)=shp(2,j)
                  Bju(3,2)=shp(1,j)

c                 TANGENTE

                  do i1=1,3
                    dsigde(i1)=0.d0
```

```
                  do j1=1,2
                    dsigdu(i1,j1)=0.d0
                    dsigde(i1)=dsigde(i1)+bbb(j1,i1)*Bjel(j1)
                    do k1=1,3
                      dsigdu(i1,j1)=dsigdu(i1,j1)+cc(i1,k1)*Bju(k1,j1)
                    enddo
                  enddo
                enddo

                do i1=1,2
                  ddelde(i1)=0.d0
                  do j1=1,2
                    ddeldu(i1,j1)=0.d0
                    ddelde(i1)=ddelde(i1)-aa(i1,j1)*Bjel(j1)
                    do k1=1,3
                      ddeldu(i1,j1)=ddeldu(i1,j1)+bbb(i1,k1)*Bju(k1,j1)
                    enddo
                  enddo
                enddo

c               Kee-terme einsortieren

                do k1=1,2
                 kmat(5*(i-1)+3,5*(j-1)+3)=
     x           kmat(5*(i-1)+3,5*(j-1)+3)
     x          +ddelde(k1)*Biel(k1)*xsj
                enddo


                kmat(5*(i-1)+3,5*(j-1)+3)=
     x           kmat(5*(i-1)+3,5*(j-1)+3)
     x             +shp(3,i)*dRho_dPhi*shp(3,j)*xsj

c               Kep-terme einsortieren

                do i1=1,2
                  hilfep(i1)=0.d0
                  do j1=1,2
                    hilfep(i1)=hilfep(i1)+Biel(j1)*ddeldp(j1,i1)
                  enddo
                enddo

                do j1=1,2
                  kmat(5*(i-1)+3,5*(j-1)+j1)=kmat(5*(i-1)+3,5*(j-1)+j1)
```

```
     x                    +hilfep(j1)*shp(3,j)*xsj
                enddo

c               Keu - terme berechnen

                do j1=1,2
                  do k1=1,2
                    kmat(5*(i-1)+3,5*(j-1)+3+j1)=
     x               kmat(5*(i-1)+3,5*(j-1)+3+j1)
     x              +Biel(k1)*ddeldu(k1,j1)*xsj
                  enddo
                enddo

c               Kpu -terme einsortieren

                do i1=1,2
                  do j1=1,2
                    hilfpu(i1,j1)=0.d0
                    do k1=1,3
                      hilfpu(i1,j1)=hilfpu(i1,j1)
     x                         +deps0dpol(k1,i1)*dsigdu(k1,j1)
     x                         +Bju(k1,j1)*hilfpu2(k1,i1)
                    enddo
                  enddo
                enddo

                do i1=1,2
                  do j1=1,2
                    kmat(5*(i-1)+i1,5*(j-1)+3+j1)=
     x                kmat(5*(i-1)+i1,5*(j-1)+3+j1)
     x                -shp(3,i)*hilfpu(i1,j1)*xsj
                  enddo
                enddo

c               Kpe -terme einsortieren
                do i1=1,3
                  do j1=1,2
                    hilfpe2(i1,j1)=0.d0
                    do k1=1,2
                      hilfpe2(i1,j1)=hilfpe2(i1,j1)-dbdpol(k1,i1,j1)
     x                *Bjel(k1)
                    enddo
                  enddo
                enddo
```

```

               do i1=1,2
                 hilfpe(i1)=0.d0
                 do j1=1,3
                   hilfpe(i1)=hilfpe(i1)+deps0dpol(j1,i1)*dsigde(j1)
     x                            +(eps(j1)-eps0(j1))*hilfpe2(j1,i1)
                 enddo
               enddo

               do k1=1,2
                 kmat(5*(i-1)+k1,5*(j-1)+3)=kmat(5*(i-1)+k1,5*(j-1)+3)
     x                 -shp(3,i)*(hilfpe(k1)-Bjel(k1))*xsj
               enddo

c              Kpp -terme einsortieren
               do i1=1,2
                 do j1=1,2
                   hilfpp(i1,j1)=0.d0
                   do k1=1,4
                     hilfpp(i1,j1)=hilfpp(i1,j1)+Bi(k1,i1)*Bj(k1,j1)
                   enddo
                 enddo
               enddo

               do i1=1,2
                 do j1=1,2
                   kmat(5*(i-1)+i1,5*(j-1)+j1)=
     x             kmat(5*(i-1)+i1,5*(j-1)+j1)
     x             +(kaps*G/epsil*dpsidpol2(i1,j1)*shp(3,i)*shp(3,j)
     x             -hilfpp2(i1,j1)*shp(3,i)*shp(3,j)
     x             -hilfpp3(i1,j1)*shp(3,i)*shp(3,j)
     x             +2.d0*kapi*G*epsil/pol0q*hilfpp(i1,j1))*xsj
                 enddo
               enddo

c              Kuu, Kup - berechnen
               do i1=1,2
                 do j1=1,2
                   do k1=1,3
                     kmat(5*(i-1)+3+i1,5*(j-1)+3+j1)=
     x                kmat(5*(i-1)+3+i1,5*(j-1)+3+j1)
     x               +Biu(k1,i1)*dsigdu(k1,j1)*xsj
                     kmat(5*(i-1)+3+i1,5*(j-1)+j1)=
     x                kmat(5*(i-1)+3+i1,5*(j-1)+j1)
```

```
     x                +Biu(k1,i1)*dsigdp(k1,j1)*shp(3,j)*xsj
                    enddo
                  enddo
                enddo

c               Kue - terme berechnen
                do i1=1,2
                  do k1=1,3
                  kmat(5*(i-1)+3+i1,5*(j-1)+3)=
     x              kmat(5*(i-1)+3+i1,5*(j-1)+3)
     x              +Biu(k1,i1)*dsigde(k1)*xsj
                  enddo
                enddo

c               Form damping matrix
                do i1=1,2
                  dmat(5*(i-1)+i1,5*(j-1)+i1)=
     x            dmat(5*(i-1)+i1,5*(j-1)+i1)
     x            +1.d0/alpha*shp(3,i)*shp(3,j)*xsj
                enddo

310           continue

            endif   ! if(isw.eq.3); LINE 631

c           compute residuals

            hilfres1(1)=0.d0
            hilfres1(2)=0.d0
            do i1=1,3
              hilfres1(1)=hilfres1(1)+deps0dpol(i1,1)*sig(i1)
              hilfres1(2)=hilfres1(2)+deps0dpol(i1,2)*sig(i1)
            enddo

            hilfres2(1)=0.d0
            hilfres2(2)=0.d0
            do i1=1,2
              do j1=1,3
                hilfres2(1)=hilfres2(1)
     x                   +(eps(j1)-eps0(j1))*dbdpol(i1,j1,1)*eel(i1)
                hilfres2(2)=hilfres2(2)
     x                   +(eps(j1)-eps0(j1))*dbdpol(i1,j1,2)*eel(i1)
              enddo
            enddo
```

```

           dpsidpol(1)=2.d0*a(2)*pol(1)+4.d0*a(3)*pol(1)**3.d0+
     x               2.d0*a(4)*pol(1)*pol2q
     x              +6.d0*a(5)*pol(1)**5.d0
           dpsidpol(2)=2.d0*a(2)*pol(2)+4.d0*a(3)*pol(2)**3.d0+
     x               2.d0*a(4)*pol(2)*pol1q
     x              +6.d0*a(5)*pol(2)**5.d0


           dpsidp(1)=+shp(3,i)*(eel(1)-kaps*G/epsil*dpsidpol(1)
     x                                  +hilfres1(1)+hilfres2(1))*xsj
     x                         -2.d0*kapi*G*epsil/pol0q*(Bi(1,1)*gradpol(1)
     x                            +Bi(2,1)*gradpol(2)
     x                            +Bi(3,1)*gradpol(3)
     x                            +Bi(4,1)*gradpol(4))*xsj

           dpsidp(2)=+shp(3,i)*(eel(2)-kaps*G/epsil*dpsidpol(2)
     x                                  +hilfres1(2)+hilfres2(2))*xsj
     x                         -2.d0*kapi*G*epsil/pol0q*(Bi(1,2)*gradpol(1)
     x                            +Bi(2,2)*gradpol(2)
     x                            +Bi(3,2)*gradpol(3)
     x                            +Bi(4,2)*gradpol(4))*xsj

           p_r(5*(i-1)+1)=p_r(5*(i-1)+1)
     x                       -1.d0/alpha*shp(3,i)*poldot(1)*xsj+dpsidp(1)
           p_r(5*(i-1)+2)=p_r(5*(i-1)+2)
     x                       -1.d0/alpha*shp(3,i)*poldot(2)*xsj+dpsidp(2)



c          compute residual for electrical problem
c
c          augmented version that considers volume charges
           do i1=1,2
             p_r(5*(i-1)+3)=p_r(5*(i-1)+3)
     x       -Biel(i1)*del(i1)*xsj
           enddo

            p_r(5*(i-1)+3)=p_r(5*(i-1)+3)-shp(3,i)*rho*xsj

c          compute residual for mechanical problem -(BI^T sigma)
           do i1=1,2
             do k1=1,3
               p_r(5*(i-1)+3+i1)=p_r(5*(i-1)+3+i1)
```

```
     x         -Biu(k1,i1)*sig(k1)*xsj
             enddo
           enddo

300      continue

       endif        !   if(mod(isw,3).eq.0); LINE 610

       if(isw.eq.4) then
         write(iow,2500) (ix(i),i=1,4),(u(i),i=1,2),(eps(i),i=1,3),
     x                   (sig(i),i=1,3),phiel,(eel(i),i=1,2),
     x                   (del(i),i=1,2)
         write(*,2500) (ix(i),i=1,4),(u(i),i=1,2),(eps(i),i=1,3),
     x                 (sig(i),i=1,3),phiel,(eel(i),i=1,2),(del(i),i=1,2)
       endif

       if (isw.eq.8) then
c          angle=datan2(pol_gl(2),pol_gl(1))
c          if(angle.lt.0.d0) then
c            angle=angle+2.d0*pi
c          endif
c          angle=angle/pi*180.d0

         del_gl(1)=Q(1,1)*del(1)+Q(2,1)*del(2)
         del_gl(2)=Q(1,2)*del(1)+Q(2,2)*del(2)

         sig_gl(1)=Q(1,1)**2.d0*sig(1)+Q(2,1)**2.d0*sig(2)
     x             +2.d0*Q(1,1)*Q(2,1)*sig(3)
         sig_gl(2)=Q(1,2)**2.d0*sig(1)+Q(2,2)**2.d0*sig(2)
     x             +2.d0*Q(1,2)*Q(2,2)*sig(3)
         sig_gl(3)=Q(1,1)*Q(1,2)*sig(1)+Q(2,1)*Q(2,2)*sig(2)
     x             +(Q(1,1)*Q(2,2)+Q(1,2)*Q(2,1))*sig(3)

         valp(1)=rho         !
         valp(2)=eel(2)      !
c          valp(3)=sig_gl(3)       !
         valp(3)=phiel
         valp(4)=rho_don
         valp(5)=rho_acc
         valp(6)=eel_gl(2)        !  E_2
c          valp(8)=abspol          !
c          valp(9)=angle           !
         valp(7)=gradpol(1) + gradpol(2)
         valp(8)=Hent+Hint+Hsep
```

```
            valp(9)=dRho_dPhi



            call elmt36plot(ix,valp,shp,xsj,
     x                      hr(nph),hr(nph+numnp),hr(ner),
     x                      4,numnp)
          endif

320     continue     ! do l=1,lint


c       Form overall element matrix

        do i=1,20
          do j=1,20
            s_r(i,j)=ctan(1)*kmat(i,j)+ctan(2)*dmat(i,j)
          enddo
        enddo

c       back-rotate residual: p = Q^T * p_r

        do i=1,4
          p(5*(i-1)+1)=QT(1,1)*p_r(5*(i-1)+1)+QT(1,2)*p_r(5*(i-1)+2)
          p(5*(i-1)+2)=QT(2,1)*p_r(5*(i-1)+1)+QT(2,2)*p_r(5*(i-1)+2)
          p(5*(i-1)+3)=p_r(5*(i-1)+3)
          p(5*(i-1)+4)=QT(1,1)*p_r(5*(i-1)+4)+QT(1,2)*p_r(5*(i-1)+5)
          p(5*(i-1)+5)=QT(2,1)*p_r(5*(i-1)+4)+QT(2,2)*p_r(5*(i-1)+5)
        enddo

c       back-rotate tangent: s = Q^T * s_r * Q

        do i=1,4
          do j=1,4
            do k=1,2
              m=k+3
              do l=1,2
                n=l+3
c       s_pp
                s_q(5*(i-1)+k,5*(j-1)+l)=QT(k,1)*s_r(5*(i-1)+1,5*(j-1)+l)
     x                                  +QT(k,2)*s_r(5*(i-1)+2,5*(j-1)+l)
c       s_uu
                s_q(5*(i-1)+m,5*(j-1)+n)=QT(k,1)*s_r(5*(i-1)+4,5*(j-1)+n)
     x                                  +QT(k,2)*s_r(5*(i-1)+5,5*(j-1)+n)
```

```
c     s_pu
              s_q(5*(i-1)+k,5*(j-1)+n)=QT(k,1)*s_r(5*(i-1)+1,5*(j-1)+n)
     x                                +QT(k,2)*s_r(5*(i-1)+2,5*(j-1)+n)
c     s_up
              s_q(5*(i-1)+m,5*(j-1)+l)=QT(k,1)*s_r(5*(i-1)+4,5*(j-1)+l)
     x                                +QT(k,2)*s_r(5*(i-1)+5,5*(j-1)+l)
            enddo ! l
          enddo ! k
c
          do k=1,2
            m=k+3
            do l=1,2
              n=l+3
c     s_pp
              s(5*(i-1)+k,5*(j-1)+l)=s_q(5*(i-1)+k,5*(j-1)+1)*Q(1,l)
     x                              +s_q(5*(i-1)+k,5*(j-1)+2)*Q(2,l)
c     s_uu
              s(5*(i-1)+m,5*(j-1)+n)=s_q(5*(i-1)+m,5*(j-1)+4)*Q(1,l)
     x                              +s_q(5*(i-1)+m,5*(j-1)+5)*Q(2,l)
c     s_pu
              s(5*(i-1)+k,5*(j-1)+n)=s_q(5*(i-1)+k,5*(j-1)+4)*Q(1,l)
     x                              +s_q(5*(i-1)+k,5*(j-1)+5)*Q(2,l)
c     s_up
              s(5*(i-1)+m,5*(j-1)+l)=s_q(5*(i-1)+m,5*(j-1)+1)*Q(1,l)
     x                              +s_q(5*(i-1)+m,5*(j-1)+2)*Q(2,l)
            enddo ! l
c     s_pe
            s(5*(i-1)+k,5*(j-1)+3)=QT(k,1)*s_r(5*(i-1)+1,5*(j-1)+3)
     x                            +QT(k,2)*s_r(5*(i-1)+2,5*(j-1)+3)
c     s_ue
            s(5*(i-1)+m,5*(j-1)+3)=QT(k,1)*s_r(5*(i-1)+4,5*(j-1)+3)
     x                            +QT(k,2)*s_r(5*(i-1)+5,5*(j-1)+3)
c     s_ep
            s(5*(i-1)+3,5*(j-1)+k)=s_r(5*(i-1)+3,5*(j-1)+1)*Q(1,k)
     x                            +s_r(5*(i-1)+3,5*(j-1)+2)*Q(2,k)
c     s_eu
            s(5*(i-1)+3,5*(j-1)+m)=s_r(5*(i-1)+3,5*(j-1)+4)*Q(1,k)
     x                            +s_r(5*(i-1)+3,5*(j-1)+5)*Q(2,k)
          enddo ! k
c     s_ee
          s(5*(i-1)+3,5*(j-1)+3)=s_r(5*(i-1)+3,5*(j-1)+3)
        enddo ! j
      enddo ! i
```

```
      return

      continue
      write(*,3000) isw
      write(iow,3000) isw
      return

c     Formatangaben

2000  format(' 4-node-element for electric mater., order parameter ',/,
     x       ' (Voigt notation)',//,
     x       ' C_ij    = ',3e12.4,/,
     x       '           ',3e12.4,/,
     x       '           ',3e12.4,//,
     x       ' B_ij    = ',3e12.4,/,
     x       '           ',3e12.4,//,
     x       ' A_ij    = ',2e12.4,/,
     x       '           ',2e12.4,/,
     x       ' P_0     = ',e12.4,/,
     x       ' eps_0   = ',e12.4,/,
     x       ' alpha   = ',e12.4,/,
     x       ' G       = ',e12.4,/,
     x       ' epsil   = ',e12.4,/,
     x       ' psi1    = ',e12.4,/,
     x       ' theta   = ',e12.4,/,
     x       ' Ef      = ',1e12.4,/,
     x       ' Ec      = ',1e12.4,/,
     x       ' Ev      = ',1e12.4,/,
     x       ' Ed      = ',1e12.4,/,
     x       ' Ea      = ',1e12.4,/,
     x       ' Nc      = ',1e12.4,/,
     x       ' Nv      = ',1e12.4,/,
     x       ' Nd      = ',1e12.4,/,
     x       ' Na      = ',1e12.4,/,
     x       ' za      = ',1e12.4,/,
     x       ' zd      = ',1e12.4,/,
     x       ' gd      = ',1e12.4,/,
     x       ' ga      = ',1e12.4,/,
     x       ' q       = ',1e12.4,/,
     x       ' k       = ',1e12.4,/,
     x       ' T       = ',1e12.4)

2500  format(' Element solution (nodes)  : ',4I4,/,
     x       ' ------------------------------------------',/,
```

```
     x         ' u_1,  u_2                        : ',2e12.4,/,
     x         ' eps_11,  eps_22  ,2eps_12        : ',3e12.4,/,
     x         ' sig_11,  sig_22  ,  sig_12       : ',3e12.4,/,
     x         ' phi                              : ',e12.4,/,
     x         ' E_1,  E_2                        : ',2e12.4,/,
     x         ' D_1,  D_2                        : ',2e12.4,/,
     x         ' ------------------------------------------',//)


3000  format(' Warning: Element  called  with  isw=',i4,' !  ',/,
     x         '            No  action  implemented  !  ',/)

      end
c-----7--------------------------------------------------------------------
      subroutine  voigt_b36(bbb,brot,dbdpol,dbrotdpol,d2bdpol,d2brotdpol)

        real*8  bbb(2,3),brot(2,2,2),dbdpol(2,3,2),dbrotdpol(2,2,2,2)
        real*8  d2bdpol(2,3,2,2),d2brotdpol(2,2,2,2,2)


        bbb(1,1)=brot(1,1,1)
        bbb(1,2)=brot(1,2,2)
        bbb(1,3)=brot(1,1,2)
        bbb(2,1)=brot(2,1,1)
        bbb(2,2)=brot(2,2,2)
        bbb(2,3)=brot(2,1,2)

        dbdpol(1,1,1)=dbrotdpol(1,1,1,1)
        dbdpol(1,1,2)=dbrotdpol(1,1,1,2)
        dbdpol(1,2,1)=dbrotdpol(1,2,2,1)
        dbdpol(1,2,2)=dbrotdpol(1,2,2,2)
        dbdpol(1,3,1)=dbrotdpol(1,1,2,1)
        dbdpol(1,3,2)=dbrotdpol(1,1,2,2)
        dbdpol(2,1,1)=dbrotdpol(2,1,1,1)
        dbdpol(2,1,2)=dbrotdpol(2,1,1,2)
        dbdpol(2,2,1)=dbrotdpol(2,2,2,1)
        dbdpol(2,2,2)=dbrotdpol(2,2,2,2)
        dbdpol(2,3,1)=dbrotdpol(2,1,2,1)
        dbdpol(2,3,2)=dbrotdpol(2,1,2,2)
        d2bdpol(1,1,1,1)=d2brotdpol(1,1,1,1,1)
        d2bdpol(1,1,1,2)=d2brotdpol(1,1,1,1,2)
        d2bdpol(1,1,2,1)=d2brotdpol(1,1,1,2,1)
        d2bdpol(1,1,2,2)=d2brotdpol(1,1,1,2,2)
        d2bdpol(1,2,1,1)=d2brotdpol(1,2,2,1,1)
```

```
        d2bdpol(1,2,1,2)=d2brotdpol(1,2,2,1,2)
        d2bdpol(1,2,2,1)=d2brotdpol(1,2,2,2,1)
        d2bdpol(1,2,2,2)=d2brotdpol(1,2,2,2,2)
        d2bdpol(1,3,1,1)=d2brotdpol(1,1,2,1,1)
        d2bdpol(1,3,1,2)=d2brotdpol(1,1,2,1,2)
        d2bdpol(1,3,2,1)=d2brotdpol(1,1,2,2,1)
        d2bdpol(1,3,2,2)=d2brotdpol(1,1,2,2,2)
        d2bdpol(2,1,1,1)=d2brotdpol(2,1,1,1,1)
        d2bdpol(2,1,1,2)=d2brotdpol(2,1,1,1,2)
        d2bdpol(2,1,2,1)=d2brotdpol(2,1,1,2,1)
        d2bdpol(2,1,2,2)=d2brotdpol(2,1,1,2,2)
        d2bdpol(2,2,1,1)=d2brotdpol(2,2,2,1,1)
        d2bdpol(2,2,1,2)=d2brotdpol(2,2,2,1,2)
        d2bdpol(2,2,2,1)=d2brotdpol(2,2,2,2,1)
        d2bdpol(2,2,2,2)=d2brotdpol(2,2,2,2,2)
        d2bdpol(2,3,1,1)=d2brotdpol(2,1,2,1,1)
        d2bdpol(2,3,1,2)=d2brotdpol(2,1,2,1,2)
        d2bdpol(2,3,2,1)=d2brotdpol(2,1,2,2,1)
        d2bdpol(2,3,2,2)=d2brotdpol(2,1,2,2,2)
      end

c-----7-----------------------------------------------------------------
      subroutine getacoef36(a,psi1,pol0)

        real*8 a(5),psi1,pol0,qq,matrix(5,5),ipiv(5),info

c         a(1)=1.d0
c         a(2)=0.d0
c         a(3)=0.d0
c         a(4)=psi1
c         a(5)=0.d0

        qq=0.88789d0-0.51696d0*psi1-0.43986d0*(psi1-.5d0)**2.d0
c         print*,qq



c         matrix(1,1)=1.d0
c         matrix(1,2)=0.d0
c         matrix(1,3)=0.d0
c         matrix(1,4)=0.d0
c         matrix(1,5)=0.d0
c         matrix(2,1)=1.d0
c         matrix(2,2)=pol0**2.d0
```

```
c        matrix(2,3)=pol0**4.d0
c        matrix(2,4)=0.d0
c        matrix(2,5)=pol0**6.d0
c        matrix(3,1)=0.d0
c        matrix(3,2)=2.d0*pol0
c        matrix(3,3)=4.d0*pol0**3.d0
c        matrix(3,4)=0.d0
c        matrix(3,5)=6.d0*pol0**5.d0
c        matrix(4,1)=1.d0
c        matrix(4,2)=2.d0*(qq*pol0)**2.d0
c        matrix(4,3)=2.d0*(qq*pol0)**4.d0
c        matrix(4,4)=(qq*pol0)**4.d0
c        matrix(4,5)=2.d0*(qq*pol0)**6.d0
c        matrix(5,1)=0.d0
c        matrix(5,2)=2.d0*qq*pol0
c        matrix(5,3)=4.d0*(qq*pol0)**3.d0
c        matrix(5,4)=2.d0*(qq*pol0)**3.d0
c        matrix(5,5)=6.d0*(qq*pol0)**5.d0
c
c        call dgetrf(5,5,matrix,5,ipiv,info)
c        call dgetrs('N',5,1,matrix,5,ipiv,a,5,info)

        a(1)=1.d0
        a(2)=-(-1.d0+psi1+2.d0*qq**6.d0)/qq**2.d0/pol0**2.d0/
     x                                                  (-1.d0+qq**4.d0)
        a(3)=(2.d0*(1.d0-psi1)-3.d0*qq**2.d0-qq**6.d0)/
     x        (pol0**4.d0*qq**2.d0*(1.d0-qq**4.d0))
        a(4)=-(2.d0*qq**6.d0-6.d0*qq**4.d0+3.d0*qq**2.d0
     x         -3.d0*qq**2.d0*psi1-1.d0+psi1)/pol0**4.d0/
     x                                         (qq**2.d0+1.d0)/qq**4.d0
        a(5)=(psi1-1.d0+2.d0*qq**2.d0)/
     x       (pol0**6.d0*qq**2.d0*(1.d0-qq**4.d0))

        print*,a(1),a(2),a(3),a(4),a(5)
      end

cc----7-----------------------------------------------------------------
      subroutine elmt36plot(ix,value,shp,xsj,dt,st,ser,nel,numnp)

        implicit none

        integer nel,numnp
        integer i,ll
        real*8  xg
```

```
        integer ix(*)
        real*8  dt(numnp),st(numnp,*),ser(*)
        real*8  xsj,shp(3,4),value(9)

        integer k

        save

c       Lumped and consistent projection routine

c       Compute lumped projection and assemble stress integrals

        do i = 1,nel
          ll = ix(i)
          if(ll.gt.0) then
            xg     = shp(3,i)*xsj
            dt(ll) = dt(ll) + xg
c           Projections of GP-Data
            do k=1,9
              st(ll,k) = st(ll,k) + value(k)*xg
            enddo
          endif
        end do
      end

cc-----7-------------------------------------------------------------------
      subroutine setzero36(eps0,deps0dpol,d2eps0dpol,bbb,dbdpol,
     x                        d2bdpol)

        real*8 eps0(3),deps0dpol(3,2),d2eps0dpol(3,2,2),bbb(2,3)
        real*8 dbdpol(2,3,2),d2bdpol(2,3,2,2)

c       print*,' ZERO POLARISATION !'
        eps0(1)=0.d0
        eps0(2)=0.d0
        eps0(3)=0.d0
        deps0dpol(1,1)=0.d0
        deps0dpol(2,1)=0.d0
        deps0dpol(3,1)=0.d0
        deps0dpol(1,2)=0.d0
        deps0dpol(2,2)=0.d0
        deps0dpol(3,2)=0.d0
        d2eps0dpol(1,1,1)=0.d0
```

```
        d2eps0dpol(1,1,2)=0.d0
        d2eps0dpol(1,2,1)=0.d0
        d2eps0dpol(1,2,2)=0.d0
        d2eps0dpol(2,1,1)=0.d0
        d2eps0dpol(2,1,2)=0.d0
        d2eps0dpol(2,2,1)=0.d0
        d2eps0dpol(2,2,2)=0.d0
        d2eps0dpol(3,1,1)=0.d0
        d2eps0dpol(3,1,2)=0.d0
        d2eps0dpol(3,2,1)=0.d0
        d2eps0dpol(3,2,2)=0.d0

        bbb(1,1)=0.d0
        bbb(1,2)=0.d0
        bbb(1,3)=0.d0
        bbb(2,1)=0.d0
        bbb(2,2)=0.d0
        bbb(2,3)=0.d0
        dbdpol(1,1,1)=0.d0
        dbdpol(1,1,2)=0.d0
        dbdpol(1,2,1)=0.d0
        dbdpol(1,2,2)=0.d0
        dbdpol(1,3,1)=0.d0
        dbdpol(1,3,2)=0.d0
        dbdpol(2,1,1)=0.d0
        dbdpol(2,1,2)=0.d0
        dbdpol(2,2,1)=0.d0
        dbdpol(2,2,2)=0.d0
        dbdpol(2,3,1)=0.d0
        dbdpol(2,3,2)=0.d0
        d2bdpol(1,1,1,1)=0.d0
        d2bdpol(1,1,1,2)=0.d0
        d2bdpol(1,1,2,1)=0.d0
        d2bdpol(1,1,2,2)=0.d0
        d2bdpol(1,2,1,1)=0.d0
        d2bdpol(1,2,1,2)=0.d0
        d2bdpol(1,2,2,1)=0.d0
        d2bdpol(1,2,2,2)=0.d0
        d2bdpol(1,3,1,1)=0.d0
        d2bdpol(1,3,1,2)=0.d0
        d2bdpol(1,3,2,1)=0.d0
        d2bdpol(1,3,2,2)=0.d0
        d2bdpol(2,1,1,1)=0.d0
        d2bdpol(2,1,1,2)=0.d0
```

```
        d2bdpol(2,1,2,1)=0.d0
        d2bdpol(2,1,2,2)=0.d0
        d2bdpol(2,2,1,1)=0.d0
        d2bdpol(2,2,1,2)=0.d0
        d2bdpol(2,2,2,1)=0.d0
        d2bdpol(2,2,2,2)=0.d0
        d2bdpol(2,3,1,1)=0.d0
        d2bdpol(2,3,1,2)=0.d0
        d2bdpol(2,3,2,1)=0.d0
        d2bdpol(2,3,2,2)=0.d0
      end
cc-----7------------------------------------------------------------------------


   Subroutines for space charge due to semiconducting feature of
   ferroelectrics

        call getFreeChargeDensity(phiel,parms,rho
     x    ,rho$\_$ele,rho$\_$hol,rho$\_$don,rho$\_$acc )
        call getTangentFreeChargeDensity(phiel,parms,dRho$\_$dPhi)




        subroutine getFreeChargeDensity(phi, p, rho,
     x       rho$\_$ele,rho$\_$hol,rho$\_$don,rho$\_$acc)

        implicit none

        real*8 phi, rho, t$\_$d, t$\_$a, p(16)

        real*8 rho$\_$ele,rho$\_$hol,rho$\_$don,rho$\_$acc

        ! Fermi-Dirac integrals provided in "fermi$\_$dirac$\_$integrals.f"
        real*8 F$\_$plusHalf, arg1, arg2, kt, qphi

        kt = p(15)*p(16)
        qphi = p(14)*phi
        arg1 = (p(4) - p(1) - qphi) / kt
        arg2 = (p(5) - p(1) - qphi) / kt

        !determine the fraction of ionized donors
        t$\_$d = 1.d0 - 1.d0 / (1.d0 + (1.d0 / p(12)) * dexp(arg1))

```

```
        !determine the fraction of ionized acceptors
        t$\_$a = 1.d0 / (1.d0 + p(13) * dexp(arg2))


        arg1 = (p(1) - p(2) + qphi) / kt
        arg2 = (p(3) - p(1) - qphi) / kt

        !determine the free charge density
        rho = -p(6) * F$\_$plusHalf(arg1)
     x     + p(7) * F$\_$plusHalf(arg2)
     x        + p(11) * p(8) * t$\_$d - p(10) * p(9) * t$\_$a
        rho = rho * p(14)

        rho$\_$ele=-p(6) * F$\_$plusHalf(arg1)
        rho$\_$hol=p(7) * F$\_$plusHalf(arg2)
        rho$\_$don=p(11) * p(8) * t$\_$d
        rho$\_$acc=- p(10) * p(9) * t$\_$a

        rho$\_$ele=rho$\_$ele*p(14)
        rho$\_$hol=rho$\_$hol*p(14)
        rho$\_$don=rho$\_$don*p(14)
        rho$\_$acc=rho$\_$acc*p(14)
      end















       subroutine getTangentFreeChargeDensity(phi, p, drho)

        implicit none

        real*8 phi, p(16), drho, dt$\_$d, dt$\_$a, arg1, arg2, kt, qphi,
   qex
```

```
        ! interface for the derivatives of Fermi-Dirac integrals as
        ! provided in ”fermi$\_$dirac$\_$integrals.f”
        real*8 F$\_$minusHalf

        kt = p(15)*p(16)
        qphi = p(14)*phi
        arg1 = (p(4) - p(1) - qphi) / kt
        arg2 = (p(5) - p(1) - qphi) / kt
        qex = p(14)**2 / kt

        ! determine the fraction of ionized donors derived w.r.t. the
        ! potential field (minus constant factors)
        dt$\_$d = dexp(arg1) / (1.d0 + (1.d0/p(12)) * dexp(arg1))**2

        ! determine the fraction of ionized acceptors derived w.r.t. to
        ! the potential field (minus constant factors)
        dt$\_$a = dexp(arg2) / (1.d0 + p(13) * dexp(arg2))**2

        arg1 = (p(1) - p(2) + qphi) / kt
        arg2 = (p(3) - p(1) - qphi) / kt

        ! determine the free charge density derived w.r.t. to the
        ! potential field
        drho = - p(6) * F$\_$minusHalf(arg1)
     x  -p(7) * F$\_$minusHalf(arg2)
     x  -p(11) * p(8) / p(12) * dt$\_$d
     x  -p(10) * p(9) * p(13) * dt$\_$a
        drho = drho * qex

          end



c     The functions provided here allow the approximation of Fermi-Dirac
c     integrals of order {-1/2, 1/2}
c
c     The specific series along with their coefficients are taken from
c     van Halen, P. and Pulfrey, D.L. ”Accurate short series
c     approximations to Fermi-Dirac integrals of order -1/2, 1/2, 3/2,
c     5/2, 3, and 7/2”, Journal of Applied Physics 57(12) (1985),
c     pp. 5271-5274, doi:10.1063/1.335269 (+ the accompanying erratum!)
c
c     The integral F$\_${1/2}(x) is approximated by four different series,
c     depending on the argument x:
```

```
c     { x <= 0; 0 < x <= 2; 2 <= x <= 4; x >= 4 }
c
c     Likewise, the integral F$\_${1/2}(x) is approximated by four series
c     over the argument ranges:
c     { x <= 0; 0 < x <= 2.5; 2.5 <= x <= 5; x >= 5 }
c


c     Series approximation for the Fermi-Dirac integral F$\_${1/2)(x)
      real*8 function F$\_$plusHalf(arg)

        implicit none

        real*8 arg, coeffs(7,4)
        integer r

        data coeffs / 1.0d0, 0.353568d0, 0.192439d0, 0.122973d0,
     x    0.077134d0, 0.036228d0, 0.008346d0,
     x                0.765147d0, 0.604911d0, 0.189885d0, 0.020307d0,
     x    -0.004380d0, -0.000366d0, 0.000133d0,
     x                0.777114d0, 0.581307d0, 0.206132d0, 0.017680d0,
     x    -0.006549d0, 0.000784d0, -0.000036d0,
     x                0.752253d0, 0.928195d0, 0.680839d0, 25.7829d0,
     x    -553.636d0, 3531.43d0, -3254.65d0 /

        F$\_$plusHalf = 0.d0
        if(arg .le. 0.d0) then
          do r=1,7
            F$\_$plusHalf = F$\_$plusHalf +
     x        (-1.d0)**(r+1.d0) * coeffs(r,1) * dexp(r*arg)
          enddo
        else
          if(arg .le. 2.d0) then
            do r=1,7
              F$\_$plusHalf = F$\_$plusHalf + coeffs(r,2)*arg**(r-1.d0)
            enddo
          else if(arg .le. 4.d0) then
          do r=1,7
              F$\_$plusHalf = F$\_$plusHalf + coeffs(r,3)*arg**(r-1.d0)
            enddo
          else ! x > 4.0
            do r=1,7
              F$\_$plusHalf = F$\_$plusHalf + coeffs(r,4) / arg**(2.d0*r-2.d0)
```

```
          enddo
          F$\_$plusHalf = F$\_$plusHalf * arg**(1.5d0)
        endif
      endif

    end function

c      Series approximation for the Fermi-Dirac integral F$\_${-1/2)(x)
       real*8 function F$\_$minusHalf(arg)

         implicit none

         real*8 arg, coeffs(9,4)
         integer r

         data coeffs / 0.999909d0, 0.706781d0, 0.572752d0, 0.466318d0,
     x     0.324511d0, 0.152889d0, 0.033673d0, 0.d0, 0.d0,
     x                 0.604856d0, 0.380080d0, 0.059320d0, -0.014526d0,
     x     -0.004222d0, 0.001335d0, 0.000291d0, -0.000159d0, 0.000018d0,
     x                 0.638086d0, 0.292266d0, 0.159486d0, -0.077691d0,
     x     0.018650d0, -0.002736d0, 0.000249d0, -0.000013d0, 0.d0,
     x                 1.12837d0, -0.470698d0, -0.453108d0, -228.975d0,
     x     8303.50d0, -118124.d0, 632895.d0, 0.d0, 0.d0 /


         F$\_$minusHalf = 0.d0
         if(arg .le. 0.d0) then
           do r=1,7
             F$\_$minusHalf = F$\_$minusHalf +
     x         (-1.d0)**(r+1.d0) * coeffs(r,1) * dexp(r*arg)
           enddo
         else
           if(arg .le. 2.5d0) then
             do r=1,9
               F$\_$minusHalf = F$\_$minusHalf + coeffs(r,2)*arg**(r-1.d0)
             enddo
           else if(arg .le. 5.d0) then
             do r=1,9
               F$\_$minusHalf = F$\_$minusHalf + coeffs(r,3)*arg**(r-1.d0)
             enddo
           else ! x > 5.0
             do r=1,7
               F$\_$minusHalf = F$\_$minusHalf + coeffs(r,4)/arg**(2.d0*r-2.
  d0)
```

```
          enddo
          F$\_$minusHalf = F$\_$minusHalf * arg**(0.5d0)
        endif
        endif

    end function

\subsection{FEAP code for ferroelectrics with defect dipoles}

Since this part of code shares many lines with the one with semiconducting feature. One makes only an excerpt from the most essential lines.
The code is for ferroelectrics with switchable defect dipoles. For static defect dipoles, one just need to remove all the $c_i$ terms and make $P_d$ a constant,
and then the case is reduced to a static one.

      do 320 l = 1,lint

      ss(1)=sg(1,l)
      ss(2)=sg(2,l)

      call shp2d(ss,xl$\_$r,shp,xsj,ndm,4,ix,.false.)
    xsj = xsj*sg(3,l)

      call shp2d(ss,xl,shp$\_$gl,xsj_gl,ndm,4,ix,.false.)
      xsj$\_$gl = xsj$\_$gl*sg(3,l)


      phiel=0.d0
      eps(1)=0.d0
      eps(2)=0.d0
      eps(3)=0.d0
    Hent=0.d0
    Hint=0.d0
    Hsep=0.d0

      do i=1,2
    u(i)=0.d0
        eele(i)=0.d0
        eelt(i)=0.d0
        eel$\_$gl(i)=0.d0
        pol(i)=0.d0
        poldot(i)=0.d0
```

```
          chd(i)=0.d0
          chddot(i)=0.d0
          gradpol(2*(i-1)+1)=0.d0
          gradpol(2*(i-1)+2)=0.d0
          gradchd(2*(i-1)+1)=0.d0  ! pay attention that gradchd not in same order like gradpol
          gradchd(2*(i-1)+2)=0.d0
          chb(i)=0.d0
          chbdot(i)=0.d0
          gradchb(2*(i-1)+1)=0.d0  ! pay attention that gradchd not in same order like gradpol
          gradchb(2*(i-1)+2)=0.d0
        enddo

        do j=1,4
          phiel = phiel + shp(3,j)*ul$\_$r(3,j,1)
           pol(1) = pol(1) + shp(3,j)*ul$\_$r(1,j,1)
          pol(2) = pol(2) + shp(3,j)*ul$\_$r(2,j,1)
         chd(1) = chd(1) + shp(3,j)*ul$\_$r(6,j,1)
          chd(2) = chd(2) + shp(3,j)*ul$\_$r(7,j,1)
         chb(1) = chb(1) + shp(3,j)*ul$\_$r(8,j,1)
          chb(2) = chb(2) + shp(3,j)*ul$\_$r(9,j,1)

         poldot(1) = poldot(1) + shp(3,j)*ul$\_$r(1,j,4)
          poldot(2) = poldot(2) + shp(3,j)*ul$\_$r(2,j,4)
           chddot(1) = chddot(1) + shp(3,j)*ul$\_$r(6,j,4)
          chddot(2) = chddot(2) + shp(3,j)*ul$\_$r(7,j,4)
           chbdot(1) = chbdot(1) + shp(3,j)*ul$\_$r(8,j,4)
          chbdot(2) = chbdot(2) + shp(3,j)*ul$\_$r(9,j,4)

      u(1)   = u(1) + shp(3,j)*ul$\_$r(4,j,1)
          u(2)   = u(2) + shp(3,j)*ul$\_$r(5,j,1)
      eps(1) = eps(1) + shp(1,j)*ul$\_$r(4,j,1)
      eps(2) = eps(2) + shp(2,j)*ul$\_$r(5,j,1)
      eps(3) = eps(3) + shp(1,j)*ul$\_$r(5,j,1) + shp(2,j)*ul$\_$r(4,j,1)
      eele(1) = eele(1) - shp(1,j)*ul$\_$r(3,j,1)
      eele(2) = eele(2) - shp(2,j)*ul$\_$r(3,j,1)
          eel$\_$gl(1) = eel$\_$gl(1) - shp$\_$gl(1,j)*ul(3,j,1)
      eel$\_$gl(2) = eel$\_$gl(2) - shp$\_$gl(2,j)*ul(3,j,1)
          gradpol(1) = gradpol(1) + shp(1,j)*ul$\_$r(1,j,1)
      gradpol(2) = gradpol(2) + shp(2,j)*ul$\_$r(2,j,1)
          gradpol(3) = gradpol(3) + shp(2,j)*ul$\_$r(1,j,1)
      gradpol(4) = gradpol(4) + shp(1,j)*ul$\_$r(2,j,1)
              gradchd(1) = gradchd(1) + shp(1,j)*ul$\_$r(6,j,1)
```

```
   gradchd(2) = gradchd(2) + shp(1,j)*ul$\_$r(7,j,1)
       gradchd(3) = gradchd(3) + shp(2,j)*ul$\_$r(6,j,1)
   gradchd(4) = gradchd(4) + shp(2,j)*ul$\_$r(7,j,1)

       gradchb(1) = gradchb(1) + shp(1,j)*ul$\_$r(8,j,1)
   gradchb(2) = gradchb(2) + shp(1,j)*ul$\_$r(9,j,1)
       gradchb(3) = gradchb(3) + shp(2,j)*ul$\_$r(8,j,1)
   gradchb(4) = gradchb(4) + shp(2,j)*ul$\_$r(9,j,1)
    enddo

                                                                   !
total electrical field
     eelt(1)= eele(1)+C0*(chb(2)-chb(1))*pd/(pi*k0)
     eelt(2)= eele(2)+C0*(chd(2)-chd(1))*pd/(pi*k0)

                                                             ! total
polarization
        polt(1)= pol(1)+(chb(2)-chb(1))*pd
         polt(2)= pol(2)+(chd(2)-chd(1))*pd

      if (pol(2)>=0.0) then
       E42=0.62
       E23=1.40
       E31=1.06
       E14=1.17
       E32=0.62
       E24=1.40
       E41=1.06
       E13=1.17
      endif

      if (pol(2)<0.0) then
       E42=1.06
       E23=1.17
       E31=0.62
       E14=1.40
       E32=1.06
       E24=1.17
       E41=0.62
       E13=1.40
      endif

            F14=omega*exp(-E14*qunit/T/kb)
            F31=omega*exp(-E31*qunit/T/kb)
```

```
              F23=omega*exp(-E23*qunit/T/kb)
              F42=omega*exp(-E42*qunit/T/kb)

              F41=omega*exp(-E41*qunit/T/kb)
              F13=omega*exp(-E13*qunit/T/kb)
              F32=omega*exp(-E32*qunit/T/kb)
              F24=omega*exp(-E24*qunit/T/kb)




            kmat(9*(i-1)+6,9*(j-1)+6)=kmat(9*(i-1)+6,9*(j-1)+6)+0.d0
     x         -(0.5*F13+0.5*F14)*shp(3,i)*shp(3,j)*xsj

            kmat(9*(i-1)+6,9*(j-1)+7)=kmat(9*(i-1)+6,9*(j-1)+7)+0.d0
    x         +0.0

            kmat(9*(i-1)+6,9*(j-1)+8)=kmat(9*(i-1)+6,9*(j-1)+8)+0.d0
     x         +0.5*F31*shp(3,i)*shp(3,j)*xsj

            kmat(9*(i-1)+6,9*(j-1)+9)=kmat(9*(i-1)+6,9*(j-1)+9)+0.d0
     x         +0.5*F41*shp(3,i)*shp(3,j)*xsj


            kmat(9*(i-1)+7,9*(j-1)+6)=kmat(9*(i-1)+7,9*(j-1)+6)+0.d0
     x         +0.0

            kmat(9*(i-1)+7,9*(j-1)+7)=kmat(9*(i-1)+7,9*(j-1)+7)+0.d0
     x         -(0.5*F23+0.5*F24)*shp(3,i)*shp(3,j)*xsj

             kmat(9*(i-1)+7,9*(j-1)+8)=kmat(9*(i-1)+7,9*(j-1)+8)+0.d0
     x         +0.5*F32*shp(3,i)*shp(3,j)*xsj

            kmat(9*(i-1)+7,9*(j-1)+9)=kmat(9*(i-1)+7,9*(j-1)+9)+0.d0
     x         +0.5*F42*shp(3,i)*shp(3,j)*xsj




               kmat(9*(i-1)+8,9*(j-1)+6)=kmat(9*(i-1)+8,9*(j-1)+6)+0.d0
     x         +0.5*F13*shp(3,i)*shp(3,j)*xsj
```

```
             kmat(9*(i-1)+8,9*(j-1)+7)=kmat(9*(i-1)+8,9*(j-1)+7)+0.d0
     x          +0.5*F23*shp(3,i)*shp(3,j)*xsj

             kmat(9*(i-1)+8,9*(j-1)+8)=kmat(9*(i-1)+8,9*(j-1)+8)+0.d0
     x          -(0.5*F32+0.5*F31)*shp(3,i)*shp(3,j)*xsj

             kmat(9*(i-1)+8,9*(j-1)+9)=kmat(9*(i-1)+8,9*(j-1)+9)+0.d0
     x          +0.0





             kmat(9*(i-1)+9,9*(j-1)+6)=kmat(9*(i-1)+9,9*(j-1)+6)+0.d0
     x         +0.5*F14*shp(3,i)*shp(3,j)*xsj

             kmat(9*(i-1)+9,9*(j-1)+7)=kmat(9*(i-1)+9,9*(j-1)+7)+0.d0
     x          +0.5*F24*shp(3,i)*shp(3,j)*xsj

             kmat(9*(i-1)+9,9*(j-1)+8)=kmat(9*(i-1)+9,9*(j-1)+8)+0.d0
     x          +0.0

             kmat(9*(i-1)+9,9*(j-1)+9)=kmat(9*(i-1)+9,9*(j-1)+9)+0.d0
     x          -(0.5*F42+0.5*F41)*shp(3,i)*shp(3,j)*xsj


     c           Form damping matrix

            do i1=1,2


           dmat(9*(i-1)+i1 ,9*(j-1)+i1 )=dmat(9*(i-1)+i1 ,9*(j-1)+i1 )
     x     +1.d0/alpha*shp(3,i)*shp(3,j)*xsj

            enddo

           dmat(9*(i-1)+6,9*(j-1)+6)=dmat(9*(i-1)+6,9*(j-1)+6)
     x     -shp(3,i)*shp(3,j)*xsj

       dmat(9*(i-1)+7,9*(j-1)+7)=dmat(9*(i-1)+7,9*(j-1)+7)
     x     -shp(3,i)*shp(3,j)*xsj

           dmat(9*(i-1)+8,9*(j-1)+8)=dmat(9*(i-1)+8,9*(j-1)+8)
     x     -shp(3,i)*shp(3,j)*xsj
```

```

        dmat(9*(i-1)+9,9*(j-1)+9)=dmat(9*(i-1)+9,9*(j-1)+9)
     x        -shp(3,i)*shp(3,j)*xsj

              p$\_$r(9*(i-1)+6)=p$\_$r(9*(i-1)+6)+0.d0
     x       +(0.5*F13*chd(1)+0.5*F14*chd(1)
     x       -0.5*F31*chb(1)-0.5*F41*chb(2))*shp(3,i)*xsj


        p$\_$r(9*(i-1)+6)=p$\_$r(9*(i-1)+6)+shp(3,i)*chddot(1)*xsj


        p$\_$r(9*(i-1)+7)=p$\_$r(9*(i-1)+7)+0.d0
     x   +(0.5*F23*chd(2)+0.5*F24*chd(2)
     x   -0.5*F32*chb(1)-0.5*F42*chb(2))*shp(3,i)*xsj


        p$\_$r(9*(i-1)+7)=p$\_$r(9*(i-1)+7)+shp(3,i)*chddot(2)*xsj


        p$\_$r(9*(i-1)+8)=p$\_$r(9*(i-1)+8)+0.d0
     x   +((0.5*F32+0.5*F31)*chb(1)
     x     -0.5*F13*chd(1)-0.5*F23*chd(2))*shp(3,i)*xsj


        p$\_$r(9*(i-1)+8)=p$\_$r(9*(i-1)+8)+shp(3,i)*chbdot(1)*xsj


       p$\_$r(9*(i-1)+9)=p$\_$r(9*(i-1)+9)+0.d0
     x   +((0.5*F42+0.5*F41)*chb(2)
     x     -0.5*F14*chd(1)-0.5*F24*chd(2))*shp(3,i)*xsj


        p$\_$r(9*(i-1)+9)=p$\_$r(9*(i-1)+9)+shp(3,i)*chbdot(2)*xsj
```

Bibliography

[1] Valasek, J., (1920). ‘Piezoelectric and allied phenomena in Rochelle salt‘. Physical Review 15: 537

[2] Busch, G., Scherer, P., (1935) Naturwiss. 23, 737.

[3] Wul, W., Goldman, I.M.C.R., (1946) *Acad. Sci. Russ.* 40, 139.

[4] Känzig, W., Ferroelectrics and Antiferroelectrics, Academic Press.

[5] Matthias, B. T., (1949) ‘New ferroelectric crystals.‘ *Phys. Rev.* **75**, 11, 1771-1771

[6] Matthias, B. T., Remeika, J. P., (1949) ‘Ferroelasticity in the ilmenite structure.‘ *Phys. Rev.* **76** 12 1886-1887.

[7] Shirane, G., Hoshino, S., Suzuki, K., (1950) ‘X-ray study of the phase transition in lead titanate.‘ *Phys. Rev.* **80**, 1105.

[8] Bernstein, S., Wong, T., Kisler, Y. and Tustison, R., (1993),‘Fatigue of ferroelectric $PbZr_xTi_yO_3$ capacitors with Ru and RuO_x electrodes. ‘ *J. Mat. Res.* **8**, 12-13.

[9] Auciello, O., Gifford, K. D., Lichtenwalner, D. J., Dat, R., Al-Shareef, H. N., Bellur, K. R., and Kingon, A., (1995) ‘A review of composition-structure-property relationships for PZT-based heterostructure capacitors.‘ *Integr. Ferro.* **6**, 173.

[10] Cross, J., Fujiki, M., Tsukada, M., Kotaka, Y., and Goto, Y., (1998) ‘Characterization of PZT capacitors with $SrRuO_3$ electrodes.‘ *Integr. Ferro.* **21**, 263.

[11] Yoo, I. K. and Desu, S. B., (1992),‘Mechanism of fatigue in ferroelectric thin-films. ‘ *Phys. Status Solidi A* **133**, 565.

[12] Tagantsev, A. K., Stolichnov, I., Colla, E. L., Setter, N., (2001) ‘Polarization fatigue in ferroelectric films: Basic experimental findings, phenomenological scenarios, and microscopic features.‘ *J. Appl. Phys.* **90**, 1384.

[13] Paton, E., Brazier, M., Mansour, S. and Bement, A., (1997) ‘A critical study of defect migration and ferroelectric fatigue in lead zirconate titanate thin film capacitors under extreme temperatures.‘ *Integr. Ferro.*

[14] Pawlaczyk, C., Tagantsev, A. K., Brooks, K., Reaney, I. M., Klissurska, R. and Setter N., (1995) ‘Fatigue, rejuvenation and self-restoring in ferroelectric thin-films.‘ *Integr. Ferro.* **8**, 293.

[15] Majumder, S. B., Mohapatra, Y. N. and Agrawal, D. C., (1997) ‘Optical and microstructural characterization of sol-gel derived cerium-doped PZT thin films.‘ *J. Mat. Sci.* **32**, 2141.

[16] AlShareef, H. N., Tuttle, B. A., Warren, W. L., Headley, T. J., Dimos, D., Voigt, J. A. and Nasby, R. D., (1996) ‘Effect of B-site cation stoichiometry on electrical fatigue of $RuO_2/Pb(Zr_xTi_{1-x})O_3/RuO_2$ capacitors.‘ *Phys. Rev.* **80**, 1105.

[17] Griswold, E. M., Sayer, M., Amm, D. T. and Calder, I. D., (1991) ‘The influence of niobium-doping on lead zirconate titanate ferroelectric thin-films.‘ *Can. J. Phys.* **69**, 260.

[18] Shimizu, M., Fujisawa, H. and Shiosaki, T. (1997) ‘Effects of La and Nb modification on the electrical properties of $Pb(Zr, Ti)O_3$ thin films by MOCVD.‘ *Integr. Ferro.* **14**, 69.

[19] Aoki, K. and Fukuda, Y., (1991) ‘The effects of La and Nb modification on fatigue and retention properties of $Pb(Ti, Zr)O_3$ thin-film capacitors.‘ *Jap. J. Appl. Phys.* **36**, 1195.

[20] Klissurska, R. D., Brooks, K. G. and Setter, N. (1998) ‘Acceptor dopant effects on endurance of PZT thin films.‘ *Ferroelectrics* **225**, 977.

[21] Stolichnov, I., Tagantsev, A., Setter, N., Cross, J. S., Fujiki, M. and Tsukada, M., (1999) ‘Degradation of asymmetrical Pt/SRO/PLZT/Pt capacitors: Role of Pt and oxide electrodes.‘ *Integr. Ferro.* **26**, 1013.

[22] Stolichnov, I., Tagantsev, A. K., Colla, E. L. and Setter, N., (1998) ‘Cold-field-emission test of the fatigued state of $Pb(Zr_xTi_{1-x})O_3$ films.‘ *Appl. Phys. Lett.* **73**, 1361.

[23] Stolichnov, I., Tagantsev, A., Setter, N., Okhonin, S., Fazan, P. and Cross, J. S., (1998) ‘Dielectric breakdown in $(Pb, La)(Zr, Ti)O_3$ ferroelectric thin films with Pt and oxide electrodes.‘ *J. Appl. Phys.* **87**, 1925.

[24] Scott, J. DeAraujo, F. C. A. P., Melnick, B. M., McMillan, L. D. and Zuleeg, R., (1998) ‘Quantitative measurement of space-charge effects in lead zirconate-titanate memories.‘ *J. Appl. Phys.* **70**, 382.

[25] Davi, F., (2001) ‘On domain switching in deformable ferroelectrics, seen as continua with microstructure.‘ *Z. Angew. Math. Phys.* **52**, 966.

[26] Kessler, H. and Balke, H., (2006) ‘A continuum analysis of the driving force of ferroelectric/ferroelastic domain wall motions.‘ *J. Mech. Phys. Solid* **54**, 113.

[27] Mueller, R., Gross, D. and Lupascu, D. C., (2006) ‘Driving forces on domain walls in ferroelectric materials and interaction with defects.‘ *Comp. Mat. Sci.* **35**, 42.

[28] Bassiouny, E., Ghaleb, A. F., Maugin, G. A., (1988) ‘Thermodynamical Formulation For Coupled Electromechanical Hysteresis Effects. 1. Basic Equations. ‘ *Int. J. Eng. Sci.* **26**(12), 1279-1295.

[29] Bassiouny, E., Ghaleb, A. F., Maugin, G. A., (1988) ‘Thermodynamical Formulation For Coupled Electromechanical Hysteresis Effects. 2. Poling Of Ceramics. ‘ *Int. J. Eng. Sci.* **26**(12), 1297-1306.

[30] Huber, J. E., (1999) ‘A constitutive model for ferroelectric polycrystals.‘ *J. Mech, Phys. Solids* **47** 8 1663-1697

[31] Chen, X., Fang, D. N., Hwang, K. C., (1997) ‘Micromechanics simulation of ferroelectric polarization switching. ‘ *Acta Mater.* **45**(8), 3181-3189.

[32] Lu, W., Fang, D. N., Li, C. Q., Hwang, K. C., (1999) ‘Nonlinear electric-mechanical behavior and micromechanics modeling of ferroelectric domain evolution.‘ *Acta Mater.*, **47**(10), 2913-2926.

[33] Shaikh, M. G., Phanish, S., Sivakumar, S. M., (2006) ‘Domain switching criteria for ferroelectrics.‘ *Comp. Mater. Sci.*, **37**, 178-186.

[34] Kamlah, M., Tsakmakis, C.,(1999) ‘Phenomenological modeling of the nonlinear electromechanical coupling in ferroelectrics.‘ *Int. J. Solids Struct.*, 1999, **36**(5), 669-695.

[35] Kamlah, M., (2001) ‘Ferroelectric and ferroelastic piezoceramics - modeling of electromechanical hysteresis phenomena.‘ *Continuum. Mech. Thermodyn.* **13**, 219.

[36] Hwang, S. C., Lynch, C. S., McMeeking, R. M., (1995) ‘Ferroelectric/Ferroelastic Interactions And A Polarization Switching Model. ‘ Acta Metal. Mater. **43**(5), 2073-2084.

[37] Hwang, S. C., Huber, J. E., McMeeking, R. M., Fleck, N. A., (1998) ‘The simulation of switching in polycrystalline ferroelectric ceramics. ‘ *J. Appl. Phys.* **84**(3), 1530-1540.

[38] Zhang, Z. K., Fang, D. N., Soh, A. K., (2006) ‘A new criterion for domain switching in ferroelectric materials.‘ *Mech. Mater.*, **38**, 25-32.

[39] Dawber, M., Scott, J.F., (2000),‘A model for fatigue in ferroelectric perovskite thin films. ‘ *Appl. Phys. Lett.* **76**(8), 1060-1062.

[40] Beale, P. D., Duiker, H. M., (1991), ‘Microscopic modeling of thin-film ferroelectrics - Fatigue.‘ *Ferroelecfrics*, **116**(1-2), 111-116.

[41] Duiker, H. M., Beale, P. D., Scott, J.F., Dearaujo, C.A.P., Melnick, B.M., Cuchiaro, J.D., McMillian, L.D., (1990), ‘Fatigue and switching in ferroelectric memories - Theory and experiment. ‘ *J. Appl. Phys.* **68**(11), 5783-5791.

[42] Brennan C., (1993), ‘Model of ferroelectric fatigue due to defect/domain interactions.‘ *Ferroelecfrics*, **150**, 199-208.

[43] Jiang, Q. Y., Subbarao, E. C., Cross, L. E., (1994) ‘Effect of composition and temperature on electric fatigue of La-doped lead zirconate titanate ceramics.‘ *J. Appl. Phys.* **75**, 74337.

[44] Yu, S. W., Yu, L., (2009), ‘Effects of fatigue and damage on the hysteresis loops of ferroelectric ceramics.‘ *Micosyst. Technol.* **15**(1), 33-38.

[45] Warren, W.L., Dimos, D., Tuttle, B.A., Nasby, R.D., Pike, G.E., (1994), ‘Electronic domain pinning in $Pb(Zr,Ti)O_3$ thin-films and its role in fatigue.‘ *Appl. Phys. Lett.* **65**(8), 1018-1020.

[46] Du, X.F., Chen, I.W., (1998), ‘Fatigue of $Pb(Zr0.53Ti0.47)O_3$ ferroelectric thin films.‘ *J. Appl. Phys.* **83**(12), 7789-7798.

[47] Yoo, I. K., Desu, S. B., (1992), ‘Fatigue modeling of lead zirconate titanate thin-films.‘ *Mat. Sci. Eng. B-Solid*, **13**(4), 319-322.

[48] Portelles, J., Garcia, S., Martinez, E., Raymond, O., Almodovar, N. S., Heiras, J. L., Siqueiros, J. M., (2005) ‘Aging behavior in $Ba0.7Sr0.3Ti0.97Zr0.03O$ ceramics.‘ *J. Appl. Phys.* **97**(5), 054105.

[49] Poykko, S., Chadi, D.J., (1999), ‘Dipolar defect model for fatigue in ferroelectric perovskites.‘ *Phys. Rev. Lett.* **83**(6), 1231-1234.

[50] Malvern, L. E., *Introduction to the Mechanics of a Continuous Medium,* (Prentice Hall, 1977).

[51] Holzapfel, G. A. *Nonlinear Solid Mechanics: A Continuum Approach for Engineering,* (Wiley, 2000).

[52] Liu, I. S. *Continuum Mechanics,* (Springer, 2009).

[53] Bonet, J., R. D. Wood, *Nonlinear Continuum Mechanics for Finite Element Analysis,* (Cambridge University Press, 2008).

[54] Ogden, R. W. *Non-linear elastic deformations,* (Dover, 1984).

[55] Haupt, P., *Continuum mechanics and theory of materials,* (Springer, 2000).

[56] Tsakmakis, C., *Kontinuumsmechanik I, Lecture Script, Department of Civil Engineering and Geodesy,* (Technische Universität Darmstadt).

[57] Pao, Y. H. *Electromagnetic forces in deformable continua,* Mechanics Today, (1978).

[58] Eringen, A. C., Maugin, G. A., *Electrodynamics of continua,* (Springer, 1989).

[59] Sze, S. M., Ng, K. K., *Physics of Semiconductor Devices,* (Wiley, 2007).

[60] van der Waals, J. D., (1894). Z. Phys. Chem. 13:657

[61] Cahn, J. W., Hilliard, J. E., (1958). 'Free Energy of a Nonuniform System. I. Interfacial Free Energy.' *J. Chem. Phys.* **28**, 258-67

[62] Cahn, J. W., (1961) 'On spinodal decomposition' *Acta Metall.* **9**, 795-801

[63] Chen, L. Q., (2002) 'Phase-field models for microstructure evolution.' *Annu. Rev. Mater. Res.* **32**, 113-140

[64] Ginzburg, V. L. and Landau, L. D., (1950) 'On the theory of superconductivity.' *Zh. Eksp. Teor. Fiz.* **20**, 1064-1082.

[65] Mueller, H.: (1940) 'Properties of Rochelle salt.' *Phys. Rev.* **57**, 829-839

[66] Mueller, H. (1940) 'Properties ofRochelle salt. III.' *Phys. Rev.* **58**, 565-573

[67] Mueller, H. (1940) 'Properties ofRochelle salt. IV.' *Phys. Rev.* **58**, 805-811

[68] Ginzburg, V.L., (1945) 'The dielectric properties of crystals of seignettcelectric substances and ofbarium titanate.' *Zh. Eksp. Teor. Fiz* **15**, 739-749

[69] Devonshire, A. F., (1954) 'Theory of ferroelectrics.' *Adv. Phys. Phil. Mag.*, **3**, 10, 85-130

[70] Cao, W. W., Barsch, G. R., (1990) 'Landau-Ginzburg model of interphase boundaries in improper ferroelastic perovskites of $D_(18)^4h$ symmetry. ' *Phys. Rev. B* **41**, 4334-4348.

[71] Li, Y. L., Hu, S. Y.,Liu, Z. K., Chen, L. Q., (2002) 'Effect of substrate constraint on the stability and evolution of ferroelectric domain structures in thin films. ' *Acta Mat.* **50**, 395-411.

[72] Wang, J., Shi, S.-Q., Chen, L.-Q., Li, Y., Zhang, T.-Y., (2004), 'Phase-field simulations of ferroelectric/ferroelastic polarization switching.' *Acta Mater.* **52**, 749 (2004).

[73] Zhang, W., Bhattacharya, K., (2005) 'A computational model of ferroelectric domains. Part I: model formulation and domain switching.' *Acta Mater.* **53**, 185.

[74] Soh, A., Song, Y., Ni, Y., (2006) ‘Phase Field Simulations of Hysteresis and Butterfly Loops in Ferroelectrics Subjected to Electro-Mechanical Coupled Loading.‘ *J. Am. Ceram. Soc.* **89**, 652.

[75] Su, Y., Landis, C. M., (2007) ‘Continuum thermodynamics of ferroelectric domain evolution: Theory, finite element implementation, and application to domain wall pinning.‘ *J. Mech. Phys. Solids* **55**(2), 280-305

[76] Schrade, D., Mueller, R., Xu, B. X., Gross, D., (2007) ‘Domain evolution in ferroelectric materials: A continuum phase field model and finite element implementation.‘ *Comp. Meth. Appl. Mech. Engng.* **196**, 4365.

[77] Müller, R., Gross, D., Schrade, D., Xu, B. X., (2007) ‘Domain evolution in ferroelectric materials: A continuum phase field model and finite element implementation.‘ *Int. J. Frac.* **147**, 173.

[78] Zhang, Y. H., Li, J. Y., Fang, D. N., (2010) ‘Size dependent domain configuration and electric field driven evolution in ultrathin ferroelectric films: A phase field investigation.‘ *J. Appl. Phys.* **107**, 034107.

[79] Wang, J., Xia, Y. F., Chen, L. Q., Shi, S. Q., (2011) ‘Effect of strain and deadlayer on the polarization switching of ferroelectric thin film.‘ *J. Appl. Phys.* **110**, 114111.

[80] Su, Y., Chen, H. T., Li, J. J., Soh, A. K., Weng, G. J., (2011) ‘Effects of surface tension on the size-dependent ferroelectric characteristics of free-standing BaTiO3 nano-thin films.‘ *J. Appl. Phys.* **110**, 084108.

[81] Stepkova, V., Marton, P., Hlinka, J., (2012) ‘Stress-induced phase transition in ferroelectric domain walls of $BaTiO_3$.‘ *J. Phys. Condens. Matter.* **24**, 212201.

[82] Xu, B. X., Schrade, D., Müller, R., Gross, D., Granzow, T., Rödel, J., (2010) ‘Phase field simulation and experimental investigation of the electro-mechanical behavior of ferroelectrics.‘ *ZAMM* **90**, 623.

[83] Peach M., Koehler J. S., (1950) ‘The Forces Exerted on Dislocations and the Stress Fields Produced by Them.‘ *Phys. Rev.* **80**, 3.

[84] Eshelby, J. D., *Inelastic Behavior of Solids,* edited by M. F. Kanninen et al. (McGraw-Hill, New York, 1970).

[85] Eshelby, J. D., (1975) ‘The elastic energy-momentum tensor.‘ *J. Elast.* **5**, 321.

[86] Gurtin, M. E., *Configurational forces as basic concepts of continuum physics,* Applied Mathematical Sciences, Vol. 137, (Springer, New York, 2000).

[87] Gross, D., Mueller, R., Kolling, S., (2002) ‘Configurational forces - morphology evolution and finite elements.‘ *Mech. Res. Commun.* **29**, 529.

[88] Arvanitakis, A. I., Chronaiou, E. I., Kalpakides, V. K., (2012) ‘ On the dynamics of moving singularities in solids under the use of the level-set method and the configurational force concept.‘ *Composites: Part B* **43**, 2628.

[89] Budiansky B., Rice, J. R., (1973), ‘Conservation Laws and Energy-Release Rates.‘ *J. Appl. Mech.* **40**, 201.

[90] Eischen, J. W., Herrmann, G., (1987) ‘Energy Release Rates and Related Balance Laws in Linear Elastic Defect Mechanics.‘ *J. Appl. Mech.*, **54**, 388.

[91] Agiasofitou, E. K., and Kalpakides, V. K., (2006) ‘The concept of a balance law for a cracked elastic body and the configurational force and moment at the crack tip.‘ *Int. J. Eng. Sci.* **44**, 127.

[92] Xu, B. X., Schrade, D., Gross, D., Mueller, R., (2010) ‘Fracture simulation of ferroelectrics based on the phase field continuum and a damage variable.‘ *Int. J. Frac.* **166**, 163.

[93] Kienzler, R., *Konzepte der Bruchmechanik: Integrale Bruchkriterien,* (Vieweg+Teubner Verlag, 1993).

[94] Maugin, G. A., *Material Inhomogeneities in Elasticity,* (Chapman & Hall/CRC, 1993).

[95] Zienkiewicz, O. C., Taylor, R. L., Zhu, J. Z. ‘The Finite Element Method: Its Basis and Fundamentals.‘ (Elsevier, 2002).

[96] Simo, J. C., Hughes, T. J. R., ‘Computational Inelasticity.‘ (Elsevier, 2002).

[97] Wriggers, P., ‘Nonlinear Finite Element Methods.‘ (Springer, 2008).

[98] van Halen, P., Pulfrey, D. L., (1985) ‘Accurate, short series approximations to Fermi-Dirac integrals of order -1/2, 1/2, 1, 3/2, 2, 5/2, 3, and 7/2.‘ *J. Appl. Phys.* **57**, 5271.

[99] Mueller R., Maugin, G. A., (2002) ‘On material forces and finite element discretizations.‘ *Comp. Mech.* **29**, 52.

[100] Xiao, Y., Shenoy, V. B., Bhattacharya, K., (2005) ‘Depletion Layers and Domain Walls in Semiconducting Ferroelectric Thin Films.‘ *Phys. Rev. Lett.* **95**, 247603.

[101] Hong, L. and Soh, A. K., Du, Q. G., Li, J. Y., (2008) ‘Interaction of O vacancies and domain structures in single crystal $BaTiO_3$: Two-dimensional ferroelectric model.‘ *Phys. Rev. B* **77**, 094104.

[102] Eichel, R. A., Erhart, P., Träskelin, P., Albe, K., Kungl, H., Hoffmann, M. J., (2008) 'Defect-dipole formation in copper-doped $PbTiO_3$ ferroelectrics.' *Phys. Rev. Lett.* **100**, 095504.

[103] Sluka, T., Tagantsev, A. K., Damjanovic, D., Gureev, M., Setter, N., (2012) 'Enhanced electromechanical response of ferroelectrics due to charged domain walls.' *Nature Commun.* **3**, 748.

[104] Sluka, T., Tagantsev, A. K., Bednyakov, P., Setter, N., (2013) 'Free-electron gas at charged domain walls in insulating $BaTiO_3$.' *Nature Commun.* **4**, 1808.

[105] Mokrý P., Tagantsev, A. K., Fousek, J., (2007), 'Pressure on charged domain walls and additional imprint mechanism in ferroelectrics.' *Phys. Rev. B* **75**, 094110 (2007).

[106] Genenko, Y. A., Hirsch, O., Erhart, P., in *2012 Internatinal symposium on applications of ferroelectrics held jointly with 11th IEEE ECAPD and IEEE PFM (ISAF/ECAPD/PFM).* Book Series: *IEEE International Symposium on Applications of Ferroelectrics,* (Aveiro, Portugal, 2012)

[107] Watanabe, Y., (1998), 'Theoretical stability of the polarization in a thin semiconducting ferroelectric.' *Phys. Rev. B* **57**, 2.

[108] Kim, S. B., and Kim, D. Y., (2000), 'Stabilization and Memory of the Domain Structures in Barium Titanate Ceramics: Microstructural Observation.' *J. Am. Ceram. Soc.* **83**, 1495.

[109] Lambeck, P. V., and Jonker, G. H., (1986), 'The nature of domain stabilization in ferroelectric perovskites.' *J. Phys. Chem. Solids.* **47**, 453.

[110] Wu X., Vanderbilt D., (2006), 'Theory of hypothetical ferroelectric superlattices incorporating head-to-head and tail-to-tail 180° domain walls.' *Phys. Rev. B* **73**, 020103.

[111] Gureev, M. Y., Tagantsev, A. K., Setter, N., (2011), 'Head-to-head and tail-to-tail 180° domain walls in an isolated ferroelectric.' *Phys. Rev. B* **83**, 184104.

[112] Gureev, M. Y., Mokrý P., Tagantsev A. K., Setter, N., (2012), 'Ferroelectric charged domain walls in an applied electric field.' *Phys. Rev. B*, **86**, 104104.

[113] Eliseev, E. A., Morozovska, A. N., Svechnikov, G. S., Gopalan, V., and Shur, V. Y., (2011), 'Static conductivity of charged domain walls in uniaxial ferroelectric semiconductors' *Phys. Rev. B*, **83**, 235313.

[114] Chen, L. Q., (2008) 'Phase-Field Method of Phase Transitions/Domain Structures in Ferroelectric Thin Films: A Review.' *J. Am. Ceram. Soc.* **91**, 1835.

[115] Landau L. D., Lifshitz, E. M., *Electrodynamics of continuous media,* (Pergamon Press, New York, 1984).

[116] Franzbach, D. J., Xu, B. X., Mueller, R., Webber, K. G., (2001) ‘The effects of polarization dynamics and domain switching energies on field induced phase transformations of perovskite ferroelectrics.‘ *Appl. Phys. Lett.* **99**, 162903.

[117] Schrade, D., Xu, B. X., Mueller, R., Gross, D., in *Proceedings of the ASME 2008 Smart Materials,* Adaptive Structures and Intelligent Systems (SMASIS2008), (Ellicot City, MD, 2008), p. 301.

[118] Different values have been used for N_d in specific examples.

[119] Wang, J., Kamlah, M., (2008) ‘Domain structures of ferroelectric nanotubes controlled by surface charge compensation.‘ *Appl. Phys. Lett.* **93**, 042906.

[120] Jia, C.-L., Mi, S.-B., Urban, K., Vrejoiu, I., Alexe, M., Hesse, D., (2008) ‘Atomic-scale study of electric dipoles near charged and uncharged domain walls in ferroelectric films.‘ *Nat. Mater.* **7**, 57

[121] Mueller, R., Kolling, S., Gross, D., (2002) ‘On configurational forces in the context of the finite element method.‘ *Int. J. Numer. Meth. Eng.* **53**, 1557.

[122] Genenko, Y. A., Lupascu, D. C., (2007) ‘Drift of charged defects in local fields as aging mechanism in ferroelectrics.‘ *Phys. Rev. B* **75**, 184107.

[123] Genenko, Y. A., (2008) ‘Space-charge mechanism of aging in ferroelectrics: An analytically solvable two-dimensional model.‘ *Phys. Rev. B* **78**, 214103.

[124] Okatan, M. B., Alpay, S. P., (2009) ‘Imprint in ferroelectric materials due to space charges: A theoretical analysis.‘ *Appl. Phys. Lett.* **95**, 092902.

[125] Zhang, X., Hashimoto, T., Joy, D. C., (1992) ‘Electron holographic study of ferroelectric domain walls.‘ *Appl. Phys. Lett.* **60**, 784.

[126] Zhang, X., Joy, D. C., Zhang, Y., Hashimoto, T., Allard, L., Nolan, T. A., (1993) ‘Electron holography techniques for study of ferroelectric domain walls.‘ *Ultramicroscopy* **51**, 21.

[127] Meier, D., Seidel, J., Cano, A., Delaney, K., Kumagai, Y., Mostovoy, M., Spaldin, N. A., Ramesh, R., Fiebig, M., ‘Anisotropic conductance at improper ferroelectric domain walls.‘ *Nat. Mater.* **11**, 284.

[128] Wang, J., Kamlah, M., Zhang, T.-Y., (2009) ‘Phase field simulations of ferroelectric nanoparticles with different long-range-electrostatic and -elastic interactions.‘ *J. Appl. Phys.* **105**, 014104.

[129] Liu, N., Su, Y., Weng, G. J., (2013) ‘A phase-field study on the hysteresis behaviors and domain patterns of nanocrystalline ferroelectric polycrystals.‘ *J. Appl. Phys.* **113**, 204106.

[130] Fridkin, V.M. *Ferroelectric Semiconductors*, Consultants Bureau, NY (1980).

[131] Zuo, Y. N., Genenko, Y. A., Klein, A., Stein, P., Xu, B. X., (2014) ‘Domain wall stability in ferroelectrics with space charges.‘ *J. Appl. Phys.* **115**, 084110.

[132] Erhart P., Albe, K., (2007) ‘Thermodynamics of mono- and di-vacancies in barium titanate.‘ *J. Appl. Phys.* **102**, 084111.

[133] Hagemann, H. J., ‘Loss mechanisms and domain stabilisation in doped $BaTiO_3$.‘ *J. Phys. C Solid State* **11**, 3333.

[134] Lambeck, P. V., Jonker, G. H., (1978) ‘Ferroelectric domain stabilization in BaTiO3 by bulk ordering of defects.‘ *Ferroelectrics* **22**, 729.

[135] Vollman, M., Waser, R., (1994) ‘Grain Boundary Defect Chemistry of Acceptor-Doped Titanates: Space Charge Layer Width.‘ *J. Am. Ceram. Soc.* **77**, 235.

[136] R. Waser, (1995) ‘Electronic properties of grain boundaries in $SrTiO_3$ and $BaTiO_3$ ceramics.‘ *Solid State Ionics* **75**, 89.

[137] Genenko, Y. A., Hirsch, O., Erhart, P., (2014) ‘Surface potential at a ferroelectric grain due to asymmetric screening of depolarization fields‘ *J. Appl. Phys.* **115**, 104102.

[138] Klein, A., (2012) ‘Energy band alignment at interfaces of semiconducting oxides: A review of experimental determination using photoelectron spectroscopy and comparison with theoretical predictions by the electron affinity rule, charge neutrality levels, and the common anion rule.‘ *Thin Solid Films* **520**, 3721.

[139] Eichel, R. A., (2007) ‘Defect structure of oxide ferroelectrics valence state, site of incorporation, mechanisms of charge compensation and internal bias fields‘ *J. Electroceram.* **19**, 9

[140] Zhang, L. X., Ren, X., (2005) ‘In situ observation of reversible domain switching in aged Mn-doped $BaTiO_3$ single crystals.‘ *Phys. Rev. B* **71**, 174108.

[141] Hagemann, H.-J., Hennings, D., (1981) ‘Reversible weight change of acceptor-doped $BaTiO_3$.‘ *J. Am. Ceram. Soc.* **64**, 590.

[142] Wechsler, B. A., Klein, M. B., (1988) ‘Thermodynamic point defect model of barium titanate and application to the photorefractive effect.‘ *J. Opt. Soc. Am.* **5**, 1711.

[143] Landauer, R., (1957) 'Electrostatic Considerations in $BaTiO_3$ Domain Formation during Polarization Reversal.' *J. Appl. Phys.* **28**, 227.

[144] Molotskii, M., Kris, R., Rosenman, G., (2000) 'Fluctuon effects in ferroelectric polarization switching.' *J. Appl. Phys.* **88**, 5318.

[145] Gerra, G., Tagantsev, A. K., Setter, N., (2005) 'Surface-Stimulated Nucleation of Reverse Domains in Ferroelectrics.' *Phys. Rev. Lett.* **94**, 107602.

[146] Neumeister, P., Balke, H., Lupascu, D. C., (2009) 'Continuum analysis of the nucleus growth of reverse domains in large ferroelectric crystals.' *J. Appl. Phys.* **105**, 084115.

[147] De Araujo, C. A. P., Cuchiaro, J. D., Mcmilan, L. D., Scott, M. C., Scott, J. F., (1995), 'Fatigue-free ferroelectric capacitors with platinum electrodes.' *Nature*(London), **374**, 627-629.

[148] Arlt, G., Neumann, H., (1988), 'Internal bias in ferroelectric ceramics: Origin and time dependence.' *Ferroelectrics*, **87**, 109-120.

[149] Ren, X., (2004), 'Large electric-field-induced strain in ferroelectric crysstals by point-defect-mediated reversible domain switching.' *Nature Mater.* **3**, 91-94.

[150] Ren, X., Zhang, L. X., (2006), 'Electro-shape-memory effect in ferroelectric martensite.' *Mater. Sci. Eng. A* 438-440, 1071-1076.

[151] Lo, V. C., Chung, W. W., Cao, H. X., Dai, X., (2008), 'Investigating the effect of oxygen vacancy on the dielectric and electromechanical properties in ferroelectric ceramics.' *J. Appl. Phys.* **104**, 064105.

[152] Zhang, Y. H., Li, J. Y., Fang, D. N., (2010), 'Oxygen-vacancy-induced memory effect and large recoverable strain in a barium in a barium titanate single crystal.' *Phys. Rev. B*, **82**, 064103.

[153] Marton, P., Elsaesser, C., (2011), ′ Switching of a substitutional-iron/oxygen-vacancy defect complex in ferroelectric PbTiO3 from first principles. ′ *Phys. Rev. B*, **83**, 020106.

[154] Zhang, L., Erdem, E., Ren, X., Eichel, R.-A., (2008) ′ Reorientation of (Mn-Ti(')-V-O(center dot center dot))(x) defect dipoles in acceptor-modified BaTiO3 single crystals: An electron paramagnetic resonance study. ′ *Appl. Phys. Lett.*, **93**, 202901.

[155] Jakes, P., Erdem, E., Eichel, R.-A., Jin, L., Damjanovic, D., (2011), ′ Position of defects with respect to domain walls in Fe3+-doped Pb[Zr0.52Ti0.48]O-3 piezoelectric ceramics. ′ *Appl. Phys. Lett.*, **98**, 072907.

[156] Morozov, M. I., Damjanovic, D., (2008), ′ Hardening-softening transition in Fe-doped Pb(Zr,Ti)O(3) ceramics and evolution of the third harmonic of the polarization response. ′ *J. Appl. Phys.*, **104**, 034107.

[157] Erhart, P., Traskelin, P., Albe, K., (2013), ‘Formation and switching of defect dipoles in acceptor-doped lead titanate: A kinetic model based on first-principles calculations.‘ *Phys. Rev. B*, **88**, 024107.

CV

Personal data

Name	Yinan Zuo
E-Mail	yinan.zuo@gmail.com
Birthday	29. April 1983 in Shenyang, Liaoning, P. R. China
Nationality	Chinese
Permanent residency	yes
Family status	married

Career experiences

03/2015 – Now	**Scientific staff**, *RWTH Aachen*, Aachen, *Civil Engineering*, Topic: Multiscale modeling of bonding processes under consideration of thermomechanical behaviors in the interface layers, Implementation in ABAQUS User Element. Teaching: WS 2015-16, Exercise of mechanics of materials, SS 2016, Exercise of theory of plasticity
10/2011 – 02/2012	**Heat treatment engineer**, *Volkswagen Automatic Transmission (Dalian) Co.,Ltd.*, Dalian, V. R. China. Test of new machines and training of new coworkers

Academic education

03/2012 – 03/2015	**Scientific staff, PhD study**, *TU Darmstadt*, Darmstadt, *Materials science*, Topic: phase field modeling of ferroelectric ceramics with point defects. Teaching: WS 2012-13, Exercise of engineering mechanics for materials science students
09/2009 – 05/2011	**M. Sc.**, *Michigan Technological University*, Hougnton, MI, USA, *Engineering Mechanics*. Average points: 3.8 (highest 4.0)
04/2006 – 07/2009	**Dipl.-Ing.**, *Karlsruhe Institute of Technologie*, Karlsruhe, *Theoretical Mechanical Engineering*. Studienarbeit: 2D Modelling of crack propagation by FEM, Diplom thesis: Phase field modeling of PTO nanotubes, Average points: 1.6 (highest 1.0)
09/2002 – 07/2005	**Bachelor study**, *Tongji-University*, Shanghai, China, *Automotive Engineering*. Average points: 4.21 (highest 5.0)

School education

09/1999 – 07/2002	**Senior middle school**, *11. Middle school of Shenyang*, Shenyang, China.
09/1996 – 07/1999	**Junior middle school**, *Northeast Yucai School*, Shenyang, China.
09/1990 – 07/1996	**Primary school**, *Ningshanlu Primary school*, Shenyang, China.